DOPED VANADIUM DIOXIDE BY HYDROTHERMAL AND GREEN PROCESSES: SYNTHESIS AND PHYSICAL PROPERTIES

By

Asratemedhin Bekele Habtemariam

Submitted in accordance with the requirement for

the degree of

DOCTOR OF PHILOSOPHY

in the subject

PHYSICS

at the

UNIVERSITY OF SOUTH AFRICA

Supervisor: Prof. Malik Maaza

Co-Supervisor: Prof. Vijaya Srinavasu Vallabhapurapu

Date Submitted: July 2018

DECLARATION

Student number: 49025155

I declare that '**Doped Vanadium Dioxide by Hydrothermal and Green Processes: Synthesis and Physical Properties**' is my own work and that all the sources that I have used or quoted have been indicated and acknowledged by means of complete references.

Mr. AB Habtemariam **Date**

DEDICATION

To my family

Acknowledgments

In the first place, I thank almighty God, who gave me the courage to be patient and achieve my big dream. Secondly, I would like to express my heartfelt gratitude to my supervisor Professor Malik Maaza who allowed me to work with his nanomaterial group in an open and friendly air. I am enlightened in his diligence, unreserved guidance and continuous follow up of my research work while I was at iThemba Labs. I am very grateful to you for your interest in helping others especially African researchers. I learnt from your extraordinary hard work, how to become an independent researcher and have developed self-confidence. You were concerned about me even when you were in a serious health condition.

I thank Professor V. S. Vallabhapurapu, my co-supervisor, for giving me important directions and detailed responses for all my academic questions.

I would like to make special mention to Dr. Zebib Yenus Nuru – whose sisterly advice, considerateness and continuous follow up of my research progress in every single minute we met was remarkable. I learnt a lot from your hard work principle how to become an independent researcher.

I have also worked in collaboration with:

- Dr. Aline Simo - who were my mentor and with me whenever I was in need of your support. Your sincere help while I am working in the Nano labs at iThemba is unforgettable.
- Dr. Bertrand T. Sone – whose constructive comments and suggestion led me to successful results. Your first trial work on the green process made me achieve the intended outcome. Especially your assistance while I am at my proposal development stage is worth mentioning.

I would like to forward my thanks to the following people as well:

- Dr. S. Zongo – you were always by my side. I will never forget the times we spent at iThemba labs. Your funny words come to my mind.
- Dr. A. Diallo – you were the first scholar I met at Cape Town airport. Your brotherly approach was unforgettable.
- Mrs. Nicozulu Losani- You are a real manager, so cool and polite. I always feel free to talk to you.
- Mrs. Phumza- I'm passionate about your smiling face to everybody at MRD. You were always positive and helpful to me.
- Dr. M. Nkosi, who was always available whenever I needed your assistance in the solid state lab for the furnace.
- Dr. R. Butcher, thank you so much for the XRD characterization of my samples at iThemba LABS.
- Dr. G. Fuku- You were always happy to advise me and your utmost assistance in helping me prepare figures and schematics. I remember the funny moments we spent in my flat.
- Dr. S. Johannes, I really thank you for your willingness in running the DSC and FTIR characterizations of my samples.

I thank the Unesco-Unisa Africa Chair in Nano Science and Nanotechnology (U2ACN2) for funding my research work, without which none of this thesis would have been materialized.

I also thank National Research Foundation (NRF)-iThemba Laboratory for allowing me to conduct my whole research work by financial and material support.

My final thank goes to my beloved family and friends who has always been supporting me in any way possible.

I thank all the MRD staff members and the security department of iThemba Labs.

In this opportunity, I would like to thank my M. Sc. supervisor, Dr. Esayas Belay Shume, who has taught me not only the technicalities but also the love for physics.

I never intend, but I am sure I've missed some names without mentioning. Thank you all!

ABSTRACT

Nanomaterials are of great interest because of their novel electrical, optical and magnetic properties which results from their small size and shape and exhibit unique features that are significantly different from their corresponding macro state. Nanomaterials synthesis, therefore, has been an important research topic due to promising signs of their implementation for various kinds of device applications.

It is well-known that vanadium dioxide is a thermochromic material and exhibits metal-insulator transition close to room temperature of about 68^0C. This metal-insulator phase transition of vanadium dioxide is followed by changes of optical properties such as increase in reflectance and decrease in emittance in the infrared region when the temperature increases above the transition value. Due to this anomalous property, vanadium dioxide is a suitable candidate material for various device applications as in optical switches, smart-window coating for energy efficiency buildings, energy storage devices, sun screening, thermal sensor, and smart radiation devices.

This research project focuses on the successful synthesis and characterization of thermochromic vanadium dioxide nanomaterials and consists of two parts. The first part of the thesis consists of hydrothermal synthesis method for the successful synthesis of undoped and Mg-, Cr-, Mo-doped vanadium dioxide nanoparticles. This is due to low cost, high throughput, environmental friendliness and scalability of the technique for large scale production. The second part of this thesis encompasses the synthesis of vanadium dioxide nanoparticles by green processing. The second part was carried out because it is nontoxic, an environmentally friendly approach and has never been done before, as to our knowledge, for the synthesis of vanadium oxides nanoparticles. All results were characterized by using XRD, SEM, HRTEM, DSC, and FTIR techniques.

Key terms:

Vanadium dioxide nanomaterials, metal- insulator transition, hydrothermal technique, green process, thermochromic property.

Table of Contents

DECLARATION ii
DEDICATION iii
Acknowledgments iv
ABSTRACT vii
List of Figures xi
CHAPTER ONE 1
INTRODUCTION 1
1.1 General Background 1
1.2 Problem Statement 3
1.3 Aims and Objectives of the Research 4
1.4 Significance of the Research 5
1.5 Outline of the Research 5
CHAPTER TWO 7
LITERATURE REVIEW 7
2.1 Physical Properties of VO_2 7
2.1.1 Crystallographic Structure of VO_2 8
2.1.1.1 Rutile structure of VO_2 9
2.1.1.2 Monoclinic M_1 structure of VO_2 10
2.1.1.3 Monoclinic M_2 structure of VO_2 11
2.1.2 Band structure of VO_2 11
2.1.3 Electrical Properties of VO_2 15
2.1.4 Optical Properties of VO_2 16
2.2 Applications of VO_2 17
CHAPTER THREE 21
DIFFERENT TECHNIQUES AND PROCESSES OF SYNTHESIS OF VO_2 21
3.1 Synthesis Techniques of VO_2 21
3.1.1 Chemical Vapour Deposition 22
3.1.2 Sol-gel 23
3.1.3 Hydrothermal 24
3.1.4 Pulsed Laser Deposition 26
3.1.5 Sputtering 27

3.1.6 Combustion Synthesis 28
3.1.7 Green Process 28
3.2 Doping Process 30
3.3 Characterization techniques 33
3.3.1 X-ray Diffraction 34
3.3.2 Scanning Electron Microscopy 35
3.3.3 Energy Dispersive X-ray Analysis 36
3.3.4 Transmission Electron Microscopy 37
3.3.5 High Resolution Transmission Electron Microscopy 37
3.3.6 Fourier Transform Infrared Spectroscopy 38
3.3.7 Differential Scanning Calorimetry 38
CHAPTER FOUR 39
EXPERIMENTAL AND RESULTS 39
4.1 Experimental Procedures 39
4.1.1 Hydrothermal Synthesis of Undoped VO_2 nanoparticles 39
4.1.2 Hydrothermal Synthesis of Mg doped VO_2 nanoparticles 40
4.1.3 Hydrothermal synthesis of Cr-doped VO_2 nanoparticles 41
4.1.4 Hydrothermal synthesis of Mo doped VO_2 nanoparticles 42
4.1.5 Hydrothermal synthesis of Mg/Mo Co-doped VO_2 nanoparticles 43
4.1.6 Synthesis of VO_2 by green process 44
4.2 Experimental Results 45
4.2.1 Hydrothermal synthesis of undoped VO_2 (M) nanoparticles 47
4.2.2 Mg doped VO_2 56
4.2.3 Cr doped VO_2 67
4.2.4 Mo doped VO_2 76
4.2.5 Magnesium/Molybdenum co-doped VO_2 87
4.2.6 Green Synthesis of VO_2 93
CHAPTER FIVE 100
CONCLUSIONS AND FUTURE WORK 100
5.1 Conclusions 100
5.2 Future Work 101
References 102

List of Figures

Figure 2.1: The Vanadium-Oxygen phase diagram [96]..... 8
Figure 2.2: Schematic diagram for the rutile structure of VO_2. Bigger (red) spheres stands for Vanadium (V) atoms and small (blue) spheres denote oxygen (O) atoms [110]. 10
Figure 2.3: Schematic diagram for monoclinic M_1 structure of VO_2 [110]. 10
Figure 2.4: Schematic diagram for monoclinic M_2 structure of VO_2 [110]..... 11
Figure 2.5: The Vanadium e_g and t_{2g} orbitals (a) $d_{3z^2-r^2}$ (b) d_{xy} (c) $d_{x^2-y^2}$ (d) d_{xz} (e) d_{yz} [119]. 15
Figure 2.6: Schematic band diagram for VO_2 [110] 13
Figure 2.7: Schematic diagram of thermochromic window during (a) summer and (b) winter seasons [138] 18
Figure 3.1: Teflon-lined autoclave (left) and Oven (right) used in this research work, at iThmba Labs..... 25
Figure 3.2: Shematic diagram of PLD [70] 27
Figure 3.3: Schematic diagram of different nanoparticle synthesis methods [61] 30
Figure 3.4: X-ray diffraction by atomic crystal 34
Figure 3.5: Schematic diagram of scanning electron microscope [183] 36
Figure 3.6: High resolution transmission electron microscope (HRTEM) at UWC used in this research..... 37
Figure 4.1: XRD patterns of undoped VO_2 nanoparticles for different hydrothermal treatment time. 48
Figure 4.2: SEM images of undoped VO_2 nanorods for 48 hours hydrothermal treatment time. 49
Figure 4.3: HRTEM images of VO_2 for 48 hours hydrothermal treatment (a-e) with clear lattice fringes of VO_2 (d). 52
Figure 4.4: SAED ring patterns of VO_2 for 48 hours hydrothermal treatment time. 53
Figure 4.5: EDS spectrum of undoped VO_2 for 48 hours hydrothermal treatment time. 54
Figure 4.6: DSC curves of undoped VO_2 nanoparticles for 6 hours hydrothermal treatment time. 55
Figure 4.7: FTIR spectrum of undoped VO_2 nanoparticles. 56
Figure 4.8 (a): XRD patterns of Mg doped VO_2 nanoparticles for different dopant concentrations. 57
Figure 4.8 (b): XRD patterns of Mg doped VO_2 with different doping concentrations, peak shift at 27.86^0. 58
Figure 4. 8 (c): XRD patterns of 2 at % Mg doped VO_2 nanoparticles for different hydrothermal treatment time. 59
Figure 4.9: SEM images of 5.0 at % Mg doped VO_2 nanoparticles. 60

Figure 4.10: HRTEM images of 5.0 at % Mg doped VO_2 nanoparticles. 61
Figure 4.11: SAED ring patterns of 5.0 at % Mg doped VO_2 nanoparticles. 62
Figure 4.12: EDS spectrum of Mg doped VO_2 nanoparticles. 63
Figure 4.13: FTIR spectrum of 5.0 at % Mg doped VO_2 nanoparticles. 64
Figure 4.14 (a): DSC curves of 1at% Mg doped VO_2 nanoparticles. 65
Figure 4.14 (b): DSC curves of 2 at% Mg doped VO_2 nanoparticles. 65
Figure 4.14 (c): DSC curves of 3 at% Mg doped VO_2 nanoparticles. 66
Figure 4.14 (d): DSC curves of 4 at% Mg doped VO_2 nanoparticles. 66
Figure 4.14 (e): DSC curves of 5 at% Mg doped VO_2 nanoparticles. 67
Figure 4.15 (a): XRD patterns of Cr doped VO_2 nanoparticles for various dopant concentrations. 68
Figure 4.15 (b): XRD patterns of Cr doped VO_2 nanoparticles, shift of peaks observed at 27.86^0 69
Figure 4.15 (c): XRD patterns of Cr doped VO_2 nanoparticles, peak shift at 37.00^0. 70
Figure 4.15 (d): XRD patterns of Cr doped VO_2 nanoparticles for different hydrothermal treatment time. 71
Figure 4.16: SEM images of Cr doped VO_2 nanoparticles. 72
Figure 4.17: HRTEM images of Cr doped VO_2nanoparticles (a-c) with clear lattice fringes (d)..... 73
Figure 4.18: SAED ring patterns of Cr-doped VO_2 nanoparticles..... 74
Figure 4.19: EDS spectrum of Cr-doped VO_2 nanoparticles by hydrothermal method..... 75
Figure 4.20: FTIR spectrum of 1.5 at % Cr doped VO_2 nanoparticles. 76
Figure 4.21 (a): XRD patterns of Mo doped VO_2 nanoparticles. 77
Figure 4.21 (b): XRD patterns of Mo doped VO_2 nanoparticles, peak shift at 27.86^0. 78
Figure 4.21 (c): XRD patterns of 1.0 at % Mo doped VO_2 with various hydrothermal treatment time. 79
Figure 4.22: SEM image of 0.5 at %Mo doped VO_2 nanoparticles. 80
Figure 4.23: HRTEM images of Mo doped VO_2 nanoparticles. 81
Figure 4.24: SAED ring patterns of Mo doped VO_2 nanoparticles. 82
Figure 4.25: EDS spectrum of Mo doped VO_2 nanoparticles. 83
Figure 4.26 (a): DSC curves for 0.5 at % Mo doped VO_2 nanoparticles. 84
Figure 4.26 (b): DSC curves for 1.0 at % Mo doped VO_2 nanoparticles. 84
Figure 4.26 (c): DSC curves for 1.5 at % Mo doped VO_2 nanoparticles. 85
Figure 4.26 (d): DSC curves for 2.0 at % Mo doped VO_2 nanoparticles. 85
Figure 4.26 (e): DSC curves for 2.5 at % Mo doped VO_2 nanoparticles. 86
Figure 4.27: FTIR spectrum of 2.0 at% Mo doped VO_2 nanoparticles. 87
Figure 4.28: XRD patterns of Mg/Mo co-doped VO_2 nanoparticles. 88
Figure 4.29: SEM images of Mg/Mo co-doped VO_2 nanoparticles. 89
Figure 4.30: HRTEM images of Mg/Mo co-doped VO_2 nanoparticles. 90
Figure 4.31: SAED ring patterns of Mg/Mo co-doped VO_2 nanoparticles. 91

Figure 4.32: EDS spectrum of Mg/Mo co-doped VO_2 nanoparticles. 92
Figure 4.33: FTIR spectrum of 2 at % Mg with 0.5 at % Mo doped VO_2 nanoparticles. 93
Figure 4.34: XRD patterns of VO_2 (M) by green process. 94
Figure 4.35: SEM images of VO_2 (M) nanoparticles synthesized by green process. 95
Figure 4.36: HRTEM images of VO_2 (M) nanoparticles by green process (a-c) with clear lattice fringes (d). 96
Figure 4.37: SAED ring patterns of VO_2 (M) by green process. 97
Figure 4.38: EDS spectrum of VO_2 (M) nanoparticles by green process. 98
Figure 4.39: FTIR spectrum of VO_2 (M) nanoparticles by green process. 99

CHAPTER ONE

INTRODUCTION

1.1 General Background

Transition metal oxides (TMOs) have been intensively investigated both theoretically and experimentally for several decades because of their strongly correlated electronic properties and potential technological applications [1-3]. TMOs demonstrate unusual physical properties, such as metal-insulator transitions (MITs), high-temperature superconductivity, and colossal magneto-resistance [1-6]. These remarkable properties arise due to the presence of partially filled 3d, 4f or 5f electronic shells, as a result of which there is strong interaction of d, f electrons with each other and with wandering electronic states of the material [6, 7]. TMOs are the most extensively studied materials in an investigation of MITs where abrupt changes in electrical and optical properties are observed [3, 8, 9]. These unique properties of TMOs are taken as important parameters for choosing several types of devices in a range of technological applications [1, 3].

Vanadium oxides (V_2O_5, V_2O_3 and VO_2) which belong to TMOs have received great attention in fundamental research and technology for decades because of their MIT phenomena [10-12]. Among these, thermochromic vanadium dioxide (VO_2) is canonical example of TMOs which has attracted researchers' attention due to its temperature dependent MIT at about 68^0C [10-16]. VO_2 undergoes a first order type phase transition reversibly from monoclinic crystal structure at low temperature to tetragonal structure at high temperature, accompanied by significantly observable electrical, optical and magnetic properties alterations [17-25]. The unique behaviors associated with VO_2 makes it to be technologically important material in many fields such as optical switches [25-28], optical storage devices [24, 29, 30], thermal sensors [12, 24, 26], smart window coatings [31-36], laser protection

[29, 30, 37], smart radiation devices [38-40] etc. However, the limited availability of vanadium over the globe initiates an economic and eco-friendly synthesis of the material [41]. Moreover, the physics of the phase transition is complex and it is still topic of research [42]; and the syntheses processes of VO_2 were challenging, as a result of which detailed investigations are still looked for.

The synthesis of VO_2 nanomaterials have been practiced for many years using different techniques since its discovery by Morin [4]. The commonly known syntheses techniques such as rf-magnetron sputtering [38, 39, 43, 44], chemical vapor deposition [45-47], pulsed laser deposition [40, 48-50], ion implantation [51, 52] etc. have been widely used. The aforementioned techniques are known in their high quality throughputs; however, they are expensive and need complicated setup arrangement [14, 53-55]. Therefore, solution based methods such as sol-gel [32, 33, 53, 6], hydrothermal [14, 54, 57], and solution combustion synthesis [58] techniques could be used as an alternative approach in preparing VO_2 nanomaterials. Both the sol-gel and hydrothermal techniques have been extensively used for VO_2 nanomaterials syntheses due to their cost-effectiveness, high yield and advantage of tailoring structure and morphology over the nanostructures [53-57]. Specifically, the hydrothermal synthesis technique does not need complicated set up, gives high quality throughput, is cost effective, flexible and can be scaled up easily for mass production [54, 55, 57]. Consequently, in this research project, the hydrothermal method has been employed for the syntheses of un-doped and doped VO_2 nanoparticles.

Although hydrothermal method is an alternate approach for the syntheses of un-doped and doped VO_2 nanoparticles, it still lacks environmental friendliness [59-62]. The increasing environmental hazards over such kind of chemical syntheses methods, therefore, have initiated the search for alternative method such as biological methods. This includes the use of bacteria, algae and plant parts for nanoparticles synthesis [59-65]. Plant extracts such as

flowers, leaves and roots have been employed to synthesize metal oxide nanoparticles, and proved to be environmentally benign [59-66]. Herein, therefore, the successfully synthesis of vanadium dioxide nanoparticles using plant extracts as a reducing and capping agent has been reported, as to our knowledge, for the first time.

1.2 Problem Statement

In the developed countries alone, about 40% of the total energy use goes into air conditioning of buildings and for the use of other indoor electrical appliances [67-69]. Due to diminishing of natural oil resources and accompanying environmental concern, in recent times, therefore, there is an increasing search for alternative energy sources than ever before [67-72]. In this regard, the study of nanomaterials for energy generation and energy saving are in the frontier of science and technology [31, 70-73]. Specifically, nano-scaled VO2 materials, due to their thermochromic property, can be the best alternative for the use of energy saving applications [23, 26, 31, 70].

Thermochromic VO_2 has interesting phase transition property which is one of the most significant factors for a range of technological applications [27, 53, 74]. This MIT can be altered to meet certain requirements by different driving mechanisms such as doping [22, 53, 74, 75], light illumination [6, 76, 77] and the application of electric field [78-80]. Understanding of the best synthesis technique and modification of the phase transition of VO_2 are essential to use in specific technological applications. Various synthesis techniques are, thus, employed since long time.

To date most technological applications, involve the use of thin films, as a result of which intensive studies of VO_2 thin films synthesis have been conducted [43-53, 81-83]. However, some of the techniques employed so far are not appropriate for coating large surface area

[22]. Moreover, most of the thin film syntheses techniques are difficult to put into practice, because of the requirement of complicated and expensive setups, complex control parameters, and scale up problems [22, 54, 83]. However, syntheses of nanopowders overcome such shortcomings and much emphasis has been given to the synthesis of nanoparticles now a day [22, 54]. Especially hydrothermal synthesis technique is more effective, environmentally friendly and less costly [54, 57, 84] and various research works have been conducted using this method for the syntheses of VO_2 nanoparticles [54, 57, 83-93].

Equally important issue is switching the phase transitions to fit specific technological applications. Among the strategies, introducing various dopants in to the VO_2 lattice are commonly practiced to get specific functionality [22, 53, 74, 75]. Extensive studies have been conducted which reveal the possibility of lowering the phase transition temperature close to ambient temperature up on doping of VO_2 [53, 54, 75, 94]. However, as these studies are not exhaustive, fundamental as well as applied studies are yet to be conducted on undoped and doped VO_2 nanomaterials. In this research work, therefore, we have studied some of the issues which require further investigation such as the effects of dopant concentration and reaction time for synthesizing un-doped and doped VO_2 nanoparticles.

In addition, due to low cost, efficiency and environmental friendliness, synthesis of VO_2 nanoparticles by the green process takes the second major part of this research project. As to our knowledge, synthesis of VO_2 by the green process is a new approach and this may make the research project novel.

1.3 Aims and Objectives of the Research

Aims of this research work are:

I. Develop cost effective and reproducible method to synthesis high quality VO_2 nanoparticles,
II. Modify phase transition temperature of VO_2 using different dopants (such as Mg, Mo, Cr).

The following specific objectives have been carried out to achieve the aims:

(a) Synthesis of undoped-VO_2 and Mg, Cr, and Mo doped-VO_2 nanoparticles through hydrothermal method,
(b) Synthesis of VO_2 nanoparticles by the green process,
(c) Structural, electrical, and optical characterizations of the synthesized nanoparticles using XRD, SEM, TEM, DSC, FTIR, and UV-Vis techniques,
(d) Comparison of results obtained from the two synthesis techniques.

1.4 Significance of the Research

World annual energy consumption studies confirmed that more than 35% of the globe's energy is consumed by buildings for lighting, heating, cooling, and air conditioning purposes on a yearly basis [68-71]. Upon maintaining the temperature balance between inside and outside of buildings, about 33% saving in energy consumption will be realized [70]. Thus, use of VO_2 as smart nano-coating in windows, for solar heat control management where cooling and air conditioning is required, i.e., for efficient and viable VO_2 coatings.

1.5 Outline of the Research

The research project is reported in five chapters. Background of the study, statement of the problem, aims and objectives of the study are discussed in the first chapter. Chapter two

deal with the physical properties of VO_2 and its possible technological applications. In chapter three different techniques and synthesis methods of VO_2 are presented. Chapter four focuses on the various experimental studies and summary of the results. Conclusion and future works of the study are presented in chapter five.

CHAPTER TWO

LITERATURE REVIEW

2.1 Physical Properties of VO_2

Vanadium, being a transition metal, has partially filled d-orbital and can exist in different oxidation states (+2, +3, +4, and +5). The major vanadium oxides like VO, V_2O_3, VO_2 and V_2O_5 form single oxidation state, whereas oxides such as V_3O_5, V_4O_7, V_6O_{11}, V_6O_{13}, V_7O_{13} etc. are found in mixed valence oxides containing two oxidation states [95-97]. The single valence oxides (VO_2, V_2O_3 and V_2O_5) are the most extensively investigated oxides for technological applications [95-97]. In these single valence oxides of vanadium, there is strong Coulombic repulsion between two electrons of same d orbital whose spin points up and down [98]. As a result, d-electrons of these oxides are considered to be strongly correlated and VO_2 is a commonly known example of strongly correlated materials [1, 7, 16, 98, 99]. These strongly correlated electrons are responsible for the extreme sensitivity of the material for small change of external factors such as pressure, temperature or dopant concentration [7, 16].

The vanadium-oxygen phase diagram in Figure 2.1 show about 13 stable vanadium oxide phases, out of which vanadium dioxide (VO_2), vanadium sesquioxide (V_2O_3) and vanadium pentoxide (V_2O_5) undergo MIT at a particular temperature (T_c) depending on oxygen vanadium stoichiometry [15]. Among them, vanadium dioxide (VO_2) is one of the intensively studied oxides of vanadium and undergoes a reversible first order type metal-insulator transition (MIT) at a critical temperature (T_c) of about 68 ^{0}C [17-19, 100]. Although, the origin of the driving force of the phase transition in VO_2 has been a controversial issue [99-103], electron-electron correlation effects are strongly supported as being the main driving forces of the phase transition phenomena [99, 102, 104].

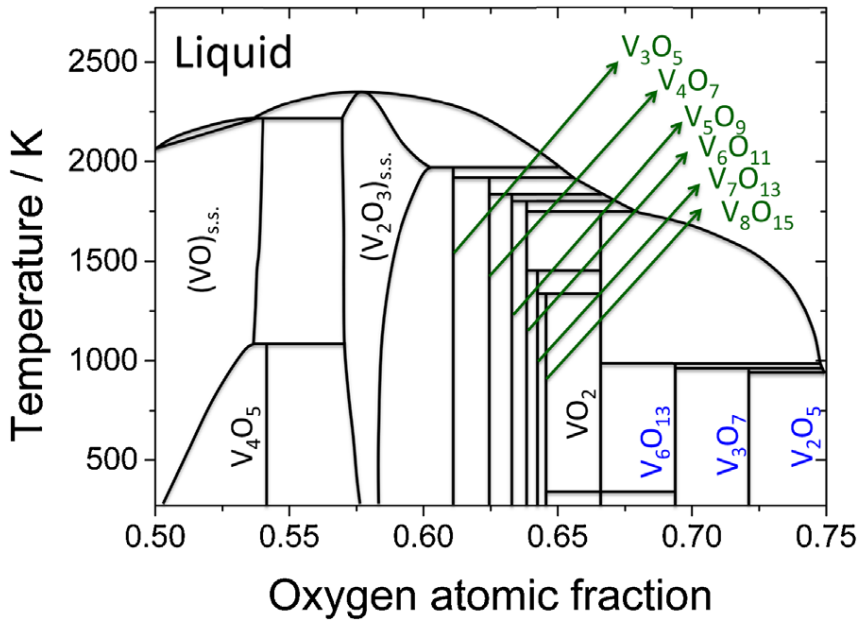

***Figure 2.1**: The Vanadium-Oxygen phase diagram [96].*

The MIT in VO_2 is accompanied by dramatic alteration in the crystallographic structure, and opto-electrical properties of the material [19-23]. Below the critical temperature (T_c), VO_2 is in semi conducting monoclinic phase state, and above T_c, VO_2 is in metallic state with rutile phase [17-24]. When it is in the monoclinic phase, the vanadium atoms pair up and open an energy band gap of 0.7 eV, giving rise to high infrared (IR) transmission [70, 97]. Whereas, when it is in the rutile phase, the existing band gap between the Fermi level and the vanadium 3d band vanishes, making the material highly reflecting in the near infrared (NIR) and optical regions [26, 44, 70]. This anomalous behavior of modulating the NIR transparency makes VO_2 a material of choice for a range of technological applications such as coating material for smart windows [14, 33, 35], thermal sensors [12, 24, 26], optical switches [19, 25, 26], etc.

2.1.1 Crystallographic Structure of VO_2

Extensive experimental studies about the crystal structure of VO_2 were made by Anderson [105], and later by McWhan et al. [106]. However, the first qualitative explanation of the

crystallographic structure of VO_2 based on the MIT was given by Goodenough [107]. In his explanation about the crystal structure of VO_2, Goodenough was using the crystal field together with the molecular orbital theory and the result was in good agreement with experiments [108].

VO_2 undergoes a first order type phase transition at a temperature of about 68 ^{0}C [17-19], that occur as a result of competing interactions between atomic structure, charge and lattice degrees of freedom [7, 99]. This phase transition in VO_2 is reversible in ultrafast time scale from an insulating low temperature state to a high temperature metallic state [23, 95, 109]. In the metallic state VO_2 exists only in one type of structure which is the rutile phase (R) [95, 107], but in the insulating state, it exists in two distinct monoclinic structures known as the M_1 and M_2 phases [95, 110]. In addition to the two phases, there is also an apparent and rarely observed triclinic insulating phase (T) [110, 111]. The rutile phase (R) and the M_1 phase are stable during the transition of bulk VO_2, while the M_2 phase is not stable in general but can be stabilized by applying external driving forces such as changing temperature, imposing an electric field or introducing dopants [110].

2.1.1.1 Rutile structure of VO_2

Above the MIT temperature, VO_2 is metallic and can be characterized by a tetragonal rutile-type structure, with lattice constants a=b ~ 0.455 nm and c ~ 0.285 nm and space group $P4_2/mnm$ [106, 107, 110]. The vanadium atoms are located at positions (2a): (0,0,0), (1/2,1/2,1/2) and the oxygen atoms are located at positions (4f): ±(u,u,0), ±(1/2+u, 1/2-u,1/2) [106, 110]. In this rutile structure, six oxygen atoms are surrounding each vanadium atom keeping the vanadium atom at the center of the octahedral structure. The rutile structure of VO_2 is shown in Figure 2.2 below.

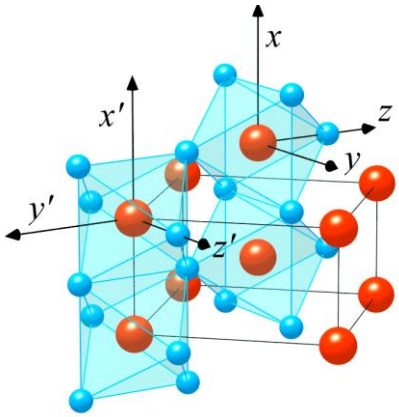

***Figure 2.2**: Schematic diagram for lattice structure of VO_2 in its rutile state. Bigger (red) spheres stands for Vanadium (V) atoms and small (blue) spheres denote oxygen (O) atoms [110].*

2.1.1.2 Monoclinic M_1 structure of VO_2

Below the MIT temperature, VO_2 exhibits a monoclinic M_1 structure and it is semiconducting and IR transparent, with lattice constants a ~ 0.575 nm, b ~ 0.4526 nm and c ~ 0.5383 nm, and space group $P2_1/c$ [105,106,110]. Both the metal atoms and the two different types of oxygen atoms occupy the general position (4e): ±(x, y, z), ±(x, 1/2-y, 1/2 +z) [107, 110]. In this semiconducting monoclinic crystal structure, the vanadium atoms can possess alternate V–V distances of ~0.2619 and ~0.312 nm [105, 107, 110]. The monoclinic M_1 structure of VO_2 (M_1) is shown in Figure 2.3, below.

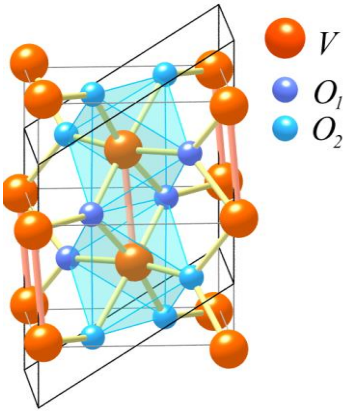

***Figure 2.3**: Schematic of lattice structure of VO_2 in its monoclinic M_1 state [110].*

2.1.1.3 Monoclinic M_2 structure of VO_2

The monoclinic M_2 structure is intermediate between the rutile and M_1 phases with lattice constants a ~ 1.209 nm, b ~ 0.3702 nm and c ~ 0.6433 nm [105, 110]. The M_2 phase consists of one set of straight vanadium chains, where half of the vanadium atoms form a zig-zag structure, and another half forms equally spaced vanadium atoms chains [110]. This phase is different from monoclinic M_1 since VO_2 crystallizes in a centered monoclinic lattice space group C_2/m in this phase [105, 110]. Two different types of metal atoms and three types of oxygen atoms are present in this structure which could occupy subsets on the general position: ±(x,y,z), ±(x,-y,z), (1/2,1/2,0)±(x,y,z), and (1/2,1/2,0)±(x,-y,z) [107, 110]. In M_2 phase, there is distortion of the basal plane of the original rutile cell and hence the new primitive translation is different from that of the M_1 phase [105, 110]. The monoclinic M_2 structure is shown in Figure 2.4, below.

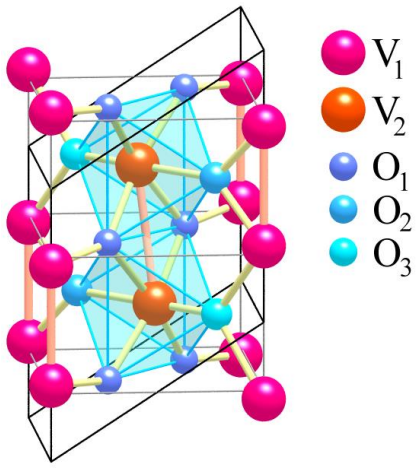

***Figure 2.4**: Schematic diagram for lattice structure of VO_2 in its monoclinic M_2 state [110].*

2.1.2 Band structure of VO_2

The successful theoretical description of metals, insulators, and the metal-insulator transitions is the classical band theory which stands on the assumption of non-interacting

electrons [7, 98]. In classical band theory, materials are classified in to metals and insulators based on the electronic bands at zero temperature, such that the highest energy band is completely filled for insulators and partially filled for metals [98]. This theory suggests that the periodic lattice structures of atoms in crystals are responsible for the formation of band structure [98].

In transition metal oxides, however, electrons occupy narrow orbitals and this spatial confinement enhances the Coulomb interaction between the electrons [98, 111-113]. This Coulombic interaction makes the electrons strongly interacting and, thus, the free-electron model fails to explain the electrical behaviour of such materials [101, 111, 112]. Even though these transition metals have partially filled d-orbitals, due to the electron-electron interaction, they exhibit insulating behaviour and the electron correlation effect gives rise to Mott (or Mott-Hubbard) transition [2, 98, 102, 114].

The MIT phenomena can also originate from electron-phonon interactions which arise from changes in the material structure and induce lattice deformation [97, 107, 115, 116]. Consequently, the band structure of the material changes since the periodic crystal structure is altered by the resulting deformation [107, 115, 116].

Another phenomenon which causes MIT is the Anderson localization, which arises due to disorder [112, 117, 118]. Anderson transition is commonly observed in materials with strong impurity scattering and strongly disordered materials and this disorder can cause localized and delocalized states in the bands [118].

In order to understand the MIT phenomenon of VO_2 and be able to develop theoretical description of metallic as well as insulating phases of VO_2, the electronic states close to the Fermi level is important [98]. The VO_2 band structure near the Fermi energy, and hence the

MIT phenomenon can be described by applying crystal field and molecular orbital theory as it was proposed by Goodenough [107]. Consequently, the VO_2 band structure result from the hybridization of the *3d* V levels and the *2p* O levels, whereby the *2p* oxygen levels are found sufficiently below the vanadium *3d* states based on electrostatic considerations [110].

The 3*d* vanadium band splits into $d_{||}$ and π^* sub-bands (Figure 2.5). The hybridization of the vanadium π^* band and the oxygen 2*p* band causes the π^* band to be shifted upwards, whereas the weak hybridization between the vanadium $d_{||}$ band and the oxygen 2*p* band keeps $d_{||}$ at the bottom state of all Vanadium 3*d* bands [107, 108, 110]. Thus, the crystal structure becomes metallic, whose structure is tetragonal with space group $P4_2/mnm$, and the metallic behavior is caused by the partially filled $d_{||}$ and π^* band. The space between oxygen 2*p* and the Fermi level E_F is the band gap corresponding to higher energy optical gap [107, 108, 110].

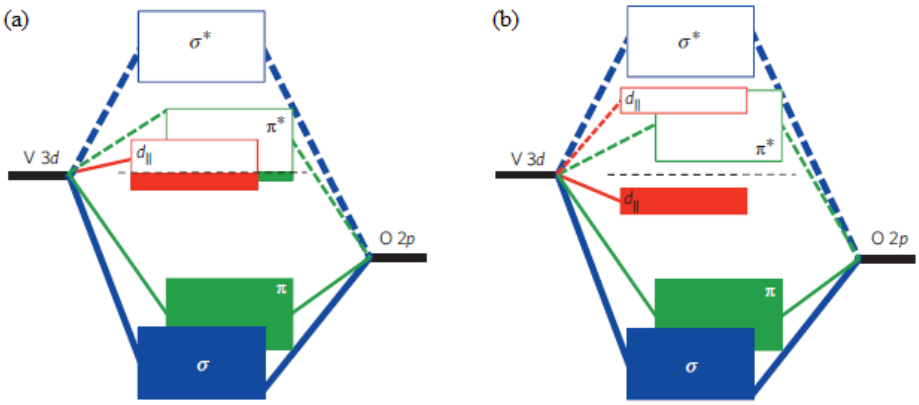

***Figure 2.5**: Energy band diagram of VO_2 in its (a) metallic (rutile) and (b) insulating (monoclinic) states [119].*

For the semiconducting state of VO_2, V atoms twist in a zig-zag pattern along the vertical-axis, resulting in distortion of the tetragonal lattice into a monoclinic lattice structure with space group $P2_1/c$ [110]. The $d_{||}$ band splits into two sub-bands, the upper $d_{||}$ band and the

lower $d_{||}$ band. The lower $d_{||}$ band is completely filled leaving the π^* band completely empty [107-110, 119, 120].

Figure 2.6 (a-e), below, clearly shows the metallic phase of the V^{4+} ion with one *3d* electron per atom placed at the center and forming the octahedral structure. VO_2 being a $3d^1$ system the *d* orbitals which comes from the metal vanadium forms relatively narrow bands. The next higher *4s* band is noticeably broader and overlaps with the entire *d* band, resulting in an occupied *4s* band [107-110]. On the other hand, the *2p* orbitals, which originate from the oxygen anion, are filled and form the valence band of the material [107-110]. Under the crystal field influence, the degenerated $3d^1$ atomic orbital of V split in to two higher energy e_g orbitals and three lower energy t_{2g} orbitals [16, 107, 110]. The e_g states, formed from the $d_{3z}{}^2-_r{}^2$ and d_{xy} orbitals, are directed towards the O ligands and are strongly hybridized with the O *2p* orbitals. In contrast, the t_{2g} states are built from the $d_x{}^2-_y{}^2$, d_{xz}, and d_{yz} orbitals. The $d_x{}^2-_y{}^2$ orbitals point along the rutile *c* axes, and, the d_{xz} and d_{yz} orbitals are directed towards the faces [108, 110].

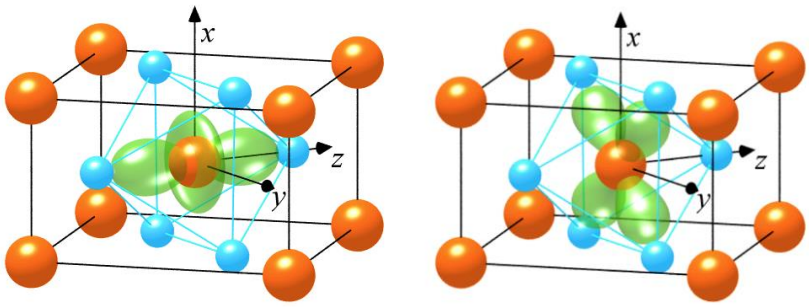

(a) $d_{3z}{}^2-_r{}^2$ (b) d_{xy}

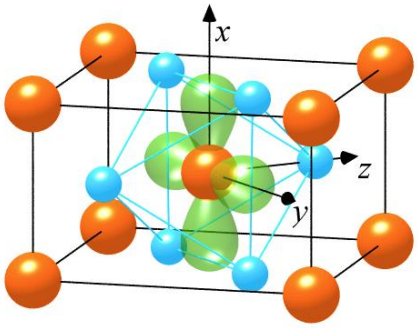

c. $d_{x^2-y^2}$

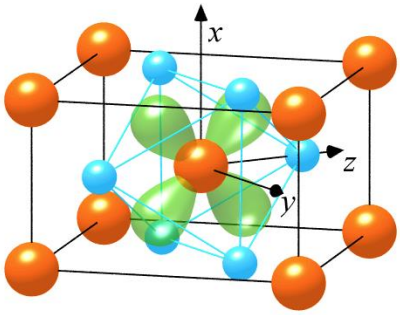

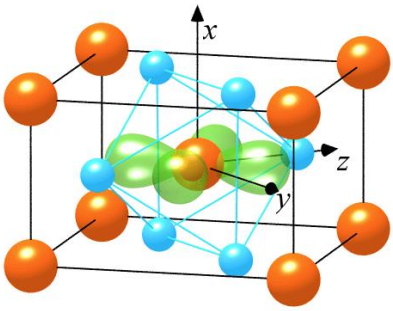

d) d_{xz} e) d_{yz}

***Figure 2.6**: The Vanadium e_g and t_{2g} orbitals (a) $d_{3z^2-r^2}$ (b) d_{xy} (c) $d_{x^2-y^2}$ (d) d_{xz} (e) d_{yz} [110].*

2.1.3 Electrical Properties of VO_2

The abrupt MIT of VO_2 from semiconductor to metal state at about 68^0C up on heating is followed by structural change [100, 121, 122]. VO_2 exhibits the rutile metallic structure above the transition temperature, and it is monoclinic below the transition temperature [19, 44, 70]. The monoclinic state which is semiconducting exhibits a band gap of ~0.7 eV [18, 123, 124]. As a result, VO_2 exhibit completely different electronic and transport properties in the two phases [116]. When VO_2 is in its metallic state, its electrical resistivity varies between 2×10^{-4} - 5×10^{-4} Ω cm^3 and, when it is in the semiconducting state it exhibits an

abrupt increment in its resistivity [122, 124]. In general, the phase transition result in remarkable changes in electrical properties between monoclinic phase at low temperature which is IR transparent and the tetragonal phase at high temperature which is opaque [37, 70, 124]. However, lowering of the phase transition close to room temperature is important to bring about significant changes in the electrical properties. Hence many different methods, such as dopant addition [83-87] and control by strain [53] have been experimentally tested to lower the transition temperature as close as possible to room temperature which in turn brings about the electrical property changes in VO_2.

2.1.4 Optical Properties of VO_2

Vanadium dioxide exhibit interesting optical properties which vary with change in temperature usually related to structural phase change on passing through the transition temperature [3, 12, 23, 121]. The phase change brings about variability in the optical properties (reflectance, transmittance, and absorbance) of the material [3, 43]. For large spectral values, VO_2 is transparent in the semiconducting state and highly reflective in the metallic state [44, 54, 70]. The cause for this change in optical properties of VO_2 is due to the fact that the carrier density increased by 3-4 orders of magnitudes across the MIT, which also accounts for the large resistivity change [17, 78, 124]. At the insulating state, VO_2 has a carrier density on the order of 10^{18} to 10^{19} cm^{-3}, while it increases to $\sim 10^{22}$ cm^{-3} after transition [78, 123]. The charge carriers, thus, play a significant role in determining the optical conductivity of VO_2 [78]. Increased carriers will intensify the scattering and absorption of photons, which results in reduction in transmittance.

2.2 Applications of VO_2

The fact that VO_2 is a thermochromic material and its phase transition takes place nearly close to room temperature made it a material of choice [19, 29, 53]. As a result of external driving forces such as electric field [78, 79], strain control [53, 102], or doping [83-87], the physical properties of VO_2 can change significantly. As a result, VO_2 exhibits unusual properties in its electrical and optical performances which can be exploited for applications in diverse areas of technology [53, 70, 121]. Consequently, optical properties such as transmittance and reflectance can be different at different temperature specifically in the infrared region [12, 17, 18]. These remarkable properties brings thermochromic VO_2 to the front line in the manufacturing of future technological devices such as smart coatings [35-37], designing terahertz (THz) optical devices [125], simple electronic switches and memories [126], holographic storage systems [127], Li-ion batteries [128,129], thermal switching [44-46], metamaterials and meta-surfaces [130-134], and thermal sensors [12, 24, 26].

One promising application of VO_2 that has been studied extensively is in thermochromic smart windows [35-37]. A thermochromic window is a type of smart material whose response to Sun's radiation varies with temperature [37, 135]. The solar radiation intake of a room can be perfectly controlled by the use of thermochromic windows, resulting in lower energy consumption than with traditional windows [33-37]. It is clearly known that optical transmittance properties changes as the material undergoes a transition from insulator to metal state [37, 54, 70]. When the room temperature is low, the MIT coating on the window glass will allow more light to pass through so that the warmness in the building is maintained [136, 137]. The situation will be reversed when the MIT coating on window glass starts reflecting most of the incoming light and keeps the inside of the building cooler [136,

137]. When VO_2 changes to a metallic state at high temperature, almost all of the longer wavelengths infrared-region (IR) light is reflected [37, 54, 70]. On the other hand, transmittance of shorter wavelength light at a metallic state remains the same through the transition [37, 54, 70]. This is the special property of thermochromic windows which allows sufficient light pass through while selectively blocking infrared radiation - induced heat at higher temperatures. Figure 2.7, below, shows the schematics.

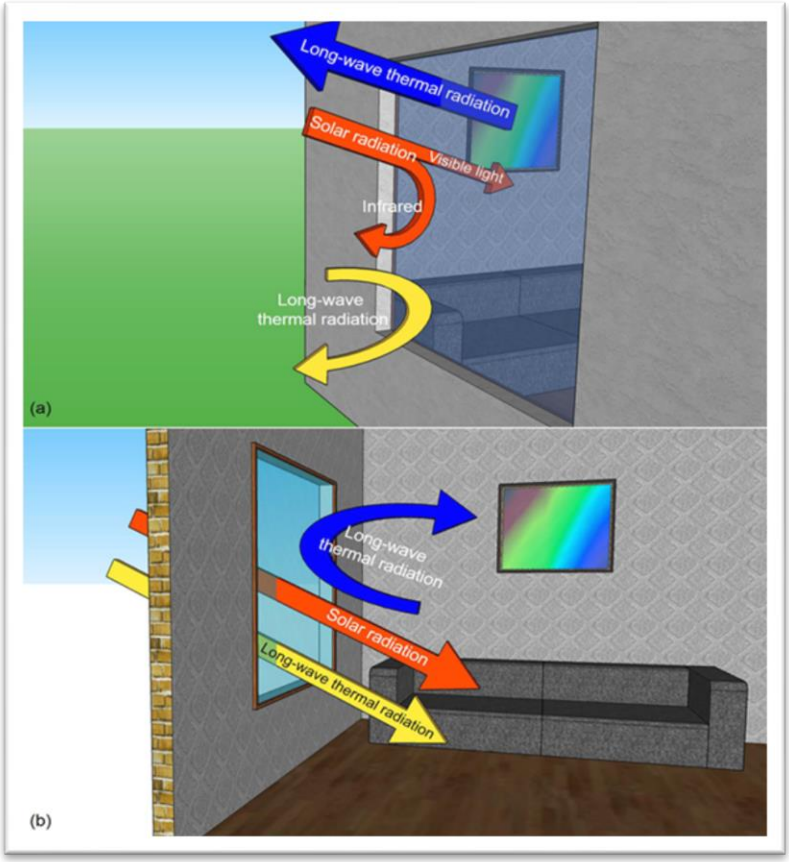

***Figure 2.7**: Schematic diagram of thermochromic window during (a) summer and (b) winter seasons [138]*

In recent times, synthesizing high purity VO_2 nanopowders with sufficient amount is highly demanded to prepare VO_2-based thin films [14]. Due to the increasing interest to use VO_2 for smart window coating application, various experimental studies have been conducted so far. For example: Li et al. [14] synthesized thermochromic VO_2 nanoparticles via

hydrothermal technique that have potential smart coating application. Xiao et al. [35] prepared a highly crystalline VO_2 powder by spray pyrolysis method which exhibit superior phase transition properties. Huang et al. [37] was able to produce nanostructured VO_2 thin film which exhibit low temperature phase transition at about 45^0C using direct magnetron sputtering method with potential application in smart window coating. Zhong et al. [57] employed the hydrothermal technique and succeeded in synthesizing star shaped VO_2 nanoparticles exhibiting improved thermochromic performance.

To date, application of VO_2 in Li-ion batteries has attracted researchers' attention due to the explosive and swelling limitations of the existing Li-ion batteries, especially those used for cell-phones, laptop etc [128]. To alleviate these types of problems, now a day, material with MIT property can be used. An MIT-material based battery can prevent overheating and explosion since the device will turn from an insulator into a metal state upon excessive heating, and this conductive metallic phase will allow the excessively stored charges inside the battery to be discharged before explosion takes place [128, 129]. Liu et al. [128] successfully synthesized VO_2 (B) nanorods prepared by the hydrothermal route and reported that VO_2 is a promising candidate for efficient Li-ion batteries. Shi et al. [129] synthesized VO_2/graphene composite hydrothermally which exhibits excellent cycling performance compared to the pure VO_2.

A new type of application area of VO_2 is passive smart radiation device (SRD) which can be used for thermal control material for spacecraft [38-40]. Compared to electronic switching or thermochromics, its application as SRD has been less investigated [39]. Thermal control of spacecraft is an issue of controlling the thermal properties of the exterior and interior subsystems of spacecrafts [31, 39, 40]. To protect electronic systems of the spacecraft from the influences of the external environment, low-cost passive thermal control systems, which balance the amounts of energy radiated and absorbed [38-40] are required. High emittance

materials are used to radiate excess heat energy into space and cool the spacecraft [39,40]. In this regard, SRDs are inevitable materials for thermal control of the internal temperature of the spacecraft [39, 40]. Thermochromic VO_2 is a suitable material for such thermal regulation application [38-40]. For instance, Benkahoul et al. [38] were able to synthesize VO_2 thin films for SRD applications on various substrates using sputtering deposition technique. Hendaoui et al. [40] deposited thermochromic VO_2 thin films for similar applications using reactive pulsed laser deposition on Al substrates.

Increasing environmental pollution and industrialization issues, globally, demanded the synthesis of various materials for gas sensing applications [139-141]. Because of their low cost and high compatibility issue, nano-scaled metal oxides have been investigated extensively as potential candidates for gas sensing applications [139, 141]. For instance, Simo et al. [140] successfully reported the synthesis of metal oxide VO_2 nanobelts using hydrothermal assisted sol-gel process useful for developing high performance H_2 gas sensors.

CHAPTER THREE

DIFFERENT TECHNIQUES AND PROCESSES OF SYNTHESIS OF VO_2

3.1 Synthesis Techniques of VO_2

Over the past few years, enormous attention has been given for the synthesis of diverse nature of nanomaterials in view of their fantastic physic-chemical properties and potential technological applications [72, 142, 143]. To date, multifunctional transition metal oxides nanomaterials of varied dimensionality have been prepared through different techniques [142]. Vanadium dioxide being one of the many transition metal oxides, its temperature dependent phase transition which is responsible for changes in its electrical and optical properties makes it interesting material [17-23].

Since single crystals structures of vanadium dioxides are unfavourable for most application purposes, synthesis of the material in the form of thin films or nanoparticles is crucial [31]. However, preparing stoichiometric VO_2 thin films and nanoparticles are challenging due to the narrow stability range of the VO_2 phase state [144]. Hence, overcoming the challenges and producing VO_2 nanomaterials of controlled size and shape are important for the understanding of their structural, electrical, and optical properties and for possible application of its phase transition phenomena. So far, many types of physical as well as chemical methods have been developed to synthesize VO_2 thin films and nanoparticles. These includes, sputtering [38, 39, 43], ion implantation [51, 52], spray pyrolysis [29, 145], pyrolysis [21-23, 35], chemical vapor deposition (CVD) [31, 45-47], pulsed laser deposition (PLD)[12, 48-50], sol-gel [33, 56, 146] and hydrothermal [14, 83-89] methods.

In these methods, thin films and nanoparticles of VO_2 with various thermochromic properties have been synthesized.

Therefore, in this section, the various synthesis methods of VO_2 thin films and nanoparticles and some of the standard characterization techniques are discussed. Synthesis methods like chemical vapour deposition (CVD), pulsed laser deposition (PLD), sputtering, sol-gel, solution combustion, hydrothermal techniques are briefly discussed. In the end, a new approach, the green process which has been proved to be efficient and environmentally friendly for the successful synthesis of metal and metal oxide nanoparticles is presented.

3.1.1 Chemical Vapour Deposition

Chemical vapour deposition (CVD) is an ideal synthesis method for large scale production of high quality thin films [45-47, 74]. Due to high deposition rates possibilities, CVD is a valuable technique [45-47]. Varying synthesis parameters such as pressure, temperature, precursors amount and flow rates, control over morphology of the nanostructure and high degree of crystalinity can be achieved [45, 74]. CVD technique has been utilized for the first time to deposit thin films of VO_2, and this method still remains to be one of the most appropriate synthesis techniques even after fifty years [74]. To prepare thin films by CVD technique, the substrate should be exposed to a suitable precursor of volatile nature which decompose on the substrate surface or react with it and produce the desired thin film [74]. CVD technique gains advantages as it has the ability to produce pure, denser materials and uniformly distributed films with better adhesion, and the deposition takes place at relatively low temperatures, and the result is reproducible [45].

Vernardou et al. [45] were able to deposit thin films of vanadium oxide of different oxidation states at a temperature of 450 ^{0}C using an atmospheric pressure chemical vapour

deposition technique (APCVD), and achieved improved electrochemical performance films. Maruyama and Ikuta [46] synthesized vanadium dioxide thin films by an APCVD method, and they observed that thin films of about 300 nm thickness demonstrated a minimum value of 44 ^{o}C transition temperature, indicating the strong dependence of optical and electrical switching behaviours on film thickness.

3.1.2 Sol-gel

Sol-gel technology was developed a couple of decades ago as an alternative technique for the synthesis of glasses and ceramics at relatively low temperature [146,147]. The sol-gel technique is based on hydrolysis of liquid precursors such as metal salts or metal alkoxides and formation of colloidal Sols [74, 82, 146]. The resulting sol is supposed to undergo through a series of steps, these are gelling, drying, pressing, and casting which results in various structural and phase transformations [146, 147]. This allows the formation of fibers, powders, coating etc from the same precursor solution [146].

The sol-gel method has so many advantages such as low cost, large surface area deposition, and the ease of metal-doping, which makes the sol-gel method to be widely employed for the synthesis of VO_2 thin films [31-34, 74]. To synthesize VO_2 thin films via sol-gel method, the precursor sol is deposited by dip-coating or spin-coating on the desired substrate [31, 74]. The required thickness of metal oxide thin film is easily achieved by the addition of extra layers. To remove the liquid phase from the gel drying process may be carried out and thus porous material can be formed. In order to obtain crystalline vanadium dioxide thin film with enhanced mechanical properties, annealing may be performed in a reducing atmosphere [74]. It is also possible to introduce dopants in the formation of thin films by the addition of adequate amount of salts or alkoxides to the precursor solution. The

fact that sol-gel method is quite simple to practice, it has been extensively used to produce undoped and doped thin films of vanadium dioxide [31, 74].

The sol-gel method being a low temperature technique, this permits the possibility of composition control over the final products [74]. Hence sol-gel method has been widely employed to synthesize doped VO_2 nanostructures with other metals, such as tungsten, molybdenum, niobium, chromium, magnesium and change its transition temperature [31]. For instance, Guzman et al. [148] prepared VO_2 thin films by spin-coating the precursor solution onto silica substrate and heat treated under a reducing atmosphere. The resulting $V0_2$ films exhibit MIT at around 67 °C and the electrical switches that have been made from such films were found to switch faster and reversibly upon applying a voltage of 50 V [148]. However, the thin film thickness plays significant influence on the optical and thermochromic properties [149]. Zhang et al. [150] synthesized thermochromic vanadium dioxide thin films of high quality that demonstrated excellent transmittance and excellent near-infrared modulation abilities. Wang et al. [52] were also able to synthesize a range of vanadium dioxide nanostructures, 0-D, 1-D and 3-D, by proper control over parameters such as aging time and annealing condition.

3.1.3 Hydrothermal

Hydrothermal synthesis is a method of nanoparticles preparation that depends on the water solubility of minerals under high temperature (around 250-300 °C) and pressure [14, 84]. A wide range of vanadium oxide nanostructures such as nanotubes, nanowires, nanorods, and nanobelts have been synthesized by hydrothermal synthesis method [142, 151]. Because of its cost-effectiveness, high production, possibility of control over the structure and morphology of the product, and environmental friendliness, this method has been widely employed to synthesize VO_2 nanoparticles [57, 83-93]. The nanoparticle synthesis is carried

out using an apparatus known as autoclave which consisting of a steel pressure vessel [84]. By adjusting simple parameters such as reaction temperature, precursor concentration, pressure, aging time, it is possible to alter the characteristics of the product particles, such as particle morphology, particle size, crystalline phase [14, 26, 142].

***Figure 3.1**: Teflon-lined autoclave (left) and Oven (right) used in this research work, at iThmba Labs.*

Hydrothermal synthesis is generally employed for synthesising a wide range of nanomaterials of different functionality [142]. As an example, Zhou et al. [54] used hydrothermal synthesis technique and successfully prepared Mg-doped VO_2 nanoparticles for utility in flexible solar modulation. Ji et al. [83] prepared high quality VO_2 powders that showed excellent optical properties. Lu et al. [84] employed a modified hydrothermal approach to synthesize high quality and high yield single crystalline $W_xV_{1-x}O_2$ nanowires with potential application in nano-optoelectronic for sensing, imaging and communications. Shi et al. [129] synthesized novel VO_2/graphene composite by an in situ hydrothermal process using V_2O_5 and graphene oxide exhibiting excellent cycling performance compared to the

pure VO_2. Zhang et al. [152] recently, employed a simple hydrothermal technique to synthesize undoped and W doped VO_2 nanopowders. Quites and Pastore [153] synthesized rod-like VO_2 nanomaterials in the B phase. Li and Liu [154] applied this technique and were able to synthesize VO_2 nanospheres that have electrochromic potential uses as electrodes for lithium-ion batteries. Zhang et al. [155] were able to synthesize nanobelts of VO_2 (A) having different absorption bands which could be used for optical switch. Guo et al [100] synthesized VO_2 (M_1) nanobelts to obtain ferromagnetic properties in vanadium oxides. Recently, Powell et al. [70] followed a direct synthesis route of VO_2 nanoparticles, and obtained highly crystalline particles exhibiting thermochromic properties of higher quality and with fully reversible phase transition at 68 °C.

3.1.4 Pulsed Laser Deposition

Pulsed laser deposition (PLD) is an excellent physical vapor deposition technique that requires a high amount of background pressure [12, 50]. PLD has been widely used for the deposition of metal oxide thin film growth such as VO_2 [48-50]. Due to the possibility of various deposition parameters control, such as substrate temperature, O_2 concentration, and pressure, PLD has become the most appropriate technique to synthesis high quality VO_2 thin films [49, 50, 156, 157]. In addition, it is a good technique for doping the VO_2 films by using either metal-doped vanadium target or dual-metal target.

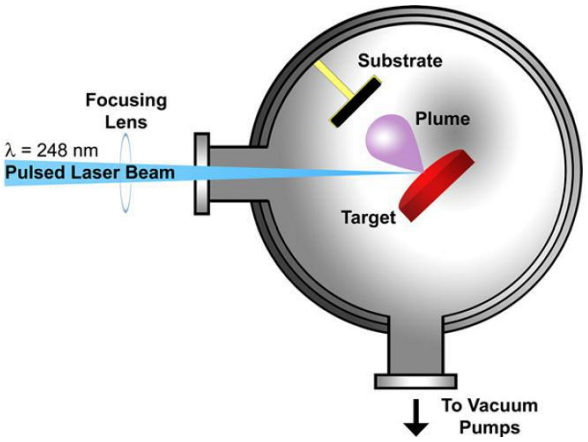

***Figure 3.2**: Schematic diagram of PLD [70]*

One of the many advantages of PLD is that the stoichiometry of the target in the deposited films is maintained properly. This is due to large ablation rate which allows all the reacting compounds of the target to evaporate simultaneously [12, 48]. For ease of management, the source of the laser is kept outside the reaction chamber. PLD is a cost-effective deposition technique and versatile, however, the limited sample size, difficulty in controlling film thickness and uniformity, are some of the side effects [49, 50].

3.1.5 Sputtering

Sputtering is the most common physical vapor deposition technique for the synthesis of vanadium dioxide thin films [36-39, 74]. Compared to other synthesis methods, the ability to produce uniform films thickness, large scale production on substrates, and efficiency in deposition are common advantages of sputtering [39, 74]. The common disadvantages of sputtering include slow growth rates, relatively poor film adhesion and the need for expensive equipment. [38, 39, 43]. Huang et al. [37] reported successfully the synthesis of VO_2 thin films possessing excellent IR properties and which ensures that the VO_2 thin films are promising nanomaterials for laser protection application. Benkahoul et al. [38] deposit

thin films of VO_2 on different substrate using RF magnetron sputtering deposition and concluded that the optical emissivity of the VO_2 deposited system strongly depend on the IR optical properties of the substrate. Miller et al. [43] employed a reactive sputter deposition of undoped VO_2 film, and achieved a transition temperature of 45^0C by restricting the particle size to approximately 30 nm. This shows that synthesizing controlled particle size plays an important role for modifying the phase transition temperature [43]. Hendaoui et al. [39] investigated the optical properties of VO_2-based smart radiation devices of different thicknesses containing SiO_2 layer.

3.1.6 Combustion Synthesis

Recently, the combustion synthesis (CS) technique is becoming an effective method to synthesize nanoscale materials [58, 158-160]. The CS technique involves a rapid heating process of solution resulting in a powder as final product and does not require an inert gas atmosphere for the synthesis process [58]. This process is cost effective, innovative, and requires short synthesis time [58, 158]. In CS techniques, relatively simple equipment is required, and desired size and shape of products are formed [158, 159]. For instance, Nagabhushana and Chandrappa [58] successfully synthesized monoclinic VO_2 via CS technique.

3.1.7 Green Process

Although the chemical and physical methods have been used widely to synthesis nanoparticles [59-62], the use of toxic and hazardous chemicals in these methods may leave harmful effect to the environment [59-61]. In recent years, thus, the use of biological methods such as plant extract is evolving as an eco-friendly alternative route [59-64]. Nanoparticles synthesized using biological methods are more stable, have diverse natures and appropriate dimensions due to the one-step synthesis procedure employed [59-61].

The biological method or the green nanoparticles syntheses procedures do not use toxic chemicals, high energy, high temperature, and high pressure [59-63]. That means; green synthesis technique can be conducted at ambient temperature, cost-effective, scalable for mass production and environmentally friendly [59-64].

The role of plant extracts during the syntheses of nanoparticles is they may function as reducing and sometimes as stabilizing agents [59, 143]. To produce nanoparticles, plant extracts will be added into the aqueous solution of the starting metal oxides precursors at ambient temperature and pressure [64]. After a couple of minutes, the reaction will be completed. However, factors that may affect the synthesis, characterization, and application of nanoparticles must be taken into consideration [61]. The commonly known factors include pH of the solution, temperature of the mixture, concentration of the extracts used, and concentration of the precursor materials [61]. This technique which has been practiced for metal nanoparticles synthesis can be adapted for synthesizing vanadium oxide nanoparticles. In Figure 3.3, below, the various syntheses techniques of nanoparticles are summarized schematically.

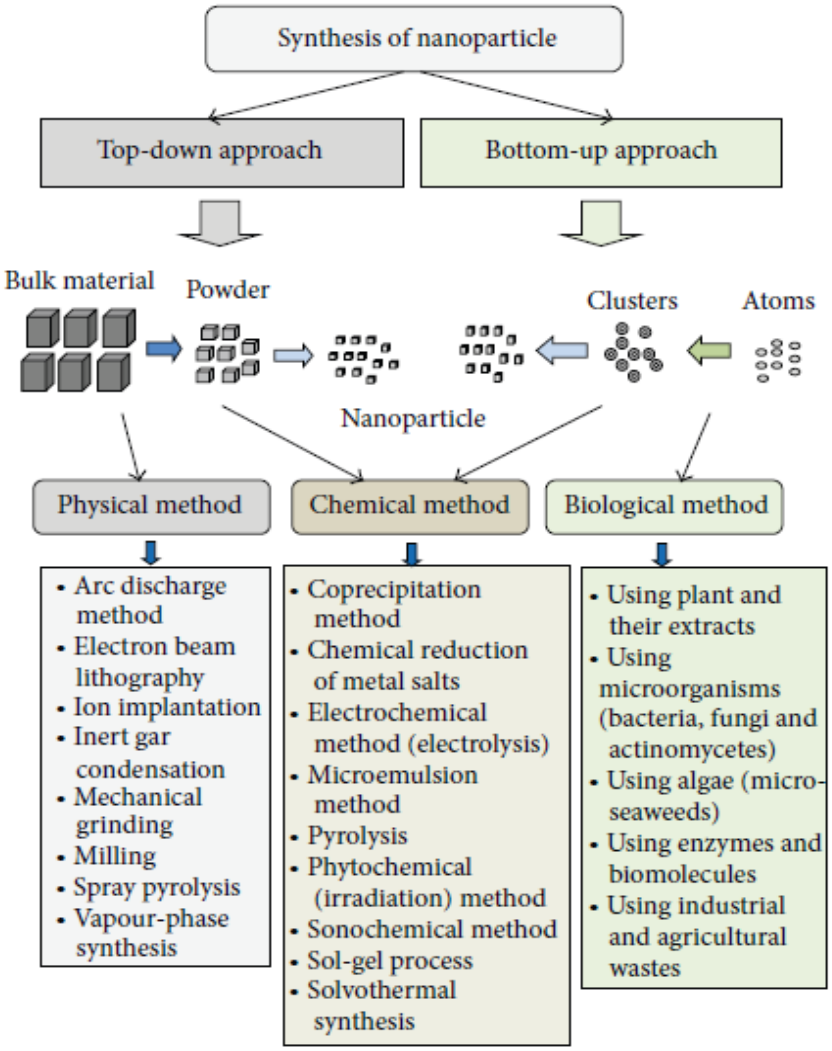

***Figure 3.3**: Schematic diagram of different nanoparticle synthesis methods [61]*

3.2 Doping Process

The introduction of impurities into a material and modifying the electrical and optical properties of the material is a commonly known technique [28-31, 74, 161]. Recently, doping vanadium dioxide crystal lattice with other members of transition elements has been observed to appreciably affect the phase transition temperature [30, 35, 161]. However, the decrease or increase in phase transition temperature can be related to the type of dopant used [30, 31, 161]. For example, when metal ions of high valences such as Co, Ni,

Mo, W and Nb, were doped by substitution into the vanadium dioxide lattice, the MIT temperature decreased significantly as low as room temperature [30, 161]. On the other hand, an increase in MIT temperature has been observed when metal ions of low valences such as Al, Ti, Ge and Cr, were doped by substitution into VO_2 lattice [30, 161].

It is obviously known that the phase transition temperature of VO_2 can be switched below or above the critical value T_c by doping certain element in to VO_2 [30, 74, 161]. For example, Futaki and Aoki [161] conducted a series of experiments on selected transition metals such as Fe, Co, Ni, W, Nb and Mo, and found that the transition temperature decreases below T_c; On the other hand, the transition temperature increases above T_c for Ti and Ge due to W doping. Marezio et al. [162] studied the change in transition phenomena by using Cr doping and showed the transition temperature of Cr-doped VO_2 decreases with increase in pressure. Mlyuka et al. [94] reported that doping of Mg on VO_2 enhances the optical transmittance while decreasing the metal-insulator transition temperature far better than that obtained by W doping. Song et al. [163] studied the effect of Ce-doped VO_2 on the phase transition property. Pergament et al. [164] made a conductivity test of W doping of VO_2 and reported the coated nanocomposite exhibited high transparency, better thermochromic performance, and extremely high strength. YaBin et al. [165] performed a study on Au doped VO_2 thin films and reported that the phase transition temperature and also the transmittance could be reduce significantly. Zhang et al. [166] carried out doping of W, Mo, Sn or Fe using hydrothermal synthesis, and they reported thermochromic properties and optical switching characters are observed in the synthesized nanostructures.

Li et al. [167] used reactive magnetron sputtering technique and prepared Mg-doped and pure VO_2 thin films on glass and carbon substrates. Their study demonstrated luminous and solar transmittances are found to be superior in Mg-doped films compared to undoped VO_2 films. Ye et al. [168] reported the successful doping of W into the VO_2 crystal lattice and the

results indicated excellent thermochromic property of tungsten-doped VO_2 nanoparticles. Dietrich et al. [169] demonstrated effective visible light transmittance of VO_2 has been enhanced by doping VO_2 with alkaline earth metals. Zhang et al. [170] carried out doping of Si on VO_2 using sputter deposition and found that 4.6 at% Si doping of VO_2 exhibited excellent terahertz modulation property.

The doping of VO_2 with alkaline earth metals such as Mg, Ca, Sr, or Ba has also been carried out and excellent switching properties were observed [169]. Dietrich et al. [169], for instance, prepared Mg, Ca, Sr, or Ba doped VO_2 thin films by sputtering, and concluded that for achieving improvement of the visible light transmittance, alkaline earth metals doping of VO_2 is an effective approach.

Shifting the phase transition temperature by doping VO_2 without substantially degrading its optical switching characteristics is not an easy task [171]. Doping of two or more ions could be used as an effective strategy to get very low thermochromic transition temperatures without degrading the optical properties of the material [31, 74, 152]. For example, Burkhardt et al. reported when two dopants W and F are simultaneously doped in to VO_2, each of the dopants are found to affect the phase transition temperature almost independently and hence the thermochromic property [172, 173]. He concluded that doping of two or more elements provides better coating properties than single element doping for applications as energy conserving smart windows [172,173].

Kong et al. [171] investigated the metal- insulator transition properties due to W and Mo co-doping of VO_2 film and found that the doping of W and Mo has demonstrated superior thermochromic property to single element doping in lowering phase transition temperature. Jiazhen et al. [174] investigated W-Mo co-doping of VO_2 thin film, and from the

transmittance hysteresis curve he concluded that co-doping lowers the transition temperature larger than when they were doped independently at the same level.

Wang et al. [175] also prepared, via sol-gel method, the simultaneous doping of Mg and W on VO_2 thin films and observed occurrence of low phase transition at 35 ^{0}C, and the two dopants have demonstrated synergetic effect. Recently, Shen et al. [75] reported synthesis of Zr-doped VO_2 and W-Zr-codoped VO_2 nanoparticles and optical properties measurements showed that with Zr doping about 60.4% enhancement of the luminous transmittance and 14.1% improvement of the solar energy modulation potentials have been detected.

3.3 Characterization techniques

Characterization of nanoparticles is one of the most important aspects in material science which are carried out by different techniques [63, 72]. Generally, size, shape, crystalline phase, structure, and porosities of nanoparticles are important parameters for characterization [63, 176, 177]. In this research, undoped VO_2 and doped-VO_2 nanoparticles were synthesized via hydrothermal technique and by the green processing. We, thus, require advanced characterization techniques for the precise control of the nanoparticles size, shape, and crystalline structure etc. to characterize these nanoparticles. Depending on the specific properties to be studied, there are different techniques available to characterize nanomaterials. These include X-ray diffraction (XRD), scanning electron microscopy (SEM), high resolution transmission electron microscopy (HRTEM), Fourier transform infrared (FTIR) spectroscopy, and differential scanning calorimetry (DSC). These techniques are widely employed for characterization of crystal structure, crystal defect, chemical analysis, phase identification, crystal or grain size etc. of the nanomaterials [176, 177]. A brief explanation of the aforementioned techniques will be made in the following sections.

3.3.1 X-ray Diffraction

X-ray diffraction (XRD) is a non-destructive technique commonly used for characterization of crystal materials and the determination of their structure. XRD provides detailed information about the crystallinity, crystallite size, and crystal orientation, phase composition and defects in crystal structure of nanomaterial [176-179].

When a beam of X-ray is incident on a crystal lattice, scattering of the rays takes place. If the scattering from different atomic planes are in phase, they interfere constructively and diffraction occurs. Each crystalline material has its own characteristic atomic structure, and diffract incident X-rays in a unique diffraction pattern which may be used as a characteristic fingerprint for its identification [180]. The working principle of XRD is based on the well-known Bragg's law ($\lambda = 2d \sin \theta$). Crystal structure analysis is based on the Joint Committee on Powder Diffraction Standards–International Center for Diffraction Data (JCPDS-ICDD) system [176, 180].

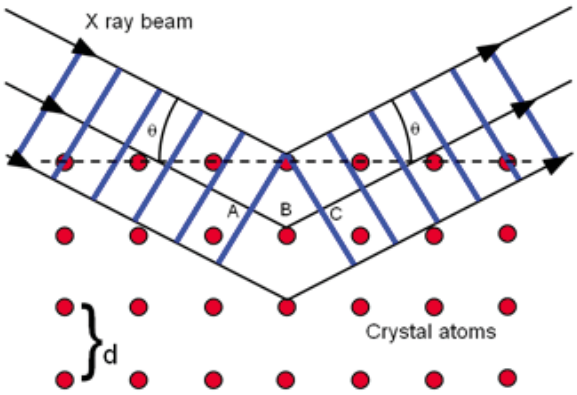

***Figure 3.4**: X-ray diffraction by atomic crystal*

The average particles size could be calculated using Scherrer formula from XRD measurement results [176, 180]:

$$a = \frac{0.9\,\lambda}{B\cos\theta},$$

where "a" is the particle size, "λ" is the X-ray wavelength, "B" is the full width of the half maxima (in radians) of the X-ray peak, and "θ" is the Bragg angle.

3.3.2 Scanning Electron Microscopy

Scanning electron microscopy (SEM) is a commonly utilized characterization technique in material science [179, 181]. High energy beam of electrons are used to scan the sample surface and results in SEM images [179-183]. For SEM analysis, the sample must be under vacuum and its surface should be electrically conductive. To avoid static charge accumulation on our sample surface, generally non-conductive solid specimens are coated with a layer of conductive material by low vacuum sputter coating or high vacuum evaporation [183]. Unique advantages of SEM includes direct examination, very large depth of focus, wide range of magnifications, minimal sample preparation, low specimen current, and sufficient resolution for most work involving direct examination of powder surface [177, 183].

When a focused beam of electrons is swept over the sample surface in a raster scan fashion, electron signals in the form of secondary, back scattered and characteristic X-rays are detected [176, 177, 181]. An image of the detected signal which contains important information about the sample's surface, composition, etc is formed on a screen by mapping the intensity of the detected signal as a function of position [176]. Using SEM much higher magnification images of a sample surface whose resolution is as good as 1-5nm can be produced [176, 179].

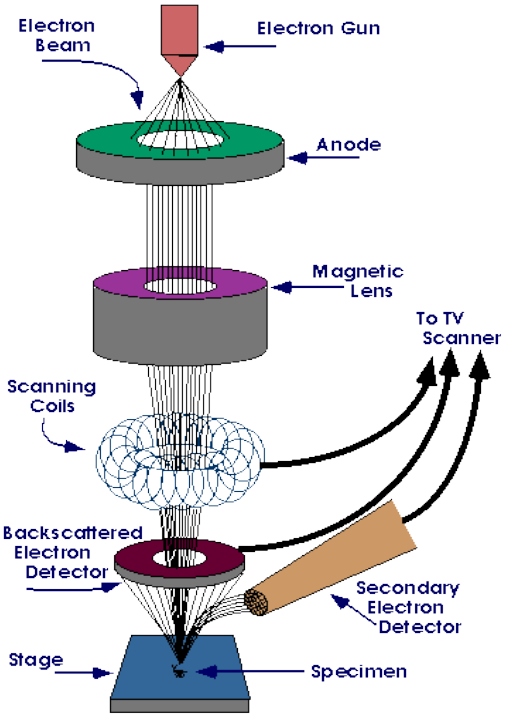

***Figure 3.5**: Schematic diagram of scanning electron microscope [183]*

3.3.3 Energy Dispersive X-ray Analysis

Energy dispersive X-ray (EDS) is a chemical analysis technique used to study types of elements found in the samples. That is EDS is used to sort the composition and distribution of various elements on the near surface of the specimen from the characteristic X-rays [176, 177, 182]. EDS is used together with SEM or TEM. A beam of electrons whose energy range lie between 10-20 KeV is used to strikes the surface of a conducting sample [182]. Upon moving the electron beam across the sample surface, the required image of each element in the sample can be obtained [176].

3.3.4 Transmission Electron Microscopy

Transmission electron microscopy (TEM) is a powerful technique which provides information on the crystal structure, particle size, size distribution and elemental composition of crystalline materials [176, 178, 179, 184]. TEM uses the interaction of energetic electrons with the sample. TEM is commonly known as amplitude or diffraction-contrast imaging technique, since only small fraction of those electrons which have passed through the sample are used to form the final image [184].

3.3.5 High Resolution Transmission Electron Microscopy

High resolution transmission electron microscopy (HRTEM) is a highly sophisticated instrument, with a number of knobs and buttons, and many adjustable parameters. HRTEM is an imaging method of the transmission microscope which allows an atomic scale imaging of the crystal structure of the sample [182, 185]. Because of its high resolution, HRTEM is an important characterization technique to study nanoscale properties of crystalline materials.

Figure 3.6: *Image of High resolution transmission electron microscope (HRTEM) at UWC used in this research.*

Both the transmitted beam of electrons and the scattered beams are used in HRTEM to create an interference image. That is, contrasted image will be formed when a directly transmitted beam interferes with one or more diffracted beams, depending on the relative phases of the various beams.

3.3.6 Fourier Transform Infrared Spectroscopy

FTIR is a commonly used non-destructive technique for finding the chemical composition of materials from their chemical bonding by the spectrum of absorption [186]. It can be used as a qualitative tool to characterize materials from the molecular vibrations of the chemical bonds in the sampling volume.

3.3.7 Differential Scanning Calorimetry

Differential Scanning Calorimetry (DSC) is a technique used to study phase transitions properties of materials as a result of heat flow. The most common type of thermal analysis report from DSC experiment is a plot of absorbed (endothermic) and released (exothermic) heat flows as a function of the temperature of the sample [179]. The possibility to use small samples (1-10 mg), and the ability to analyse solids and liquids within short period of times (10-30 minutes) are some of the commonly known advantages of DSC [179]. Moreover, the ease of sample preparation and auto analysis possibilities makes most commercial DSCs techniques preferable [179].

CHAPTER FOUR

EXPERIMENTAL AND RESULTS

Synthesis and characterization of nanomaterials such as nanorods, nanowires, nanospheres, nanobelts and nanotubes, are technologically important since they are the building block for constructing novel functional devices [72, 73, 168, 178]. There exist a number of synthesis techniques of nanomaterials (section 3.1), and their characterization techniques (section 3.3). In this regard, this research project reports the successful synthesis of un doped and doped VO_2 nanorods by hydrothermal method and synthesis of nearly spherical VO_2 nanoparticles by the green process. Characterization of the nanomaterials to analyse the various physical properties of the nanomaterials were also carried out. In the following sections the details about each experimental procedure and corresponding results are presented with discussion.

4.1 Experimental Procedures

4.1.1 Hydrothermal Synthesis of Undoped VO_2 nanoparticles

(a) Chemicals

The chemicals used in this experiment were oxalic acid ($C_2H_2O_4{\cdot}2H_2O$), vanadium pentoxide (V_2O_5), and distilled ionized water. The chemicals were standard grade and were obtained at the nano-labs from the materials research department (MRD) at iThemba Labs and used without purifying them further.

(b) Sample preparation

Synthesis of undoped VO_2 nanoparticles were carried out via hydrothermal technique as described in earlier report [171]. In detail, the synthesis procedure is as follows, 100 mL doubly ionized water was used to dissolve 3.56g of $C_2H_2O_4{\cdot}2H_2O$ under uniform magnetic stirring at room temperature. Added 2.0g of V_2O_5 to the above solution while heating at about 60 °C to obtain yellow suspension. The resulting solution turned first into green and then into dark-blue color with a pH value in the range of 2 - 3. After sufficient reaction time, the mixture was divided in to five equal parts. One fifth of the mixture was poured into a 20 mL Teflon-lined autoclave and hydrothermally treated at 240 °C for 6 hours. This procedure was repeated for 12 hours, 24 hours, and 48 hours. After cooling down the solution to room temperature, the resulting blue-black precipitate was centrifuged and washed three times with deionized water. The final precipitate was then collected and dried in oven at 80 °C and annealed at 500 °C to get the black VO_2 nanoparticles.

4.1.2 Hydrothermal Synthesis of Mg doped VO_2 nanoparticles

(a) Chemicals

The chemicals used in this experiment were oxalic acid ($C_2H_2O_4{\cdot}2H_2O$), vanadium pent oxide (V_2O_5), magnesium chloride hexahydrate ($MgCl_3.6H_2O$) and distilled ionized water. The chemicals were standard grade and were obtained at the nano-labs from the materials research department (MRD) and used without additional purification.

(b) Sample preparation

Magnesium doped VO_2 nanoparticles were synthesized hydrothermally using the method described in earlier report [171]. In detail, the synthesis procedure is as follows, 3.56g of $C_2H_2O_4{\cdot}2H_2O$ was dissolved in 100 mL doubly ionized water under slow and uniform magnetic stirring at room temperature. Added 2.0g of V_2O_5 to the above solution while

heating at about 60 °C and obtain the yellow suspension. The resulting solution turned first into green and then into dark-blue color with a pH value in the range of 2-3. After sufficient reaction, different concentrations of magnesium chloride hexahydrate ($MgCl_2$. $6H_2O$) (1.0 at% Mg, 2.0 at % Mg, 3.0 at % Mg, 4.0 at % Mg, 5.0 at % Mg) of the dopant were added into 15 mL of the above solution and the suspension was continuously magnetic stirred. One fifth of the above mixture was poured into a 20 mL Teflon-lined autoclave and hydrothermally treated at 240 °C for 6 hours. This procedure was repeated for 12 hours, 24 hours, and 48 hours for the remaining parts. After cooling the solution to room temperature, the resulting blue-black precipitate was centrifuged and washed three times with deionized water. The final precipitate was then collected and dried in oven at 80 °C and annealed at 500 °C to obtain the black Mg-doped VO_2 nanoparticles.

4.1.3 Hydrothermal synthesis of Cr-doped VO_2 nanoparticles

(a) Chemicals

The chemicals used in this experiment were oxalic acid ($C_2H_2O_4{\cdot}2H_2O$), vanadium pent oxide (V_2O_5), chromium chloride hexahydrate ($CrCl_2.6H_2O$) and distilled ionized water. All the chemicals were analytically graded and used without any further purification. The chemicals were obtained at the nano-labs from the materials research department (MRD), iThemba Labs, South Africa.

(b) Sample preparation

Hydrothermal synthesis of chromium doped VO_2 nanoparticles were carried out as described in earlier report [171]. In detail, the synthesis procedure is as follows, 3.56g of $C_2H_2O_4{\cdot}2H_2O$ was dissolved in 100 mL doubly ionized water under slow magnetic stirring at room temperature. Added 2.0g of V_2O_5 to the above solution while heating at about 60 °C

and obtain the yellow suspension. The resulting solution turned first into green and then into dark-blue color with a pH value in the range of 2-3. After sufficient reaction, different concentrations of chromium chloride hexahydrate ($CrCl_2.6H_2O$) (0.5 at% Cr, 1.0 at % Cr, 1.5 at % Cr, 2.0 at % Cr, 2.5 at % Cr) of the dopant were added into 15 mL of the above solution and the suspension was continuously magnetic stirred. One fifth of the above mixture was poured into a 20 mL Teflon-lined autoclave for hydrothermal treatment at 240 °C for 6 hours. This procedure was repeated for 12 hours, 24 hours, and 48 hours for the remaining parts. After cooling the solution to room temperature, the resulting blue-black precipitate was centrifuged and washed three times with deionized water. The final precipitate was then collected and dried in oven at 80 °C and annealed at 500 °C to obtain the black Cr-doped VO_2 nanoparticles.

4.1.4 Hydrothermal synthesis of Mo doped VO_2 nanoparticles

(a) Chemicals

The chemicals used in this experiment were oxalic acid ($C_2H_2O_4{\cdot}2H_2O$), vanadium pent oxide (V_2O_5), ammonium molybdate ($(NH_4)_6Mo_7O_{24}.4H_2O$) and distilled ionized water. The chemicals were analytically graded and used without any further purification. They were obtained at the nano-labs from the materials research department (MRD)-iThemba Labs, South Africa.

(b) Sample preparation

Hydrothermal synthesis of molybdenum doped VO_2 nanoparticles were carried out as described in earlier report [171]. In detail, the synthesis procedure is as follows, in 100 mL doubly ionized water 3.56g of $C_2H_2O_4{\cdot}2H_2O$ was dissolved under slow magnetic stirring at room temperature. Added 2.0g of V_2O_5 to the above solution while heating at about 60 °C

and obtain the yellow suspension. The resulting solution turned first into green and then into dark-blue color with a pH value in the range of 2-3. After sufficient reaction, different concentrations of ammonium molybdate (0.5 at% Mo, 1.0 at % Mo, 1.5 at % Mo, 2.0 at % Mo, 2.5 at % Mo) of the dopant were added into 15 mL of the above solution and the suspension was continuously magnetic stirred. One fifth of the above mixture was poured into a 20 mL Teflon-lined autoclave for hydrothermal treatment at 240 °C for 6 hours. This procedure was repeated for 12 hours, 24 hours, and 48 hours for the remaining parts. After cooling the solution to room temperature, the resulting blue-black precipitate was centrifuged and washed three times with deionized water. The final precipitate was then collected and oven dried at 80 °C, and annealed at 500 °C and the black Mo-doped VO_2 nanoparticles were obtained.

4.1.5 Hydrothermal synthesis of Mg/Mo Co-doped VO_2 nanoparticles

(a) Chemicals

The chemicals used in this experiment were oxalic acid ($C_2H_2O_4{\cdot}2H_2O$), vanadium pent oxide (V_2O_5), ammonium molybdate ($(NH_4)_6Mo_7O_{24}.4H_2O$), magnesium chloride hexahydrate ($MgCl_2.\ 6H_2O$) and distilled ionized water. The chemicals were standard grade and were obtained at the nano-labs from the materials research department (MRD) at iThemba labs and used without any further purification.

(b) Sample preparation

Hydrothermal synthesis of Magnesium/Molybdenum co-doped VO_2 nanoparticles were carried out as described in earlier report [171]. In a typical synthesis procedure, 100 mL of doubly ionized water was used to dissolve 3.56g of $C_2H_2O_4{\cdot}2H_2O$ under slow magnetic stirring at room temperature. Added 2.0g of V_2O_5 to the above solution while heating at

about 60 °C and obtain the yellow suspension. The resulting solution turned first into green and then into dark-blue color with a pH value in the range of 2-3. After sufficient reaction, 0.5 at % of $(NH_4)_6Mo_7O_{24}.4H_2O$ were mixed with 15 mL of 1.0 at %, 2.0 at % and 3 at % $MgCl_2$. $6H_2O$, respectively, and the resulting suspension of each mixture was continuously magnetic stirred. One fifth of the above mixture was poured into a 20 mL Teflon-lined autoclave for hydrothermal treatment at 240 °C for 6 hours. This procedure was repeated for 12 hours, 24 hours, and 48 hours for the remaining parts. After cooling down the solution to room temperature, the resulting blue-black precipitate was centrifuged and washed three times with deionized water. The final precipitate was then collected and oven dried at 80 °C, annealed at 500 °C to obtain the black Mg/Mo co-doped VO_2 nanoparticles.

4.1.6 Synthesis of VO_2 by green process

(a) Chemicals

Fresh flowers of *Callistemon viminalis* were collected from a population distributed along the road near Eresteriver, South Africa, during the flowering phase in May 2015. All other chemicals were obtained from iThemba Laboratories, MRD, South Africa.

(b) Sample preparation

Fresh flowers of *Callistemon viminalis* were dried at ambient temperature and the dried *Callistemon viminalis* flowers were added in to DI water and the suspension was filtered. On the other hand, 20 ml of doubly ionized water was used to dissolve 3.5g of V_2O_5 and mixed with a 20 mL aqueous solution of 1gm of hydrazine dihydrochloride with constant magnetic stirring until a yellow suspension solution is obtained.

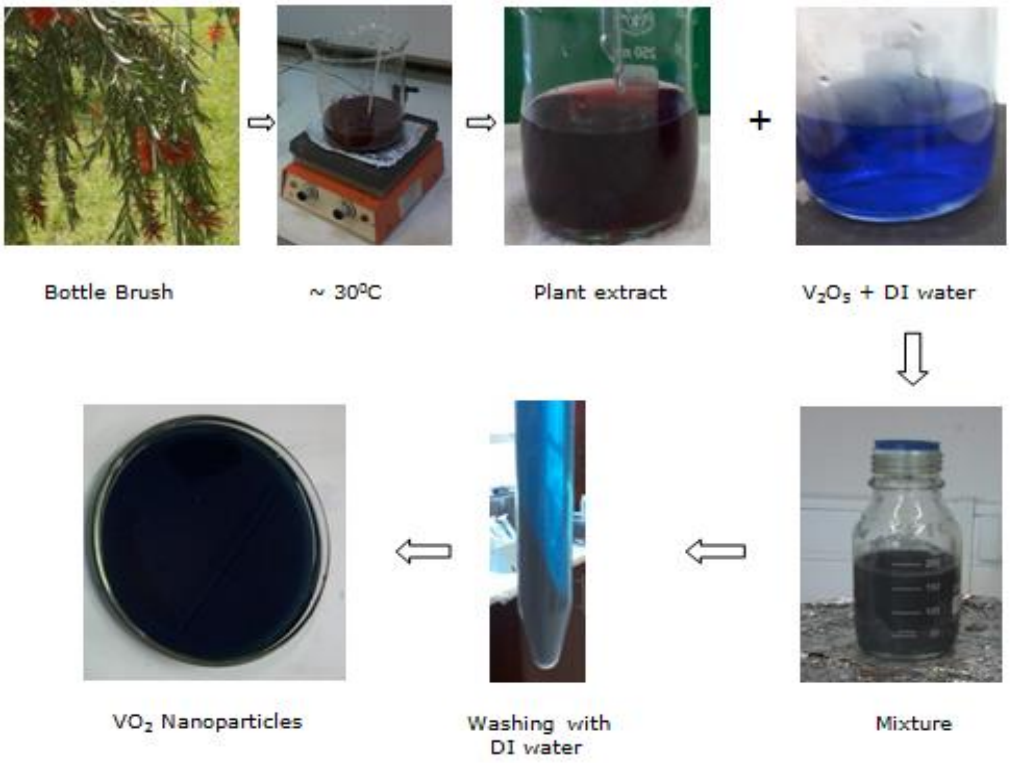

The solution turned slowly into light green and then to blue color. Adequate amount of the plant extract was then added into the above suspension with continuous and slow stirring for about 10 minutes at ambient temperature. The resulting dark blue mixture was oven-dried. Finally, the obtained black nanopowder was annealed at 450 ºC for an hour to remove biological materials and get the VO_2 nanoparticles.

4.2 Experimental Results

Undoped VO_2 (M) nanoparticles were synthesized by hydrothermal method for different treatment time and characterizations of results were carried out. Then hydrothermal synthesis of Mg-doped VO_2, Cr-doped VO_2, Mo-doped VO_2, and Mg/Mo co-doped VO_2 nanoparticles were conducted followed by characterization of results. In addition, synthesis of VO_2 (M) by the green process was carried out and results are presented. Finally, discussions of results are made in each section of the experiments.

The techniques used to characterize undoped VO_2 and doped VO_2 nanoparticles are X-ray diffraction (XRD), scanning electron microscopy (SEM), high resolution transmission electron microscopy (HRTEM), differential scanning calorimetry (DSC), and Fourier transform infrared (FTIR). All these techniques confirmed the successful synthesis of undoped and doped VO_2 nanoparticles by hydrothermal method, and green processes synthesis of pure VO_2.

The X-ray diffraction (XRD) patterns of the synthesized undoped and Mg-doped VO_2, Cr-doped VO_2, Mo-doped VO_2, and Mg/Mo co-doped VO_2 nanoparticles were observed on a Brucker D8 advance GER, x-ray diffractometer recorded in the 2-theta range 15^0–90^0 using CuKα1 radiation (wavelength = 1.5406 Å). The operating voltage of the device was 40 kV, 300 mA current. The XRD characterization was carried out at iThemba LABS, South Africa.

The Scanning Electron Microscopy (SEM) image of the synthesized undoped and Mg-doped VO_2, Cr-doped VO_2, Mo-doped VO_2, and Mg/Mo co-doped VO_2 nanoparticles were obtained using ZEISS, Oxford instruments, field emission scanning electron microscopy. No special sample preparation was required for SEM measurement. The synthesized nano powders of each sample were carefully spread over the sample holder, and were made conducting. The SEM characterizations were carried out in Physics department at University of Western Cape (UWC), South Africa.

The high resolution transmission microscopy (HRTEM) image of synthesized undoped and Mg-doped VO_2, Cr-doped VO_2, Mo-doped VO_2, and Mg/Mo co-doped VO_2 nanoparticles were recorded on a TECNAI G2-F20 at the University of the Western Cape (UWC), South Africa. For high resolution transmission electron microscopy (HRTEM), about 0.1 mg nanoparticles was dispersed in 5 mL ethanol. Then, to prepare HRTEM sample, one drop of the solution were placed on a carbon-coated copper grid and dried at ambient temperature. Elemental

composition was examined through Energy Dispersive X-Ray Spectroscopy Analysis (EDS) on the same high resolution electron microscopy unit.

FTIR spectrum of undoped and Mg-doped VO_2, Mo-doped VO_2, and Mg/Mo co-doped VO_2 nanoparticles were recorded on a Perkim Elmer Spectrum 100 spectrometer in the 4000-500 cm^{-1} range at the University of the Western Cape (UWC), South Africa. Samples were heated from 20^0C-90^0C and cooled back from 90^0C-20 ^{0}C at a rate of 5^0C/min using STA6000 temperature scan. Same equipment was employed for DSC characterization of samples.

4.2.1 Hydrothermal synthesis of undoped VO_2 (M) nanoparticles

X-Ray diffraction (XRD)

X-ray diffraction (XRD) patterns of undoped VO_2 nanoparticles are shown in Figure 4.1. Peaks of the corresponding XRD patterns are indexed to monoclinic VO_2 (M) phase (space group: P21/c) with lattice parameters of a = 5.753 Å, b = 4.526 Å, c = 5.383 Å, and β= 122.60^0 (JCPDS no. 44-0252). The XRD patterns of VO_2 (M), Figure 4.1, exhibits diffraction peaks at 26.93^0, 27.86^0, 33.38^0, 37.01^0, 39.76^0, 42.25^0, 52.84^0, 55.42^0, 57.53^0, 65.16^0, and 70.45^0 corresponding to (11-1), (011), (10-2), (200), (002), (210), (31-1), (22-2), (022), (031) and (202) patterns, respectively, with prominent peak at (011). Other phases of vanadium oxide or impurities are not detected in the spectra, and this reveal pure phase of VO_2 (M) nanoparticles structure. Experiment was conducted for various hydrothermal reaction times (6, 12, 24, and 48 hours). From XRD pattern it is clearly seen that there is a weakening of intensity of the peaks while becoming slightly broader with increasing hydrothermal reaction time, indicating that crystalline phase formation of VO_2 (M) is decreasing with increasing reaction time.

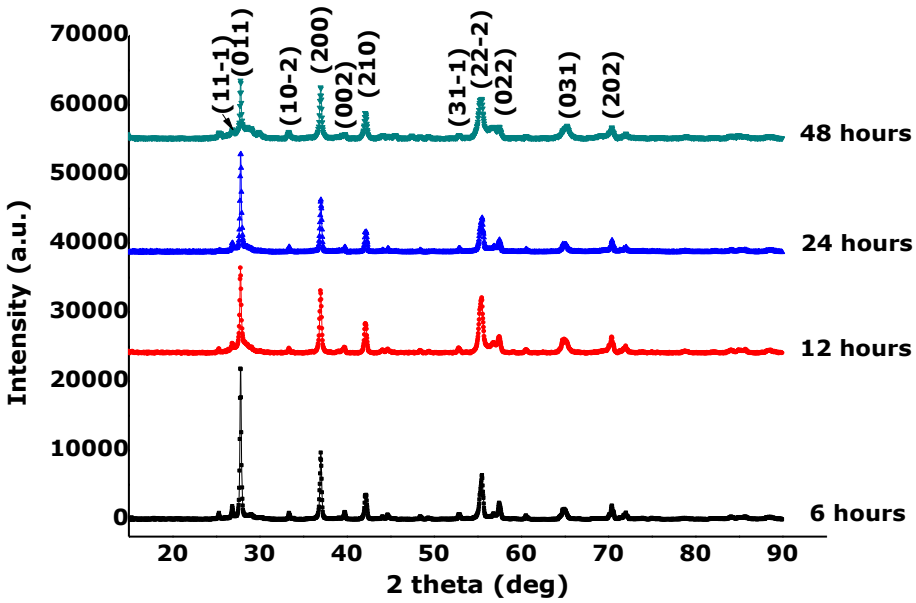

***Figure 4.1**: XRD patterns of undoped VO_2 nanoparticles for different hydrothermal treatment time.*

Scanning electron microscopy (SEM)

Scanning electron microscopy (SEM) was used to examine size and morphology of the products. Figure 4.2 shows SEM image of the synthesized nanoparticles for (a) 6 hours, (b) 24 hours and (c, d) 48 hours. The magnified SEM image shown in (Figure 4.2c), reveal nanoparticles with an average of 131.6 nm wide and 470.3 nm length.

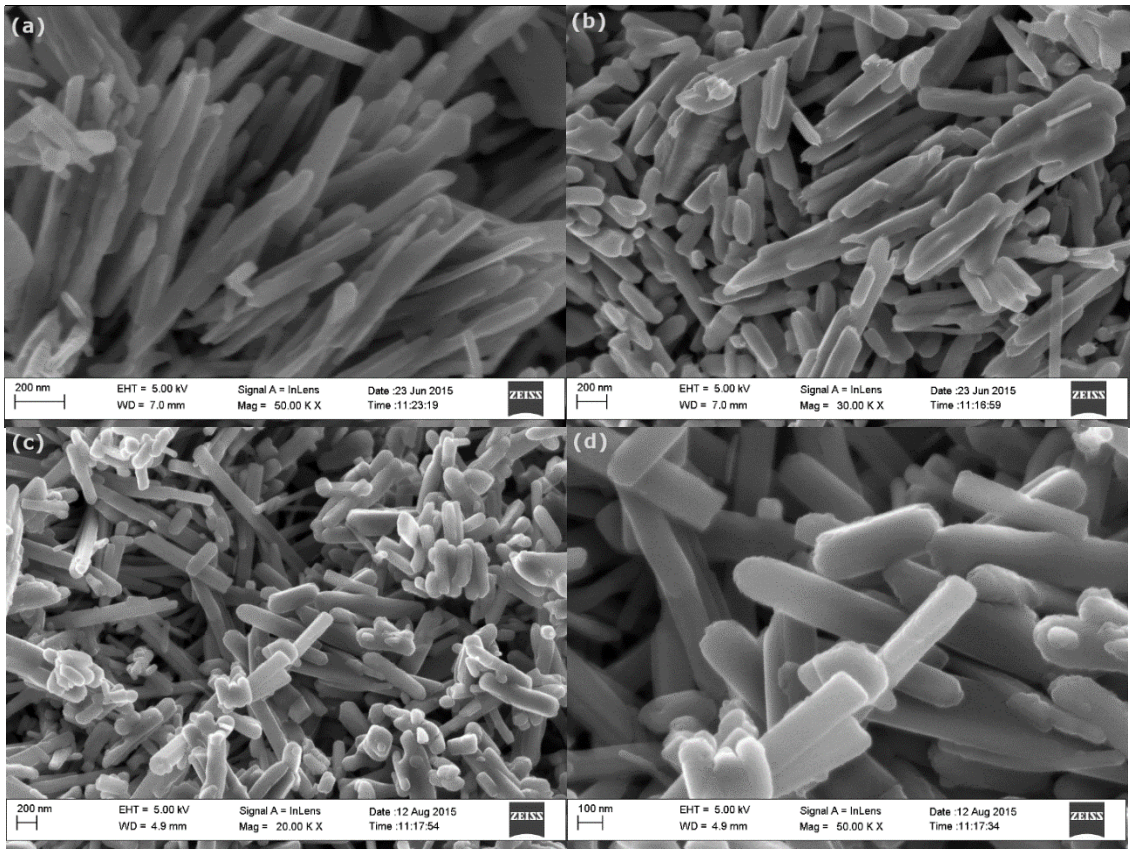

***Figure 4.2**: SEM images of undoped VO_2 microrods for (a) 6 hours (b) 24 hours (c) and (d) 48 hours hydrothermal treatment time.*

High-resolution transmission electron microscopy (HRTEM)

High resolution transmission electron microscopy (HRTEM) images of undoped VO_2 nanoparticles confirmed formation of VO_2 nanoparticles of the VO_2 (M) phase. As shown in Figures 4.3(1) (a-d), 4.3(2)(a-d), and 4.3(3) (a-d) for 6 hours, 24 hours and 48 hours, respectively, the nanoparticles exhibited crystalline structures and clear lattice fringes of VO_2 (M) phase.

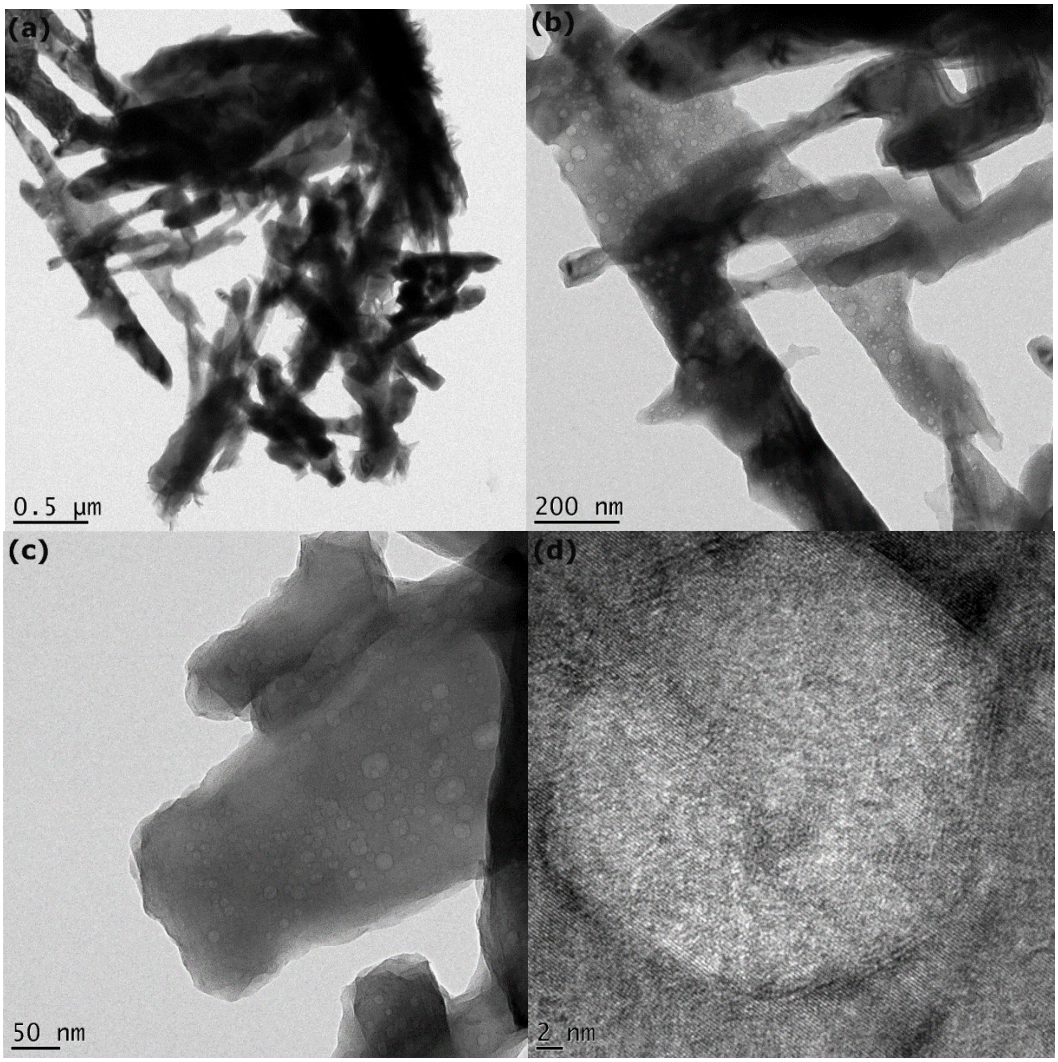

Figure 4.3(1): *HRTEM images of undoped VO_2 for 6 hours hydrothermal treatment time.*

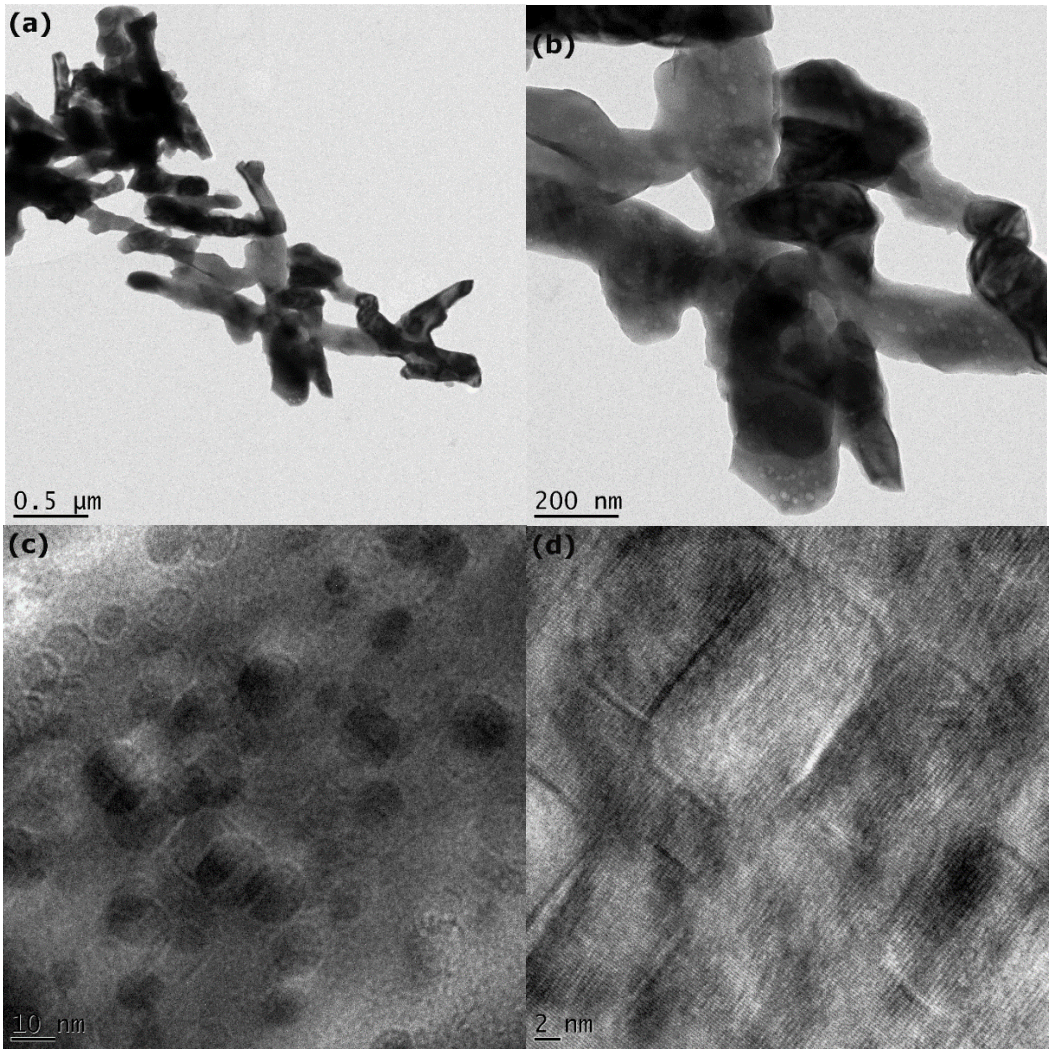

Figure 4.3(2): *HRTEM images of undoped VO_2 for 24 hours hydrothermal treatment time.*

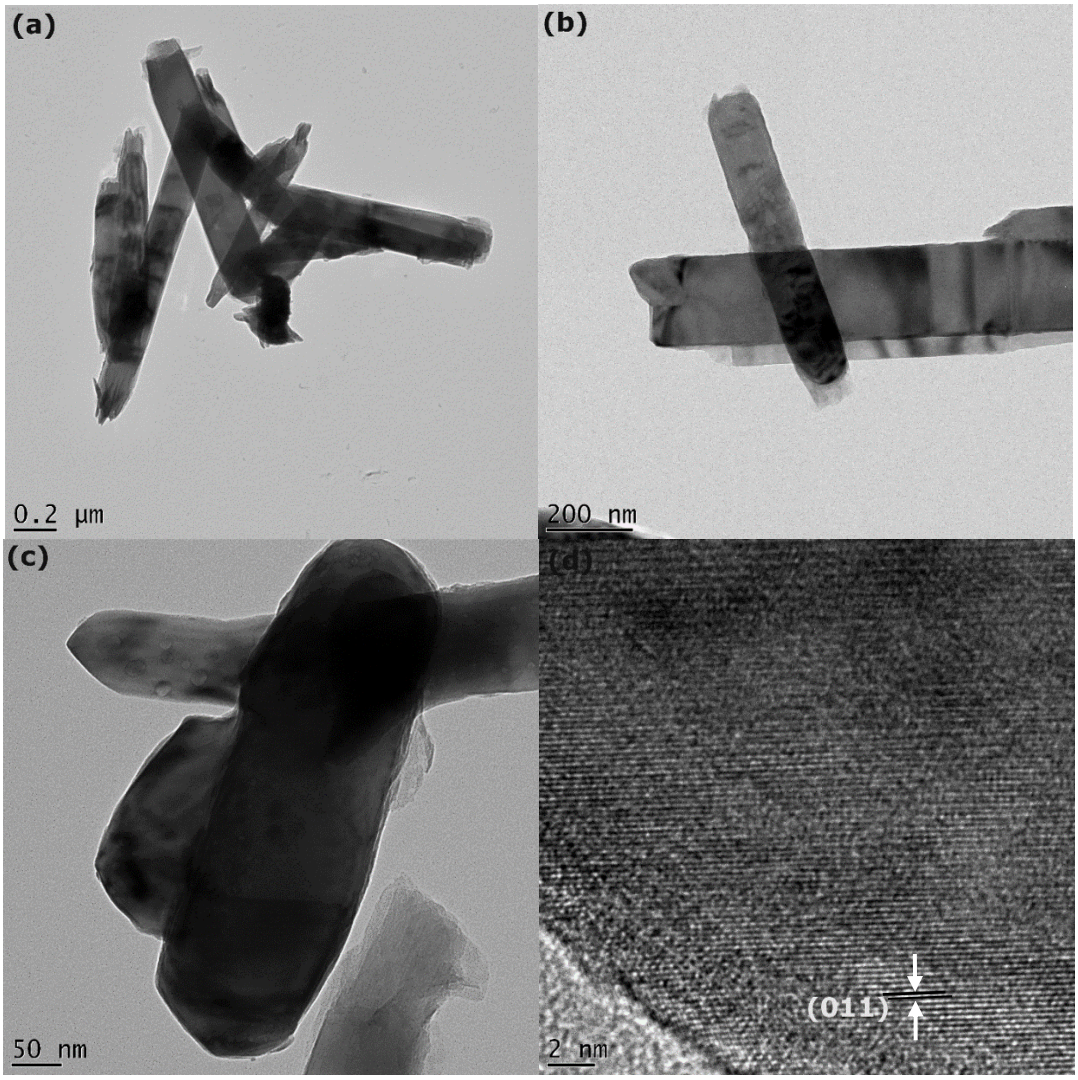

***Figure 4.3(3)**: HRTEM images of VO_2 for 48 hours hydrothermal treatment (a-e) with clear lattice fringes of VO_2 (d).*

The spacing between two successive crystal planes was calculated to be around 3.2Å, which is consistent with the spacing between two (011) crystal planes of VO_2 (M).

Figure 4.4, below, shows selected area electron diffraction (SAED) patterns of undoped VO_2 microrods and this reveal that the nanoparticles are crystalline.

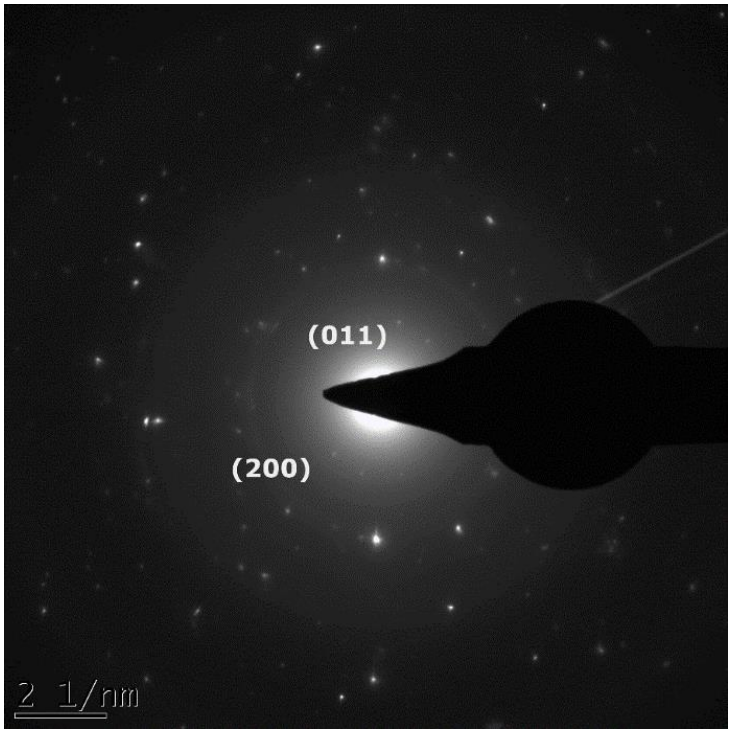

***Figure 4.4**: SAED ring patterns of VO_2 for 48 hours hydrothermal treatment time.*

Energy-dispersive X-ray spectroscopy (EDS)

Figure 4.5, below, shows EDS spectrum of undoped VO_2 nanoparticles taken on a randomly selected specimen of the nanoparticles assumed to be representative. The EDS result indicates that VO_2 (M) nanoparticles have been successfully synthesized by the hydrothermal process. The Cu peaks observed in the spectrum were from the instrument.

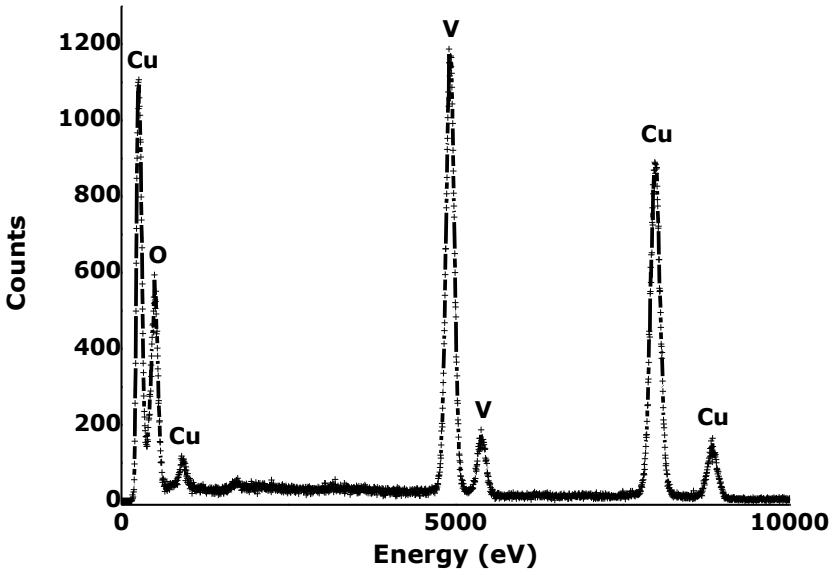

***Figure 4.5**: EDS spectrum of undoped VO_2 for 48 hours hydrothermal treatment time.*

Differential scanning calorimetry (DSC)

Differential scanning calorimetry (DSC) was used to characterize phase change temperature (T_c) properties of undoped VO_2 nanoparticles. Un-doped VO_2 sample was heated from 20°C to 90°C at a rate of 5°C/min and then cooled back to 20°C. As shown in Figure 4.6, an endothermic peak at 66°C and an exothermic peak at 52.2°C were observed. This shows the metal-insulator phase change occurs at 66°C, a lower transition than formerly reported values of 68.6 ^{0}C [75]. Furthermore, the presence of endothermic and exothermic peaks in DSC curves for the return process also confirms first-order type phase change of monoclinic VO_2 (M) [75].

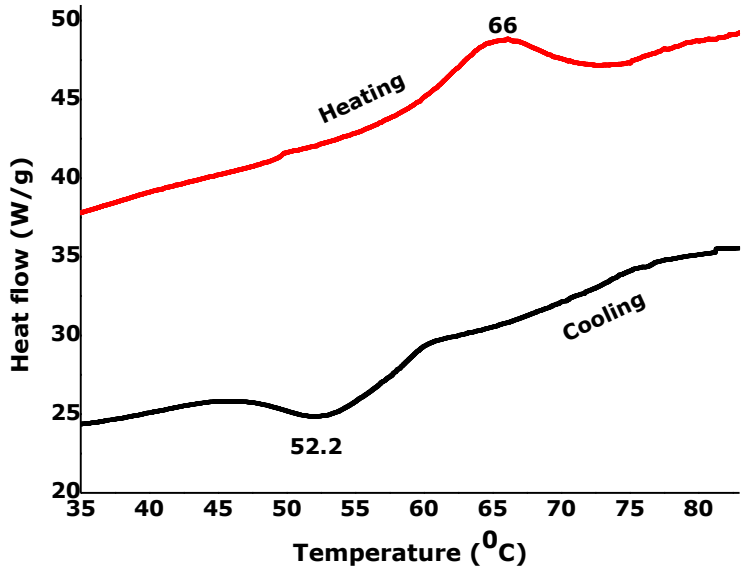

***Figure 4.6**: DSC curves of undoped VO_2 nanoparticles for 6 hours hydrothermal treatment time.*

Fourier transformed infrared spectroscopy (FTIR)

To investigate the thermochromic characteristics of hydrothermally synthesized undoped VO_2 nanoparticles, temperature dependent FTIR measurement of infrared transmittance between 500 and 4000 cm^{-1} were made. As observed from Figure 4.7, small absorption peak at 1613.3 cm^{-1} is due to the stretching and bending vibration of H_2O. The other small peak at 2027.5 cm^{-1} is due to CO_2 in the instrument [74,154]. The sharp peaks of absorption at 996.3 cm^{-1}, 593.8 cm^{-1}, 493.5 cm^{-1}, and 418.4 cm^{-1} corresponds to stretching of V=O and V–O–V coupled vibration [153,154].

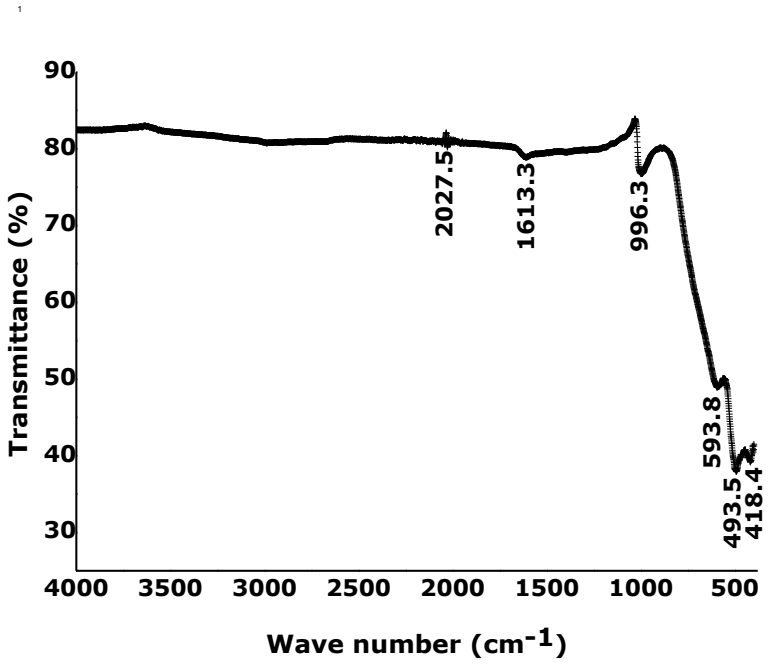

***Figure 4.7**: FTIR spectrum of undoped VO_2 nanoparticles.*

4.2.2 Mg doped VO_2

X-Ray diffraction (XRD)

X-ray diffraction (XRD) patterns of Mg doped VO_2 nanoparticles with different Mg dopant concentrations are shown in Figure 4.8 (a). Peaks of the corresponding XRD patterns are indexed to VO_2 (M) phase (space group: P21/c) with lattice parameters of a = 5.752 Å, b = 4.538 Å, c = 5.383 Å, and β= 122.64^0 (JCPDS no. 43-0251). The XRD patterns of Mg-doped VO_2, Figure 4.8(a), exhibit diffraction peaks at 26.89^0, 27.85^0, 33.40^0, 37.00^0, 39.74^0,42.16^0, 52.97^0,55.47^0, 57.48^0, 64.93^0, 70.48^0 and 72.03^0 corresponding to (110), (011), (-102), (200), (002), (-212), (121), (220), (022), (031), (202), and (-411), respectively, with prominent peak at (011). Other phases of vanadium oxide or impurities are not detected in the spectra, and this reveal pure phase of VO_2 (M) nanoparticles structure. From the XRD pattern it is clearly seen that there is weakening of intensity of the

peaks with increasing dopant concentration, indicating monoclinic phase formation of Mg-doped VO_2 nanoparticles and decreasing intensity with increasing dopant level.

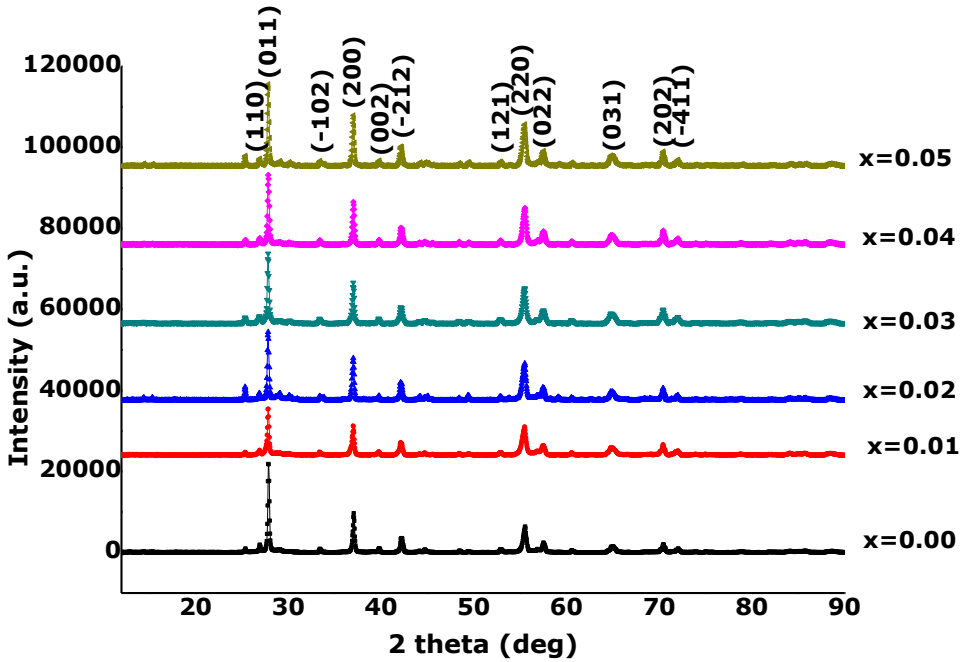

***Figure 4.8 (a)**: XRD patterns of Mg (0- 0.05%) doped VO_2 nanoparticles for different dopant concentrations.*

The magnification of the (011) peaks of the XRD patterns, Figure 4.8 (b), show shift of prominent peak position of Mg doped VO_2 (M) XRD patterns. With increasing doping level of Mg, XRD peaks of the Mg doped samples were slightly shifted towards a lower 2θ value. This phenomenon could be due to the replacement of vanadium atom by magnesium atom of relatively bigger radius [14, 81].

Further experiments were conducted on Mg doping of VO_2 varying the hydrothermal treatment time (12hours, 24hours, and 48hours) while the dopant concentration remains uniform (at x = 0.005). From the XRD patterns of Mg doped VO_2 nanoparticles, Figure 4.8

(c), the hydrothermal treatment time effect show that the synthesized nanoparticles were in monoclinic phase and highly crystalline.

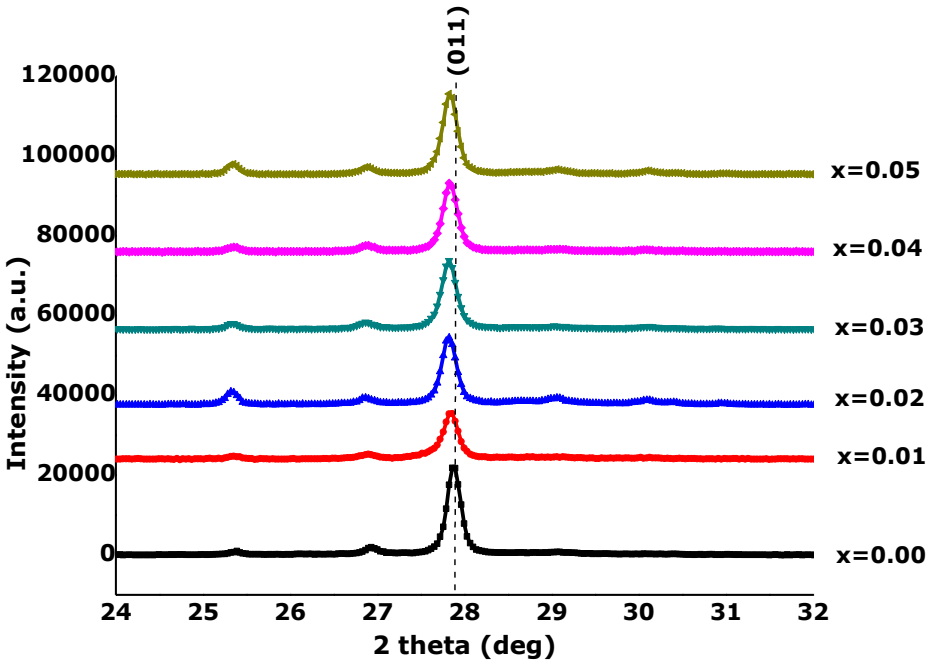

***Figure 4.8 (b)**: XRD patterns of Mg doped VO_2 with different doping concentrations, peak shift at 27.86^0.*

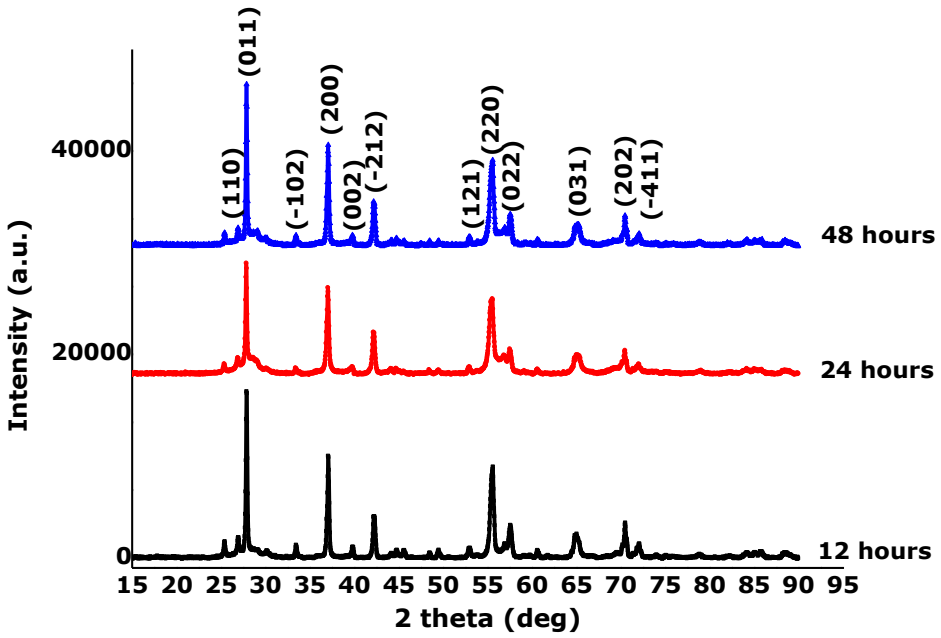

***Figure 4. 8 (c)**: XRD patterns of 2 at % Mg doped VO_2 nanoparticles for different hydrothermal treatment time.*

Scanning electron microscopy (SEM)

Scanning electron microscopy (SEM) was used to examine size and morphology of Mg doped VO_2 nanoparticles. As shown in Figure 4.9, the magnified SEM images of the nanoparticles are nanorods with an average length of about 54.5 nm and width of 20.6nm.

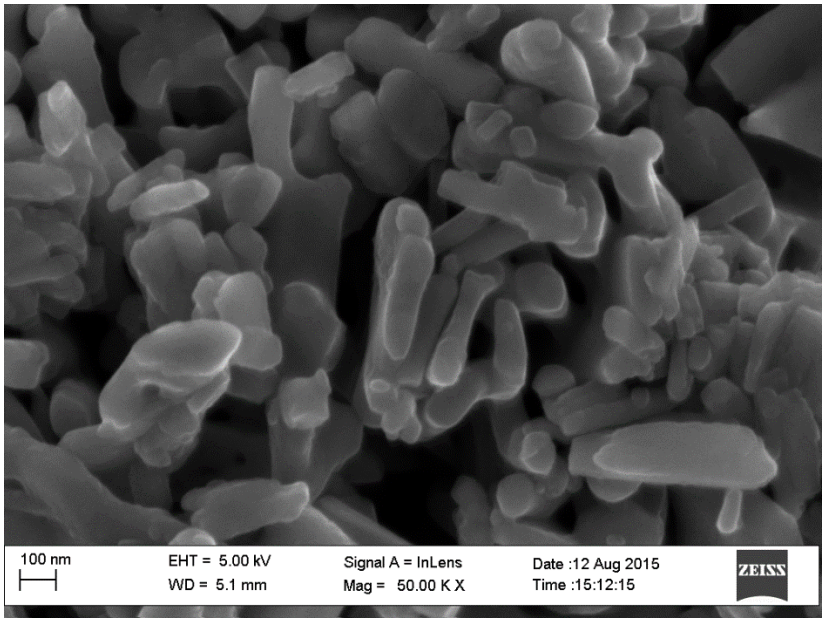

***Figure 4.9**: SEM images of 5.0 at % Mg doped VO_2 nanoparticles.*

High resolution transmission electron microscopy (HRTEM)

High resolution transmission electron microscopy (HRTEM) image of Mg doped VO_2 nanoparticles provide detailed information of the VO_2 (M) sample. As shown in Figure 4.10 (a-d), the nanoparticles exhibited crystalline structures and clear lattice fringes of VO_2 (M) phase. The spacing between two successive crystal planes was calculated to be around 3.21Å, which is consistent with distance between two (011) crystal planes of VO_2 (M). From Figure 4.10 (a, b), it could be observed that morphology of the synthesized VO_2 (M) nanoparticles are nanorods.

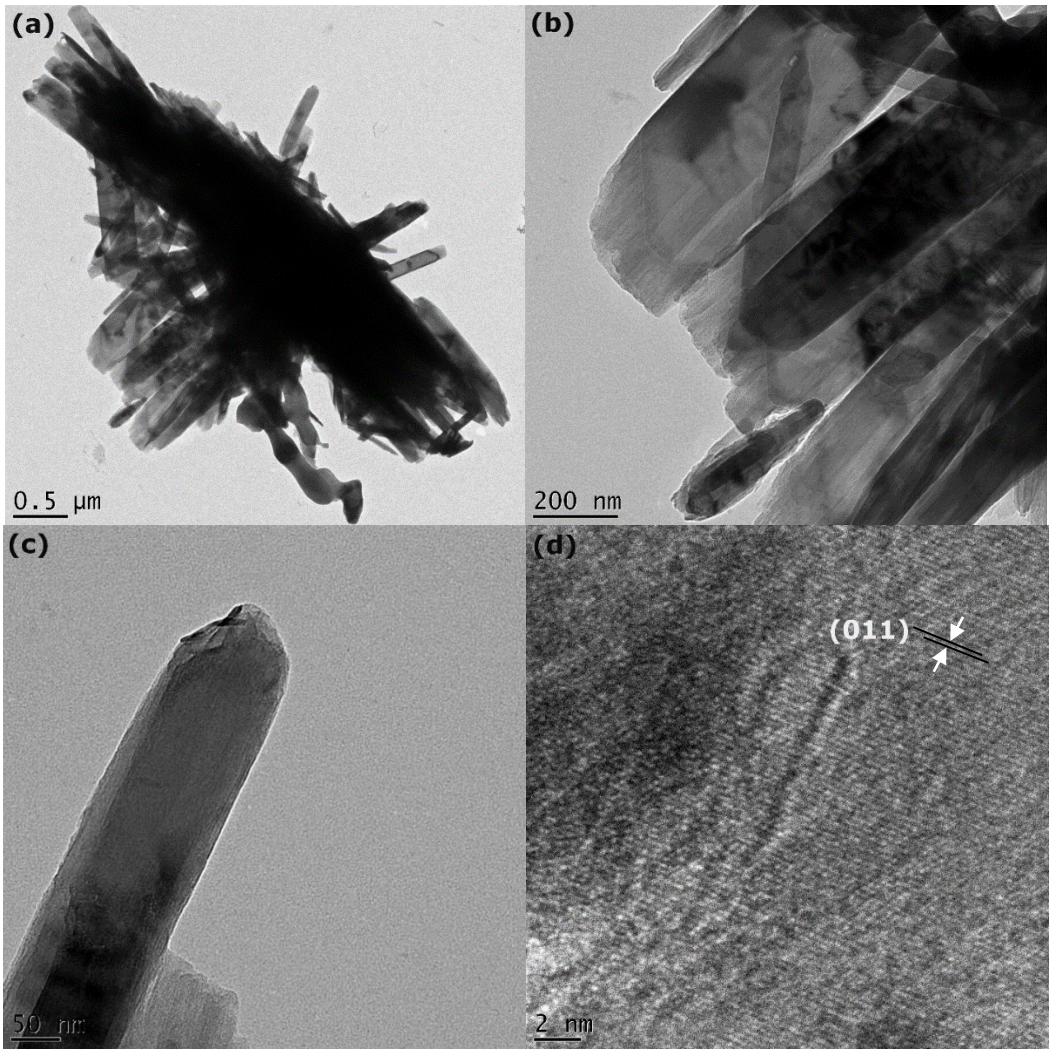

***Figure 4.10**: HRTEM images of 5.0 at % Mg doped VO_2 nanoparticles.*

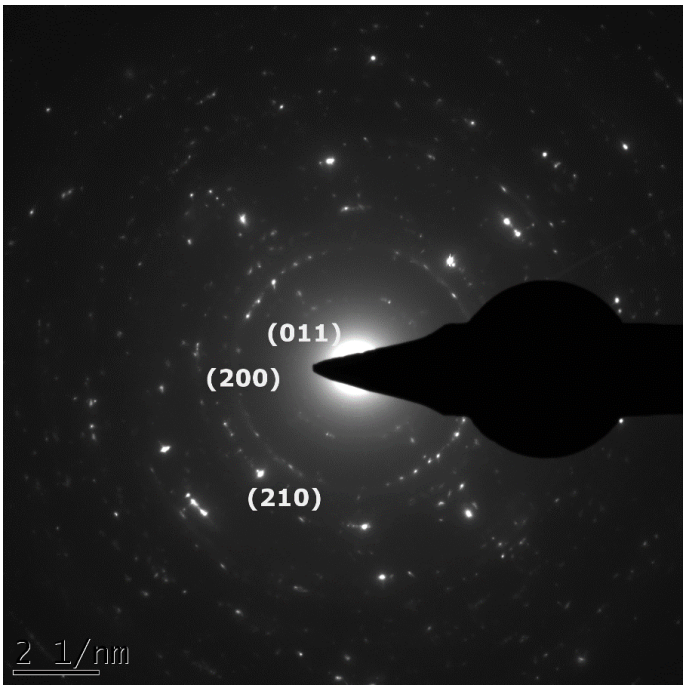

***Figure 4.11**: SAED ring patterns of 5.0 at % Mg doped VO_2 nanoparticles.*

Figure 4.11, above, shows the SAED patterns of Mg-doped VO_2 nanorods which reveal that crystalline nanoparticles have been synthesized.

Energy-dispersive X-ray spectroscopy (EDS)

Energy dispersive X-ray spectroscopy (EDS) measurement was taken on a representative specimen to determine the chemical composition of Mg doped VO_2 nanoparticles. The EDS result in Figure 4.12 shows that the synthesized nanoparticles are composed of V, Mg, and O. Moreover, the result reveals that the VO_2 nanoparticles were doped with about 1.64 at% Mg. The C and Cu peaks observed in the spectrum were from the instrument.

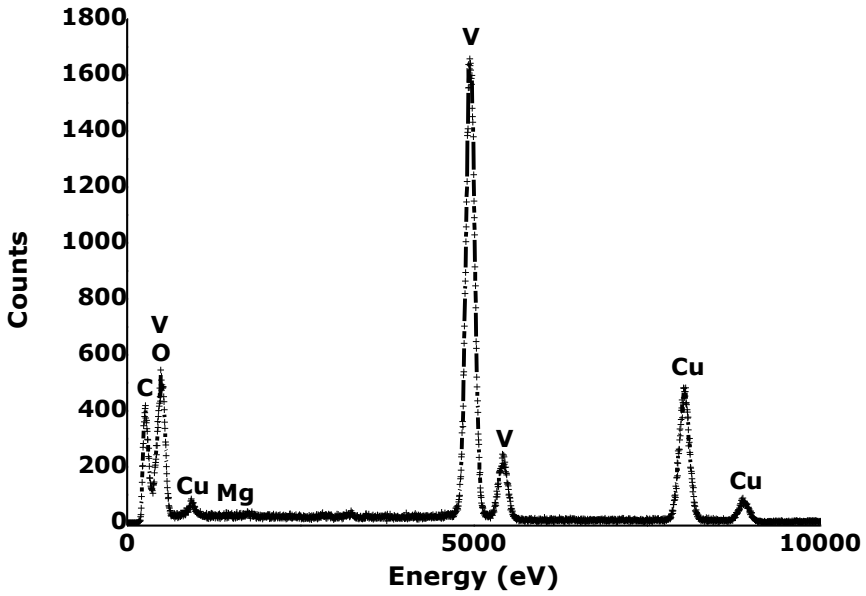

***Figure 4.12**: EDS spectrum of Mg doped VO_2 nanoparticles.*

Fourier transformed infrared spectroscopy (FTIR)

As shown in Figure 4.13, the FTIR measurement of Mg doped VO_2 nanoparticles was carried out to examine the chemical bonding between vanadium, oxygen and magnesium atoms in the nanostructure. The absorption bands 607.1 cm^{-1}, 504.5 cm^{-1}, and 434.8 cm^{-1} could be associated to V–O–V stretching modes [153, 154]. A small peak observed at 2028.3 cm^{-1} was due to stretching vibrations of C=O in the instrument [154]. No other peaks were observed due to the elimination of surfactants.

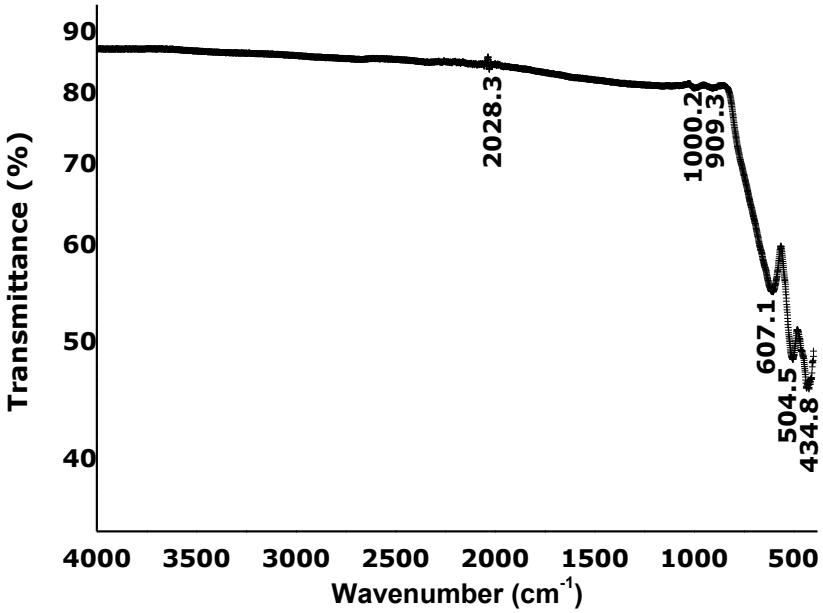

***Figure 4.13**: FTIR spectrum of 5.0 at % Mg doped VO_2 nanoparticles.*

Differential scanning calorimetry (DSC)

Differential scanning calorimetry (DSC) technique was used in studying the phase change temperature (T_c) properties of Mg-doped VO_2 nanoparticles. Mg-doped VO_2 sample was heated from 20°C to 90°C at the rate of 5 °C/min and then back to 20°C. As shown in Figure 4.14 (a), an endothermic peak at 69.3°C and an exothermic peak at 58.1°C were observed. The result obtained with Mg doping was larger than the undoped VO_2 phase transition which was at 66°C. However, T_c value decreases slightly with Mg doping, reaching 68.9 ^{0}C at 5 at% Mg dopant concentration.

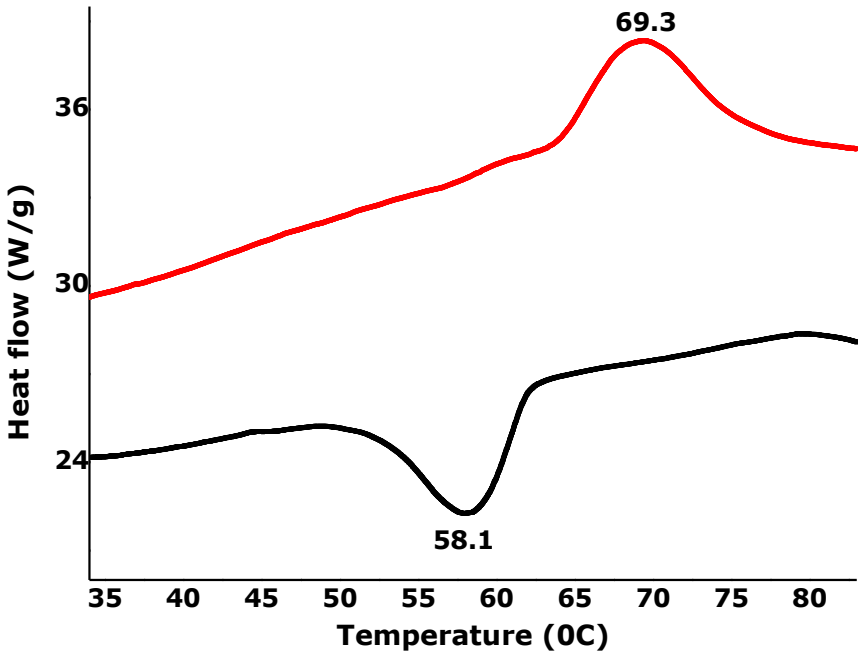

***Figure 4.14 (a)**: DSC curves of 1at% Mg doped VO_2 nanoparticles.*

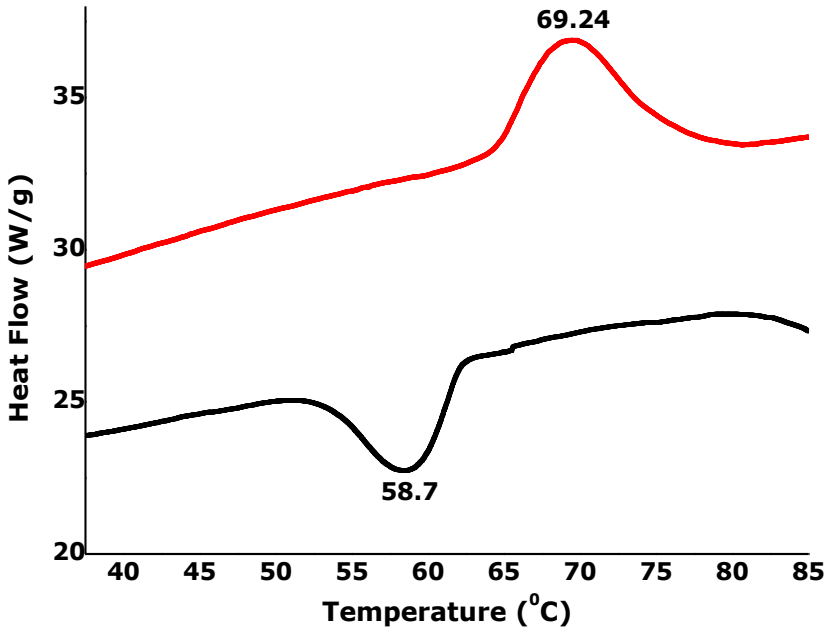

***Figure 4.14 (b)**: DSC curves of 2 at% Mg doped VO_2 nanoparticles.*

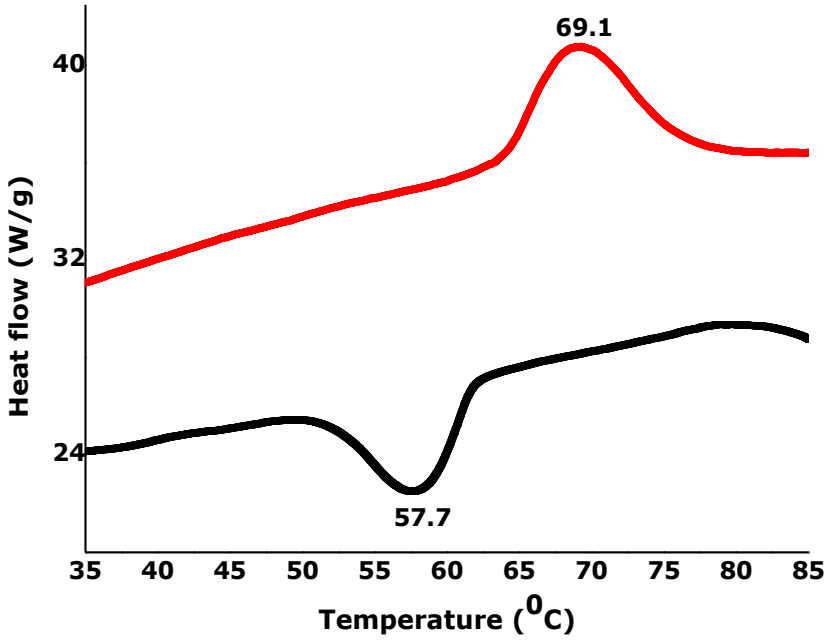

***Figure 4.14 (c)**: DSC curves of 3 at% Mg doped VO_2 nanoparticles.*

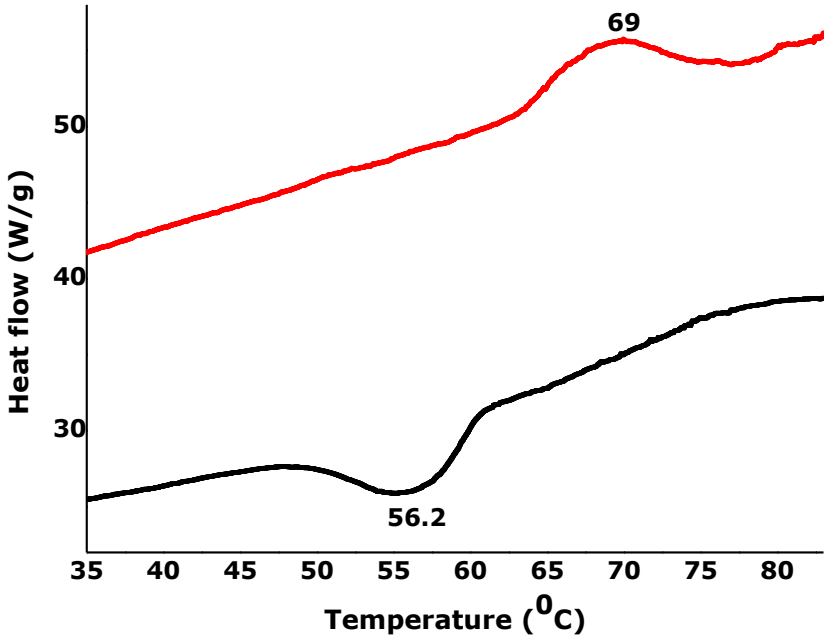

***Figure 4.14 (d)**: DSC curves of 4 at% Mg doped VO_2 nanoparticles.*

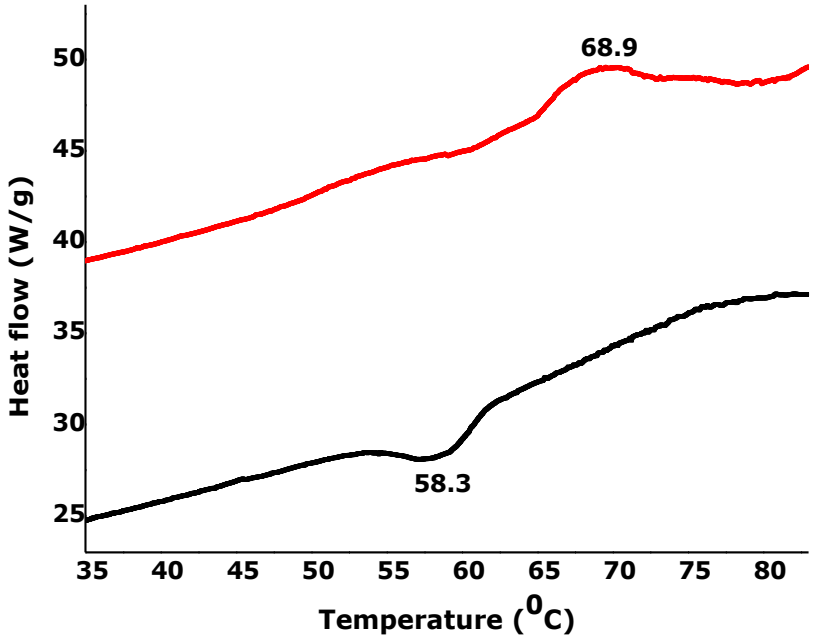

***Figure 4.14 (e)**: DSC curves of 5 at% Mg doped VO_2 nanoparticles.*

4.2.3 Cr doped VO_2

X-Ray Diffraction (XRD)

X-ray diffraction (XRD) patterns of Cr-doped VO_2 nanoparticles with various Cr-doping concentrations are shown in Figure 4.15 (a). Peaks of the corresponding XRD patterns are indexed to VO_2 (M) phase (space group: P21/c) with lattice constants of a = 5.752 Å, b = 4.538 Å, c = 5.383 Å, and β= 122.64^0 (JCPDS no. 43-1051). The XRD patterns of Cr doped VO_2 (M), Figure 4.15 (a), exhibits diffraction peaks at 26.82^0, 27.83^0, 33.42^0, 36.97^0, 39.76^0, 42.27^0, 55.57^0, 56.84^0, 64.47^0 70.29^0 and 72.04^0 corresponding to (110), (011), (-102), (-211), (002), (210), (211), (-113), (130), (-231) and (-411), respectively, with prominent peak at (-211).

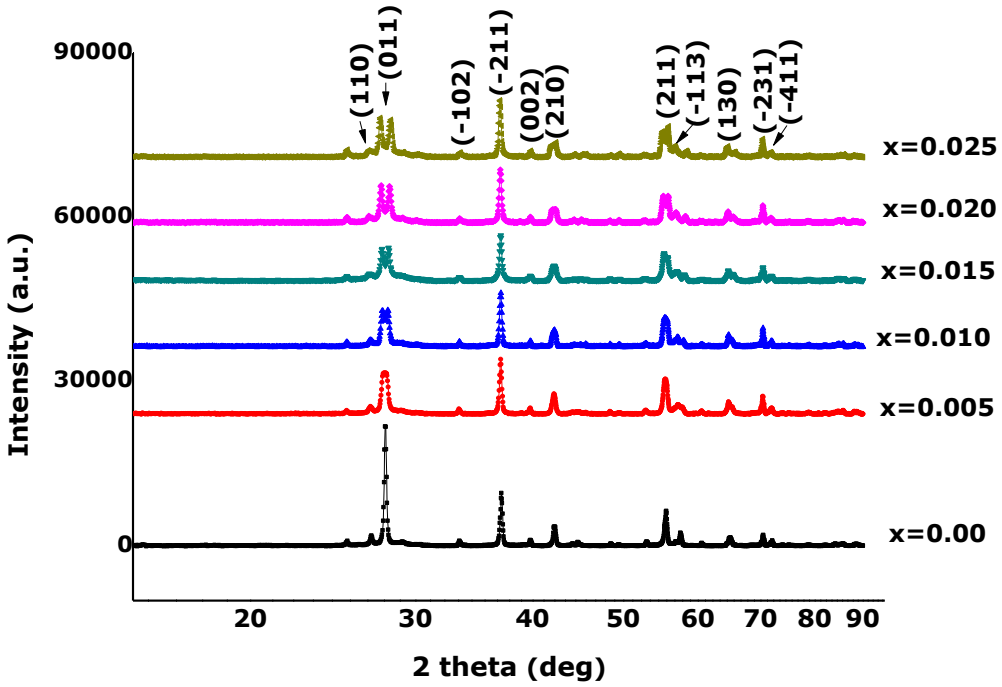

***Figure 4.15 (a)**: XRD patterns of Cr doped VO_2 nanoparticles for various dopant concentrations.*

Figure 4.15 (b) shows that the peak for undoped VO_2 at 27.83^0 splits in to two peaks due to various level of Cr doping. Peaks of the resulting XRD patterns are indexed to VO_2 (M) phase (space group: C2/m) with lattice constants of a = 9.083 Å, b = 5.763 Å, c = 4.532 Å, and $\beta = 91.50^0$ (JCPDS no. 33-1441). As a result, the 27.83^0 XRD diffraction peak of Cr doped VO_2 (M) splits in to 27.54^0, and 28.23^0, corresponding to (-201), and (201), values, respectively. This splitting of VO_2 (M) (011) peak into the (-201) and (201) indicates the occurrence of the structural phase transition [89, 187]. This indicates that the phase transition can be enhanced by proper amount of Cr doping. Since the radius of Cromium atoms are slightly larger than that of vanadium atoms, peak value at (011) shifts towards smaller angles, Figure 4.15 (c). Furthermore, the level of shifting increased slightly with increasing concentration of Cr doping.

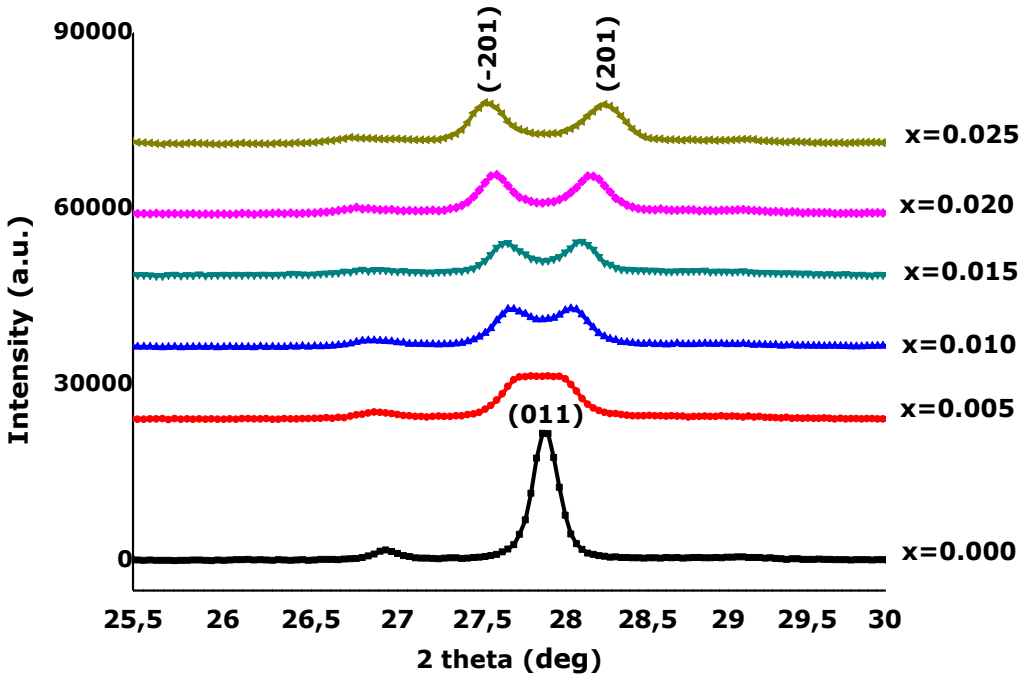

***Figure 4.15 (b)**: XRD patterns of Cr doped VO_2 nanoparticles, shift of peaks observed at 27.86^0*

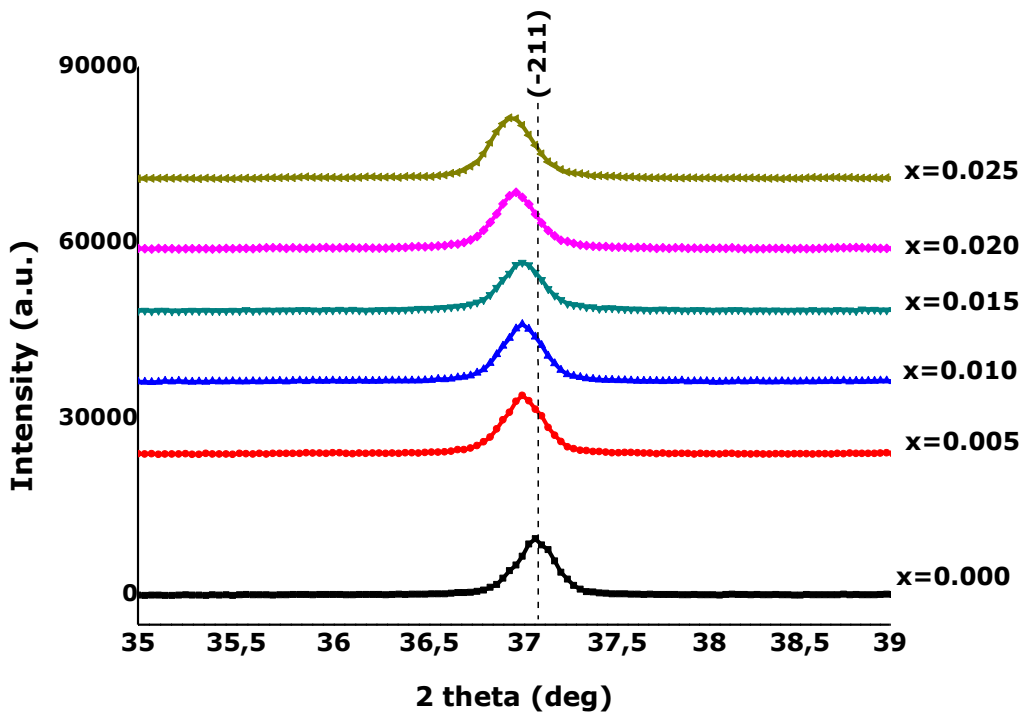

***Figure 4.15 (c)**: XRD patterns of Cr doped VO_2 nanoparticles, peak shift at 37.00^0.*

All the peaks in Figure 4.15(d) show weakened intensity peaks with increasing hydrothermal treatment time from 12hours to 48 hours at 0.5 at% Cr doping. This show the synthesized nanoparticles were smaller in size, and became less crystalline for larger treatment time.

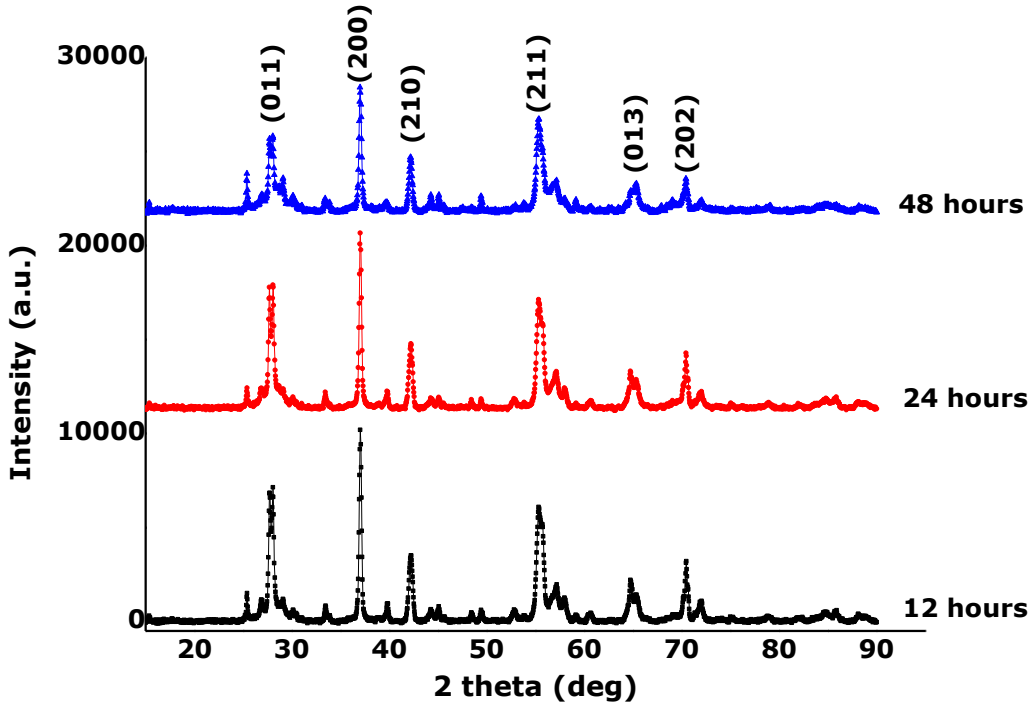

***Figure 4.15 (d)**: XRD patterns of Cr doped VO_2 nanoparticles for different hydrothermal treatment time.*

Scanning electron microscopy (SEM)

Size and morphology of Cr doped VO_2 nanoparticles were examined by scanning electron microscopy (SEM). From the magnified SEM image in Figure 4.16, it can be observed that nanoparticles of an average length of about 490.4 nm and width of 137.6 nm have been synthesized.

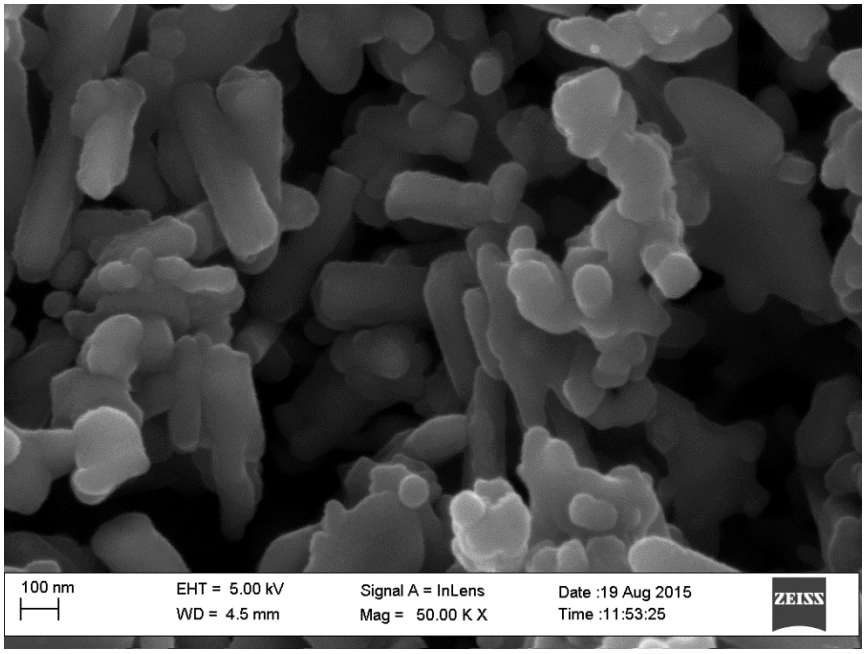

***Figure 4.16**: SEM image of Cr doped VO_2 nanoparticles.*

High resolution transmission electron microscopy (HRTEM)

High resolution transmission electron microscopy (HRTEM) images of Cr doped VO_2 nanoparticles provide detailed information of the VO_2 (M) sample. As shown in Figure 4.17 (a-d), the nanoparticles exhibited crystalline structures and very clear lattice fringes of VO_2 (M) phase. The spacing between two successive crystal planes was calculated to be around 3.21Å, which is consistent with distance between two (011) crystal planes of VO_2 (M). Moreover, HRTEM images, Figure 4.17 (a, b), reveals that morphology of synthesized Cr-doped VO_2 (M) nanoparticles are microrods.

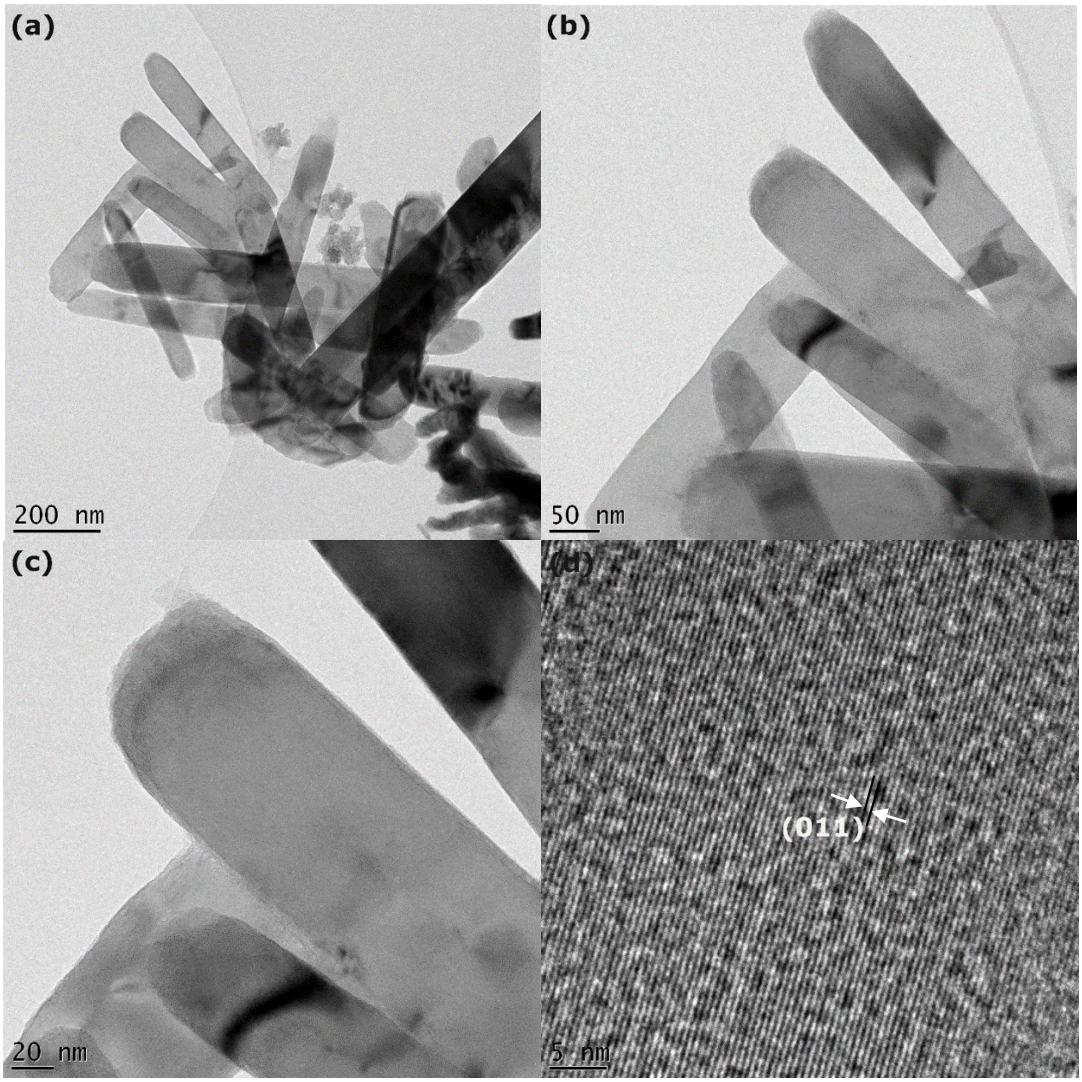

***Figure 4.17**: HRTEM images of Cr doped VO_2nanoparticles (a-c) with clear lattice fringes (d).*

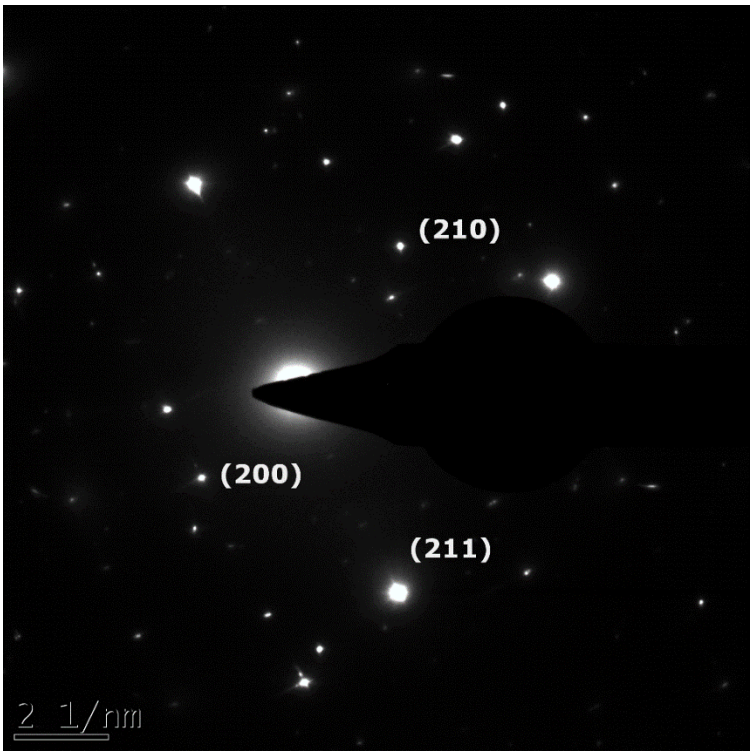

***Figure 4.18**: SAED ring patterns of Cr-doped VO_2 nanoparticles.*

Energy-dispersive X-ray spectroscopy (EDS)

Energy dispersive X-ray spectroscopy (EDS) measurement was made on representative specimen to determine the chemical composition of Cr doped VO_2 nanoparticles. The EDS result in Figure 4.19 shows that the nanoparticles contain V, Cr, and O. From EDS spectrum it was observed that the VO_2 nanoparticles were doped with about 1.5 at% Cr. The C and Ni peaks observed in the spectrum were from the instrument.

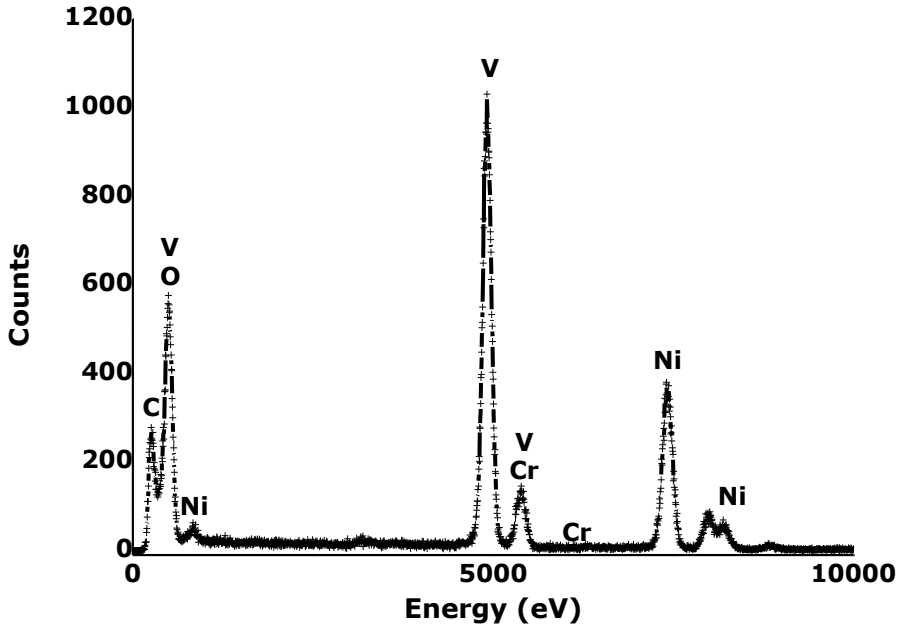

***Figure 4.19**: EDS spectrum of Cr-doped VO_2 nanoparticles by hydrothermal method.*

Fourier transformed infrared spectroscopy (FTIR)

FTIR measurement of Cr doped VO_2 nanoparticles were carried out to examine the chemical bonding between vanadium, oxygen and Chromium atoms in the prepared nanostructures. in Figure 4.20, the small peak at 2014.3 cm^{-1} is attributed to CO_2 in the instrument [154]. The other four peaks at 1000.4 cm^{-1}, 609.5 cm^{-1}, 467cm^{-1}, and 417 cm^{-1} are due to stretching and coupled vibrations of V=O and V–O–V, respectively [153, 154].

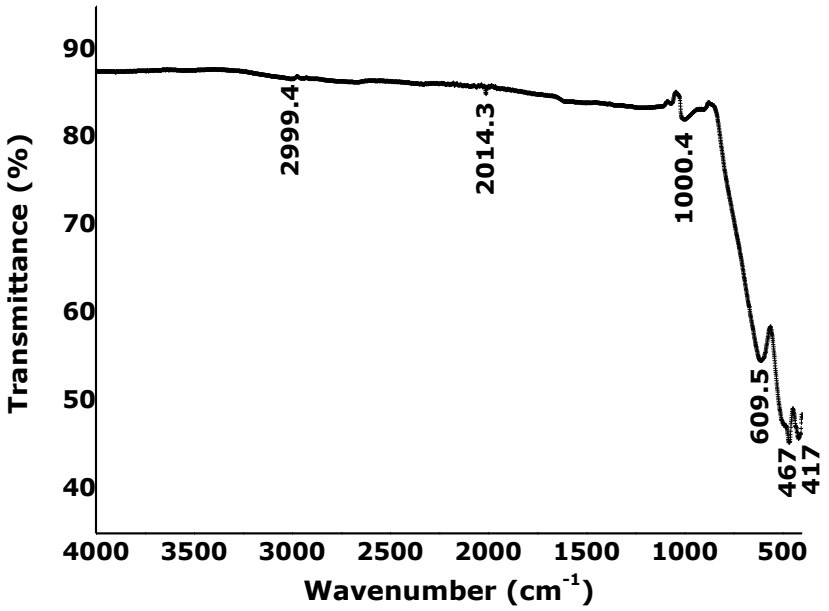

***Figure 4.20**: FTIR spectrum of 1.5 at % Cr doped VO_2 nanoparticles.*

4.2.4 Mo doped VO_2

X-ray diffraction

X-ray diffraction (XRD) patterns of Mo doped VO_2 nanoparticles with various Mo doping concentrations are shown in Figure 4.21 (a). Peaks of the corresponding XRD pattern are indexed to VO_2 (M) phase (space group: P21/c) with lattice constants of a = 5.753 Å, b = 4.526 Å, c = 5.383 Å, and β= 122.60^0 (JCPDS no. 44-0252). XRD patterns of Mo-doped VO_2, Figure 4.21 (a), exhibit diffraction peaks at 26.96^0, 27.82^0, 33.44^0, 37.00^0, 39.78^0,42.21^0, 52.96^0, 55.40^0, 57.51^0, 65.01^0, 70.430 and 72.03^0, corresponding to (110), (011), (10-2), (200), (002), (210), (102), (22-2), (022), (013), (202) and (41-1), respectively, with prominent peak at (011). Peaks of other phases or impurities were not detected in the spectra, which reveal the formation of pure phase of VO_2 (M) nanoparticles structure. From the XRD pattern it is clearly seen that there is weakening of intensity of the

peaks with increasing dopant concentration, indicating the crystalline VO_2 (M) nanoparticle formation is decreasing with increasing dopant level. As exhibited by the XRD patterns, monoclinic phase of Mo-doped VO_2 nanoparticles were synthesized, and Mo atom doping had no or little influence on the crystal lattice of VO_2.

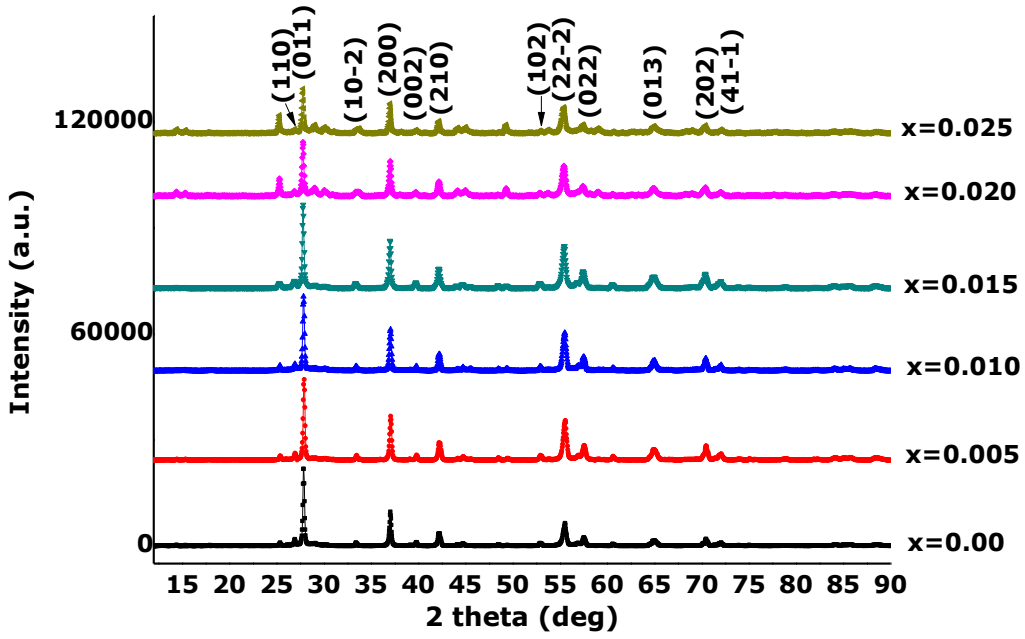

***Figure 4.21 (a)**: XRD patterns of Mo doped VO_2 nanoparticles.*

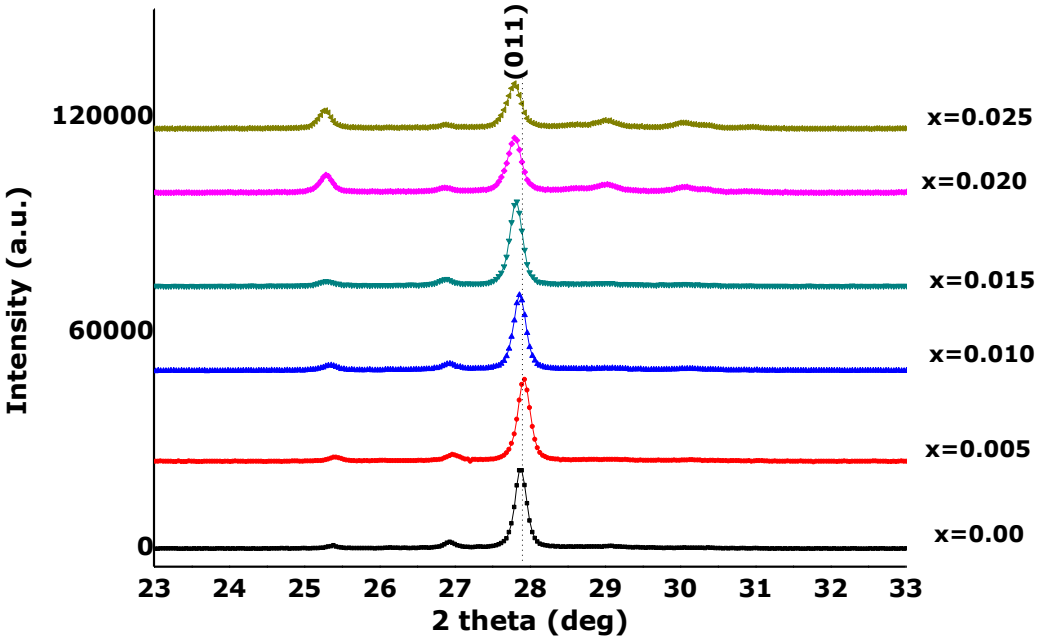

***Figure 4.21 (b)**: XRD patterns of Mo doped VO_2 nanoparticles, peak shift at 27.86^0.*

Since the radius of Mo atoms are slightly larger than that of V atoms, the peak at (011) shits towards smaller angles, Figure 4.21 (b). Hence, the level of peak shifting slightly increased with increasing concentration of Mo atoms. Furthermore, unseen peaks became visible with increasing dopant concentration.

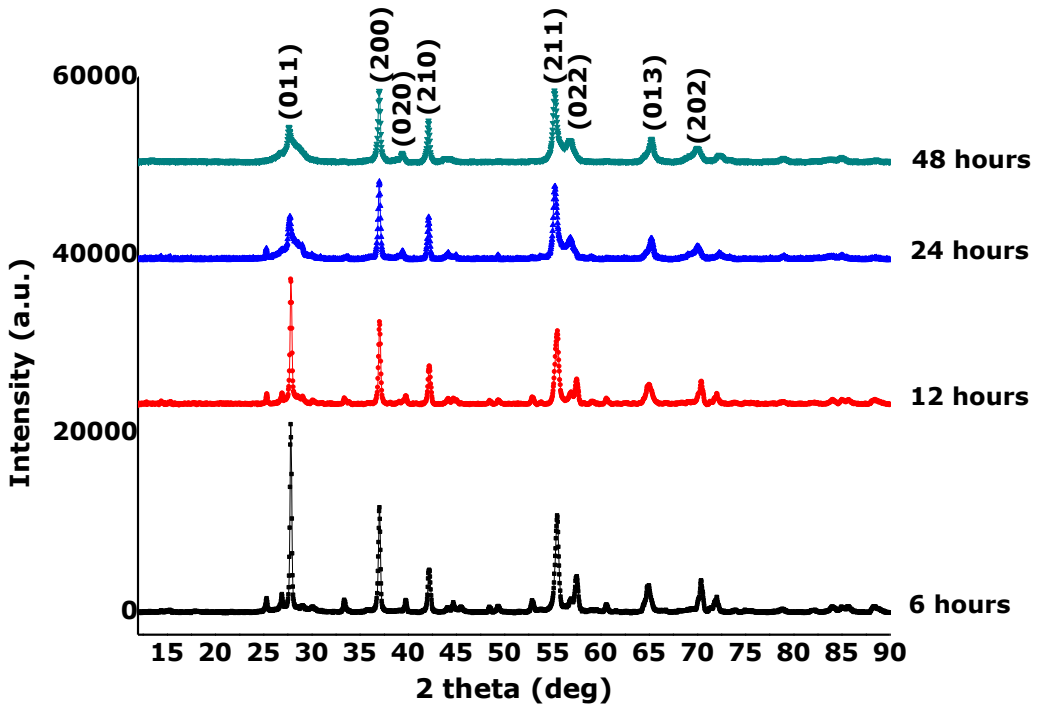

***Figure 4.21 (c)**: XRD patterns of 1.0 at % Mo doped VO_2 with various hydrothermal treatment time.*

From XRD patterns in Figure 4.21 (c), it can be observed that the peaks intensity weakens and became broader with increasing hydrothermal treatment time.

Scanning electron microscopy (SEM)

Scanning electron microscopy (SEM) measurements were employed to examine size and morphology of Mo doped VO_2 nanoparticles. As shown in Figure 4.22, the magnified SEM image reveals that the products are rod-shaped nanoparticles with an average length of about 296.4 nm and width of 68.3 nm.

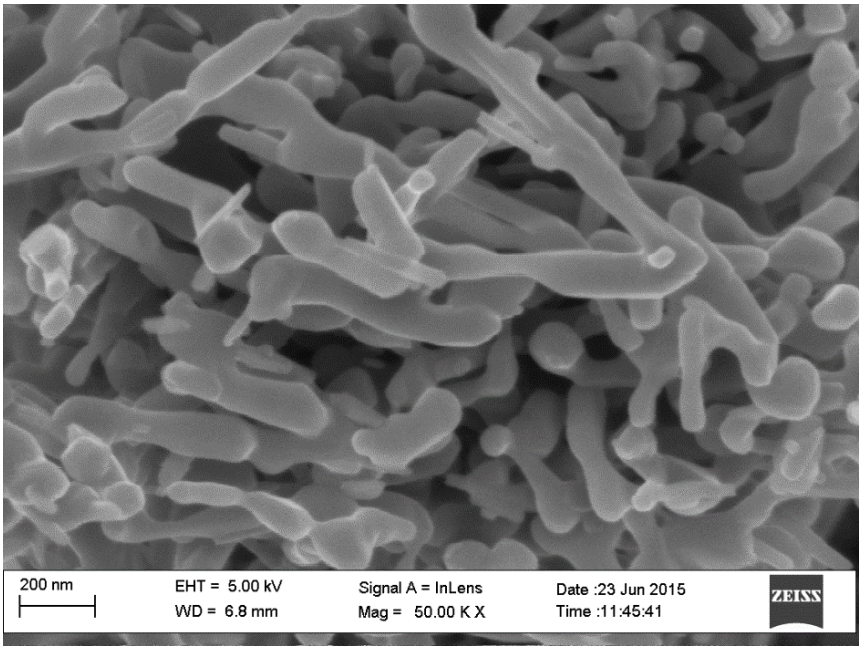

***Figure 4.22**: SEM image of 0.5 at %Mo doped VO_2 nanoparticles.*

High resolution transmission electron microscopy (HRTEM)

High resolution transmission electron microscopy (HRTEM) images of Mo doped VO_2 nanoparticles provide detailed information of VO_2 (M) sample phase. As shown in Figure 4.23 (a-d) the nanoparticles exhibited crystalline structures and clear lattice fringes of VO_2 (M) phase. The spacing between two successive crystal planes was calculated to be around 3.21 Å, which is consistent with the calculated distance between two (011) crystal planes of VO_2 (M). As shown in Figure 4.23 (a, b), morphology of the VO_2 (M) nanoparticles are rod-shaped.

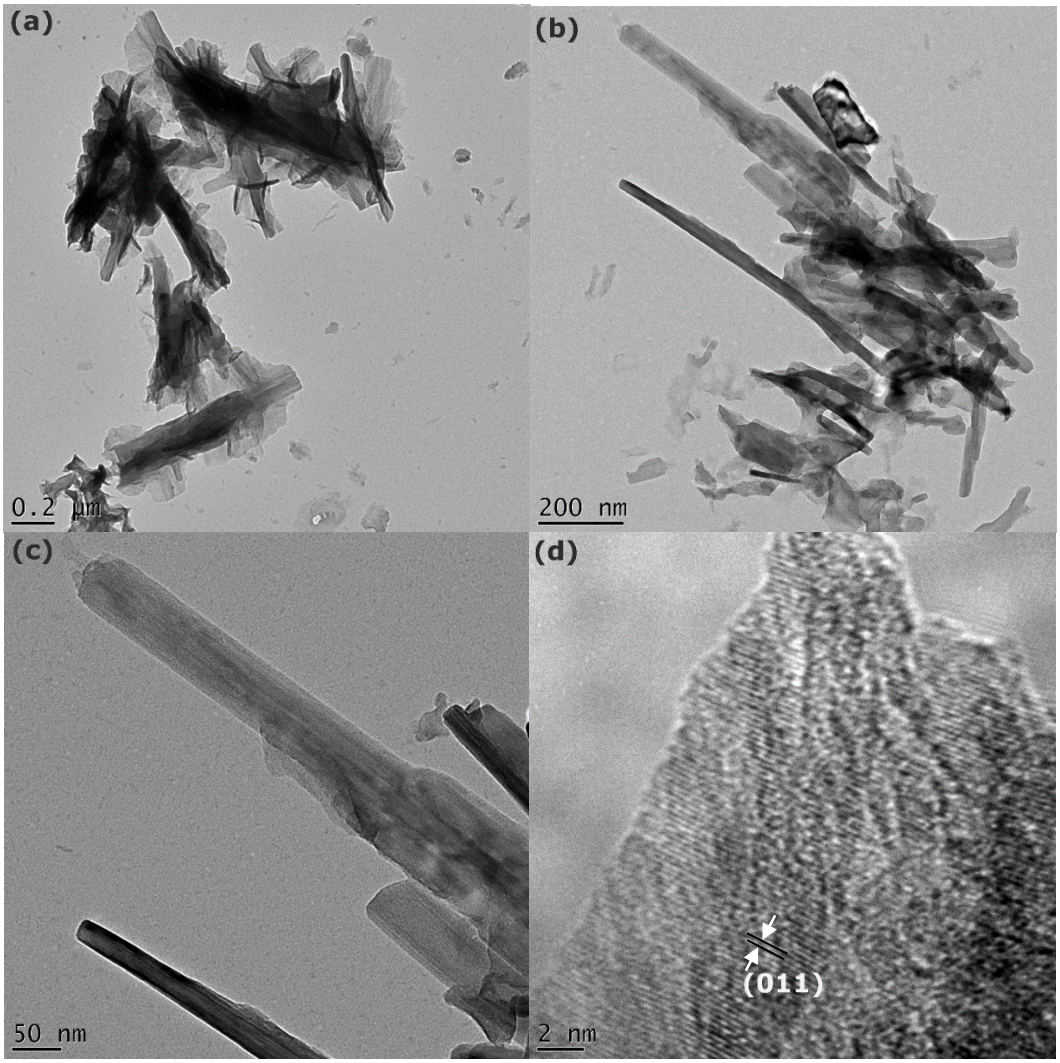

***Figure 4.23**: HRTEM images of Mo doped VO_2 nanoparticles.*

Figure 4.24, below, shows SAED patterns of Mo-doped VO_2 nanorods. The SAED patterns reveal that the synthesized nanoparticles are crystalline.

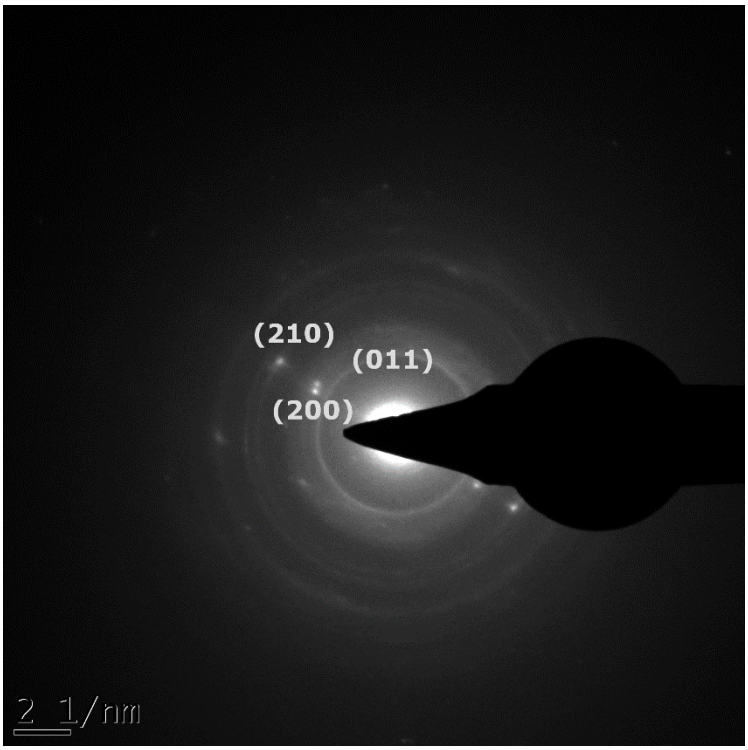

***Figure 4.24**: SAED ring patterns of Mo doped VO_2 nanoparticles.*

Energy-dispersive X-ray spectroscopy (EDS)

Energy dispersive X-ray spectroscopy (EDS) measurement was carried out on representative specimen to examine the chemical composition of Mo doped VO_2 nanoparticles. The EDS result as shown in Figure 4.25 reveal that the nanoparticles contain V, Mo, and O. From the EDS spectrum it is clearly seen that the VO_2 nanoparticles were doped with about 1.84 at% Mo. The Cu peaks observed in the spectrum were from the instrument.

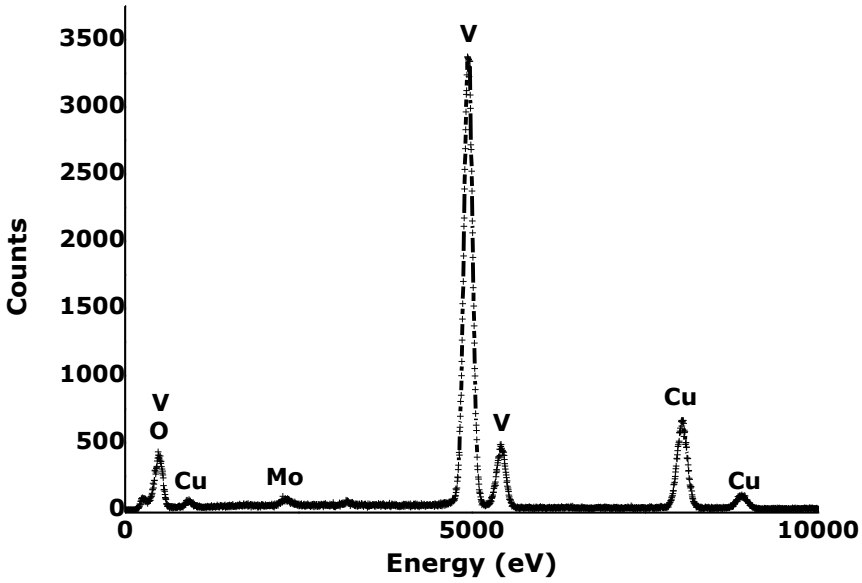

***Figure 4.25**: EDS spectrum of Mo doped VO_2 nanoparticles.*

Differential scanning calorimetry (DSC)

Differential scanning calorimetry (DSC) measurements were carried out to characterized the phase transition temperature (T_c) of Mo doped VO_2 nanoparticles. Mo-doped VO_2 sample was heated from 20°C to 90°C at the rate of 5°C/min and then cooled back to 20°C. It can be seen from Figure 4.26 (a), an endothermic peak was observed at 67.2°C and an exothermic peak at 52.5°C. The T_c result obtained with Mo doping was slightly larger than the undoped VO_2 phase transition which was at 66°C, but still it was lower than the previously reported value 68.6^0C [82]. This shows the semiconductor-metallic phase transition occurs at 67.2°C. Moreover, the T_c value slightly decreases with increasing Mo doping, reaching 64.2^0C at 2.5weight % doping of Mo, Figure 4.26 (e). The DSC results, Figure 4.26 (a-e), show that the change in temperature (ΔT) between the endothermic peak and exothermic peak decreases with increasing dopant concentration from about 14.7 at 0.5 at % doping to 7.9 ^{0}C at 2.5 at % doping.

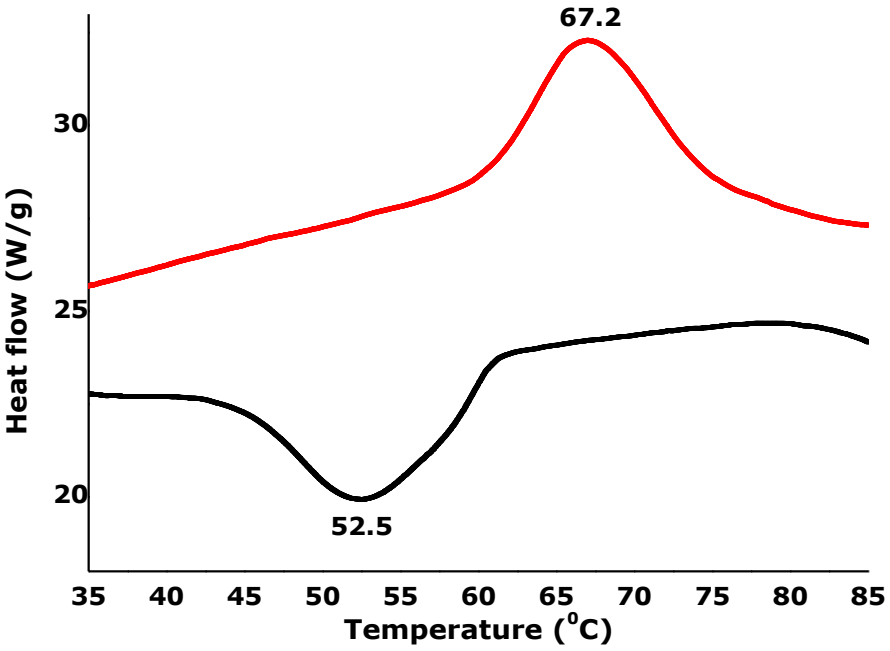

***Figure 4.26 (a)**: DSC curves for 0.5 at % Mo doped VO_2 nanoparticles.*

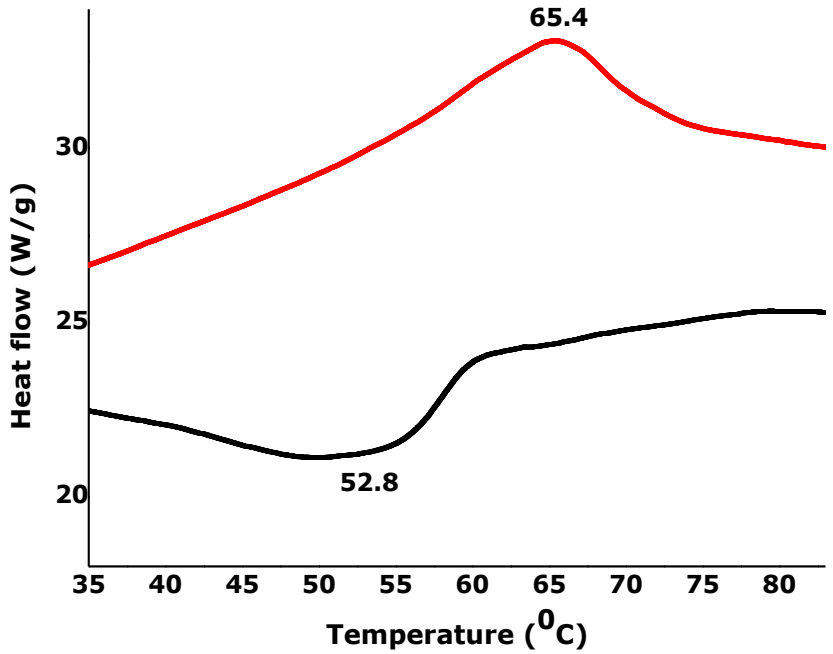

***Figure 4.26 (b)**: DSC curves for 1.0 at % Mo doped VO_2 nanoparticles.*

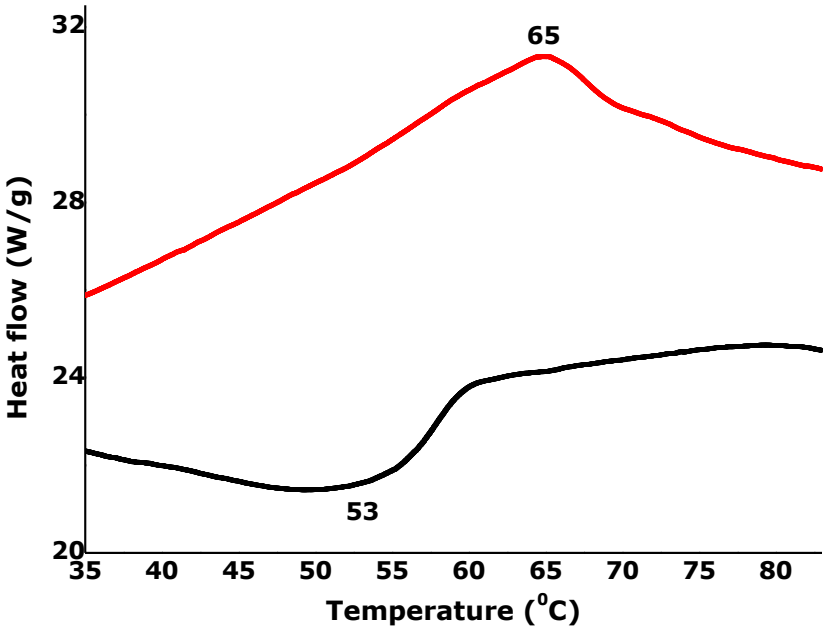

***Figure 4.26 (c)**: DSC curves for 1.5 at % Mo doped VO_2 nanoparticles.*

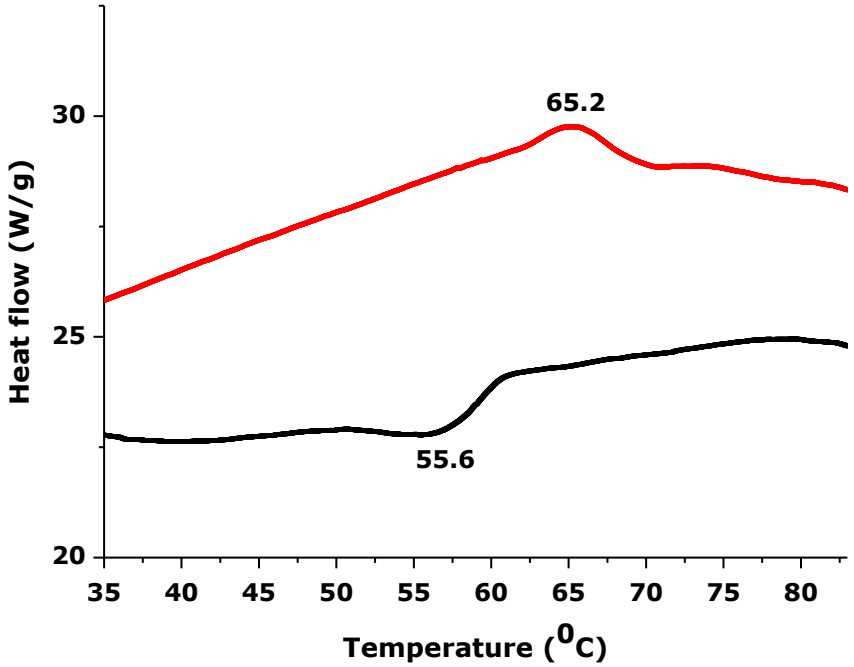

***Figure 4.26 (d)**: DSC curves for 2.0 at % Mo doped VO_2 nanoparticles.*

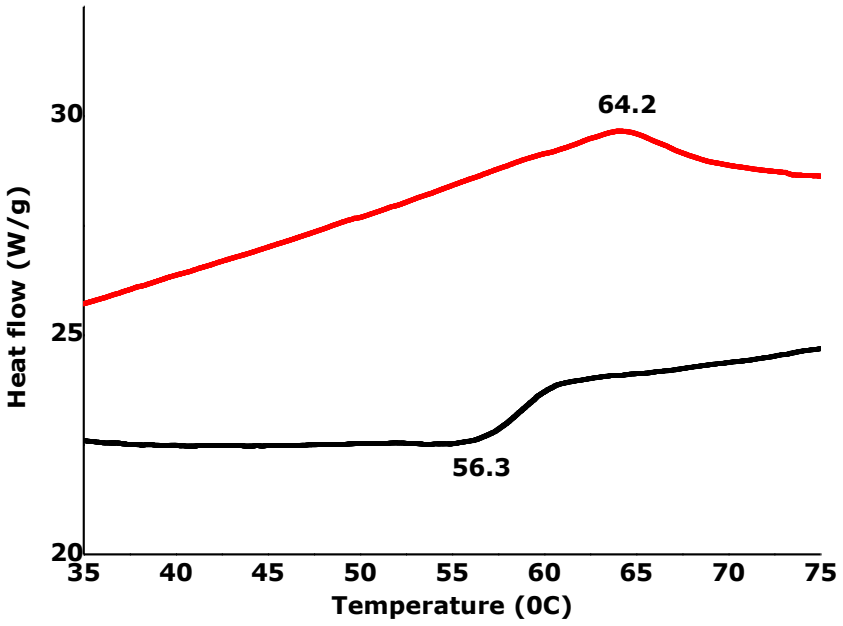

***Figure 4.26 (e)**: DSC curves for 2.5 at % Mo doped VO_2 nanoparticles.*

Fourier transformed infrared spectroscopy (FTIR)

FTIR measurement of Mo doped VO_2 nanoparticles were performed to examine chemical bonding between vanadium, oxygen and molybdenum atoms in the prepared nanostructures. As shown in Figure 4.27, the absorption at 1607.7 cm^{-1} and 2985.5 cm^{-1} are assigned to the stretching and bending vibration of H_2O [74, 90], and small peak is observed at 2028.5 cm^{-1} which is due to CO_2 in the instrument [154]. The other two peaks at 978.5 cm^{-1} and 490.5 cm^{-1} are as a result of the stretching of V=O and V–O–V coupled vibration, respectively [153, 154].

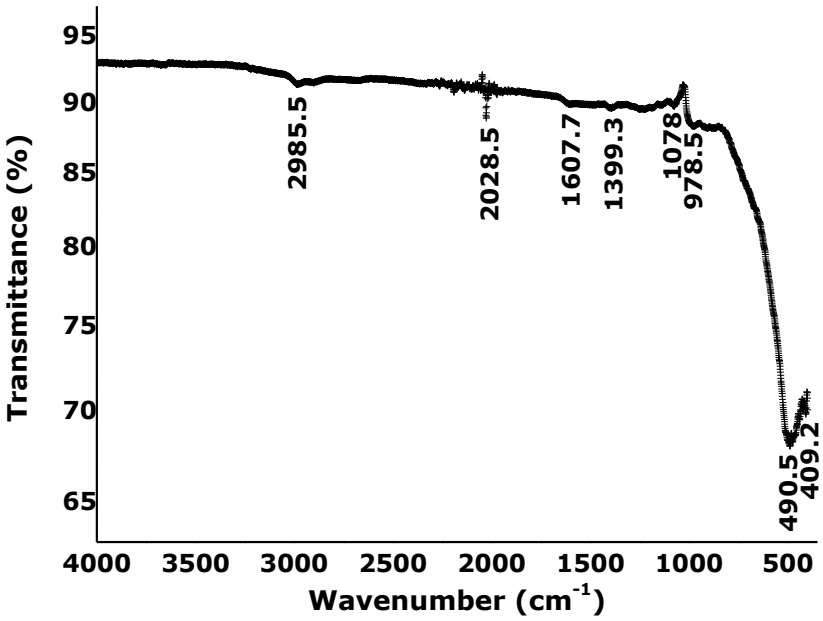

***Figure 4.27**: FTIR spectrum of 2.0 at% Mo doped VO_2 nanoparticles.*

4.2.5 Magnesium/Molybdenum co-doped VO_2

X-Ray diffraction (XRD)

XRD patterns of Mg/Mo co-doped VO_2 nanoparticles for 0.5 at % Mo and various doping concentrations of Mg (1at %, 2 at %, 3 at %) are shown in Figure 4.28. Peaks of the corresponding XRD patterns are indexed to VO_2 (M) phase (space group: P21/c) with lattice constants of a = 5.753 Å, b = 4.526 Å, c = 5.383 Å, and β= 122.60^0 (JCPDS no. 44-0252). XRD patterns of Mg/Mo co-doped VO_2 exhibit diffraction peaks at 26.93^0, 27.86^0, 33.46^0, 37.03^0, 39.83^0, 42.19^0, 44.67, 52.94^0 55.51^0, 57.48^0, 65.08^0, 70.43^0 and 72.03^0 corresponding to (110), (011), (10-2), (200), (002), (210), (021), (102), (211), (022), (031), (202) and (41-1), respectively, with prominent peak at (011) (JCPDS no. 44-0252). The XRD patterns exhibited that the Mg/Mo co-doped VO_2 nanoparticles were monoclinic phase. No significant peaks of other phase or impurities were detected in the spectra,

revealing pure phase of VO_2 (M) nanoparticles structure. From the XRD pattern it is clearly seen that enhanced peak intensity exhibit a slight increment with increasing dopant concentration, which means that crystalline VO_2 (M) phase is increasing with dopant level. XRD patterns exhibited that the Mg/Mo co-doped VO_2 nanoparticles are in monoclinic phase, and Mo atom doping has little influence on the lattice structure of VO_2.

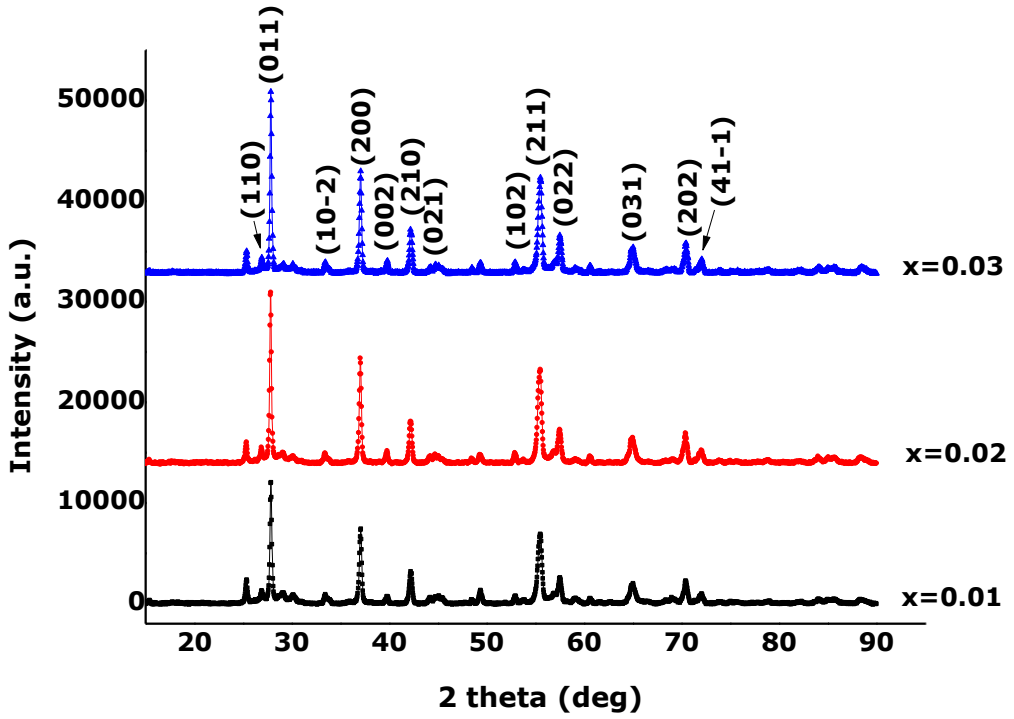

***Figure 4.28**: XRD patterns of Mg/Mo co-doped VO_2 nanoparticles.*

Scanning electron microscopy (SEM)

Scanning electron microscopy (SEM) image was taken to examine size and morphology of Mg/Mo co-doped VO_2 nanoparticles. As shown in Figure 4.29, the magnified SEM image reveal that the products are rod-shaped nanoparticles with an average length of about 490 nm and width of 137.6 nm.

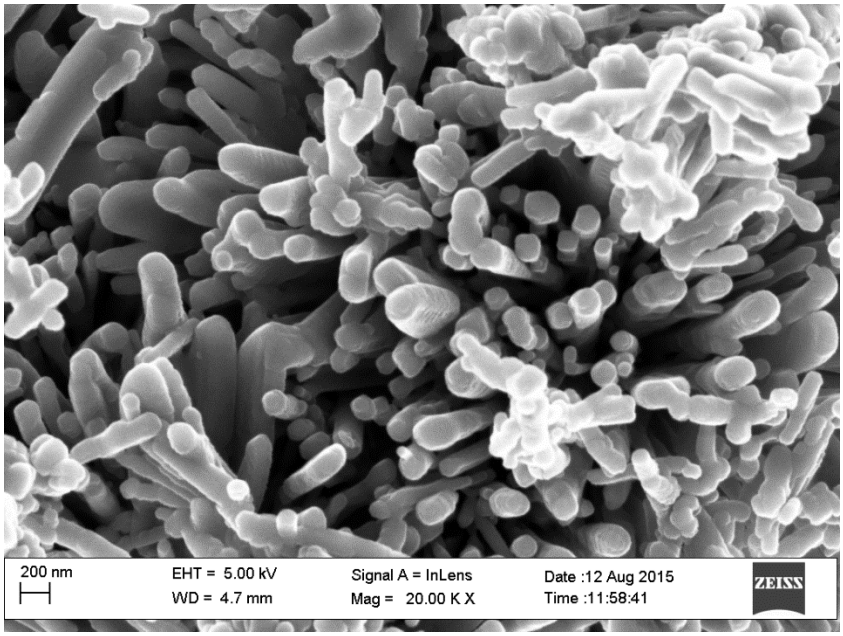

***Figure 4.29**: SEM image of Mg/Mo co-doped VO_2 nanoparticles.*

High resolution transmission electron microscopy (HRTEM)

High resolution transmission electron microscopy (HRTEM) images of Mg/Mo co-doped VO_2 nanoparticles provide additional information of the VO_2 (M) sample. From Figure 4.30 (a-d), it can be observed that the nanoparticles exhibited crystalline structures and clear lattice fringes of VO_2 (M) phase. By using digital micrograph, the spacing between two successive crystal planes was calculated to be around 3.21Å, which is consistent with the calculated distance, from prominent XRD peak, between two (011) crystal planes of VO_2 (M). From Figure 4.30 (a, b), rod-shaped morphology of the VO_2 (M) nanoparticles have been observed.

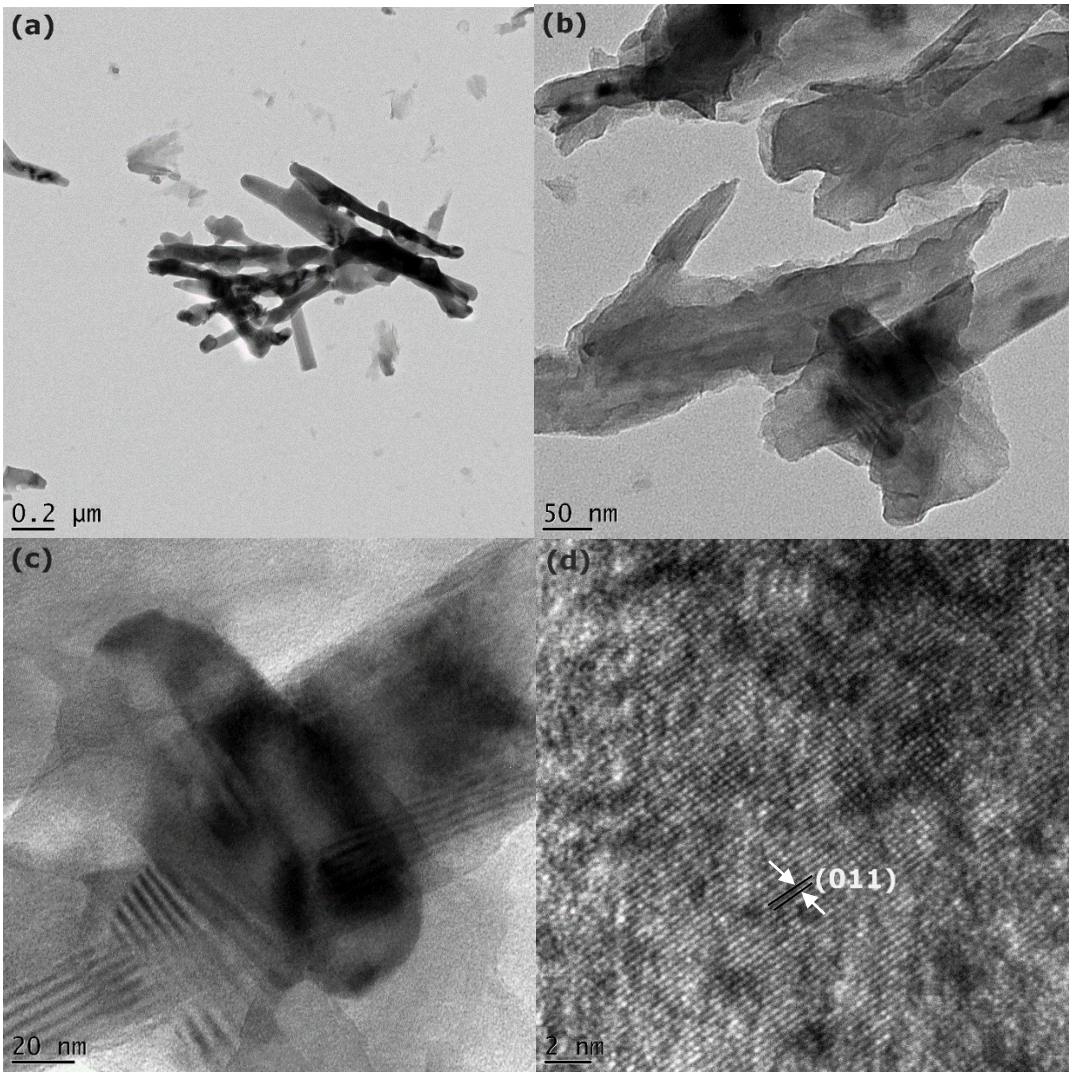

***Figure 4.30**: HRTEM images of Mg/Mo co-doped VO_2 nanoparticles.*

The SAED patterns in Figure 4.31 show the rods exhibited crystalline structures and clear lattice fringes of VO_2 (M) phase. Using digital micrograph, for HRTEM image of Figure 4.30 (d), the spacing between two successive crystal planes was calculated to be around 3.21Å. This result is consistent with the calculated distance, from prominent XRD peak in Figure 4.28, between two (011) crystal lattices of VO_2 (M).

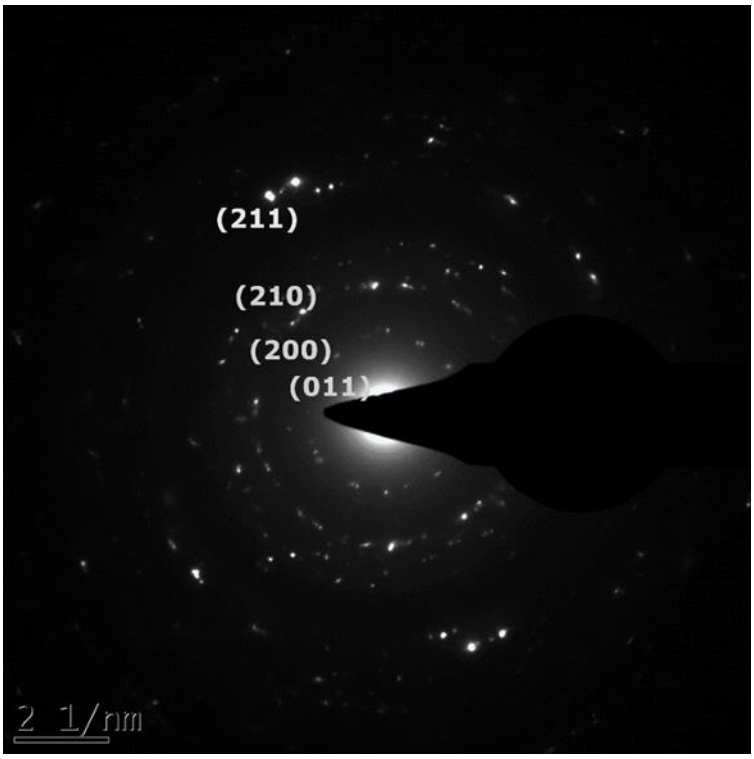

Figure 4.31: SAED ring patterns of Mg/Mo co-doped VO_2 nanoparticles.

Energy-dispersive X-ray spectroscopy (EDS)

Energy dispersive X-ray spectroscopy (EDS) measurement was taken on a representative specimen to determine the chemical composition of Mg/Mo co-doped VO_2 nanoparticles. The EDS result as shown in Figure 4.32 reveals that the nanoparticles contain V, Mg, Mo, and O. The VO_2 nanoparticles were doped with about 1.0 at% Mg and 1.2 at% Mo as observed from EDS spectrum. The C and Cu peaks observed in the spectrum were from the instrument.

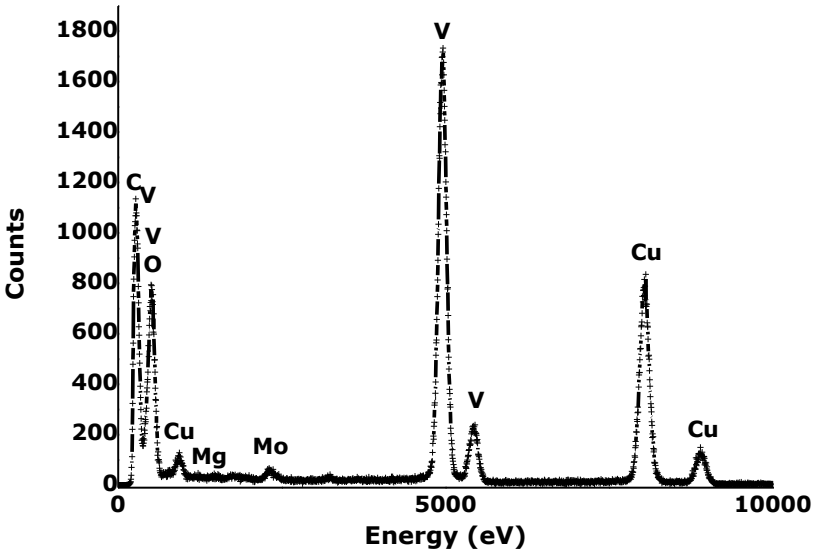

***Figure 4.32**: EDS spectrum of Mg/Mo co-doped VO_2 nanoparticles.*

Fourier transformed infrared spectroscopy (FTIR)

As shown in Figure 4.33, the FTIR measurement of Mg/Mo co-doped VO_2 nanoparticles was carried out to examine chemical bonding between atoms of vanadium, oxygen, molybdenum and magnesium in the nanostructure. The absorption band at 989.5 cm^{-1}, 493.4 cm^{-1} and 413.2 cm^{-1} can be associated to stretching vibrations of V-O and V=O [74, 90, 153]. A small peak at 1608.6 cm^{-1} was observed which is due to the adsorbed water molecules [90]. No other peaks were observed due to the elimination of surfactants.

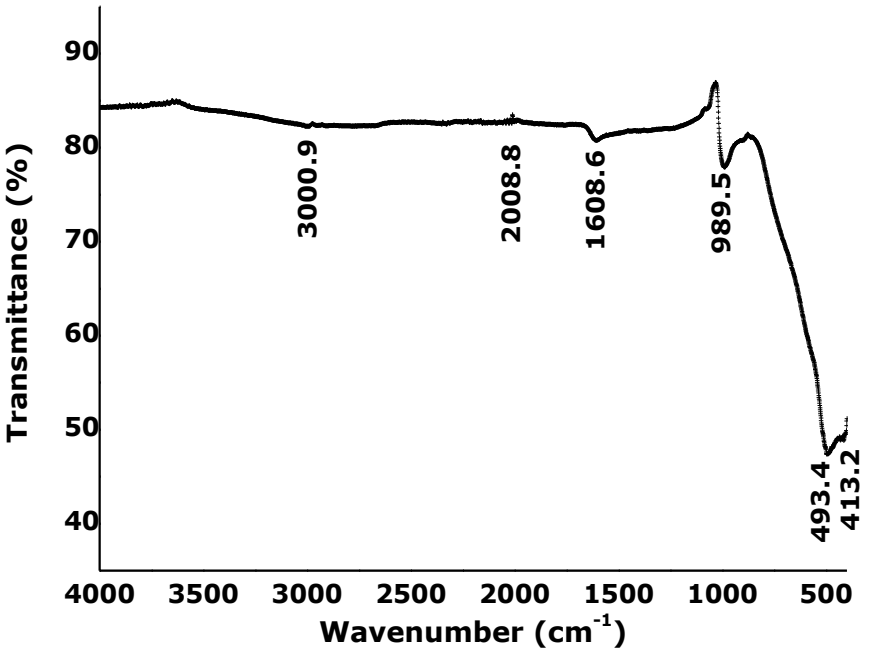

***Figure 4.33**: FTIR spectrum of 2 at % Mg with 0.5 at % Mo doped VO_2 nanoparticles.*

4.2.6 Green Synthesis of VO_2

X-Ray Diffraction (XRD)

XRD patterns of VO_2 nanoparticles synthesized by green process are shown in Figure 4.34. Prominent diffraction peaks are exhibited at 26.92^0, 27.82^0, 36.90^0, 39.27^0, 42.05^0, 55.25^0, 65.13^0, 68.49^0, 72.02^0 and 79.04^0 corresponding to (110), (011), (20-2), (111), (21-2), (21-3), (031), (41-2), (41-1) and (400), respectively, with prominent peaks at (20-2), (21-2) and (21-3). Peaks of the corresponding XRD patterns are indexed to VO_2 (M) phase (space group: P21/c) with lattice constants of a = 5.753, b = 4.526, c = 5.383 Å, and β= 122.60^0 (JCPDS no. 44-0252). However, minor peaks of impurities have been detected in the spectra.

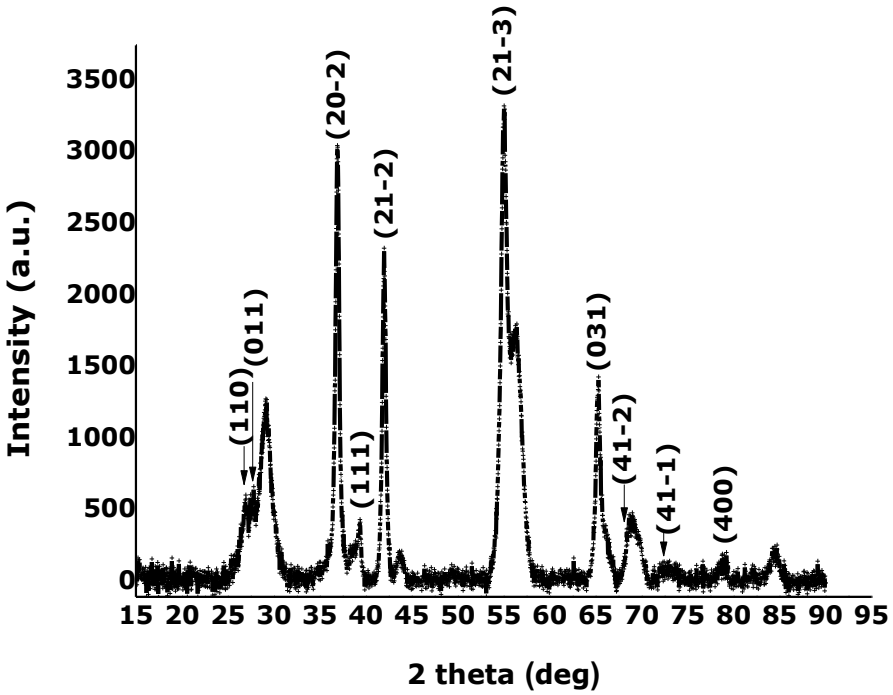

***Figure 4.34**: XRD patterns of VO_2 (M) by green process.*

The average particle size can be calculated from the largest peak at (20-2) for VO_2, using Scherrer formula $d=\kappa\lambda/\beta\cos\theta$, here d is the mean crystallites size, k is a proportionality constant commonly taken to be equal to 0.89, λ is the incident X-ray wave length, β is the half-width at full diffracted peak, and θ is the diffraction peak position. Thus for the Bragg reflection at $2\theta = 36.90^0$, corresponding to the (20-2) reflection, the calculated average value is about 150 nm.

Scanning electron microscopy (SEM)

SEM images of VO_2 nanoparticles synthesized by green process taken at (a) 200 nm and (b) 100 nm after annealing at 450^0C are shown in Figure 4.35, below. From scanning electron microscopy (SEM) measurements, size and morphology of the VO_2 nanoparticles are

examined, and the nanoparticles are observed to be granular with an average size of 64.5 nm.

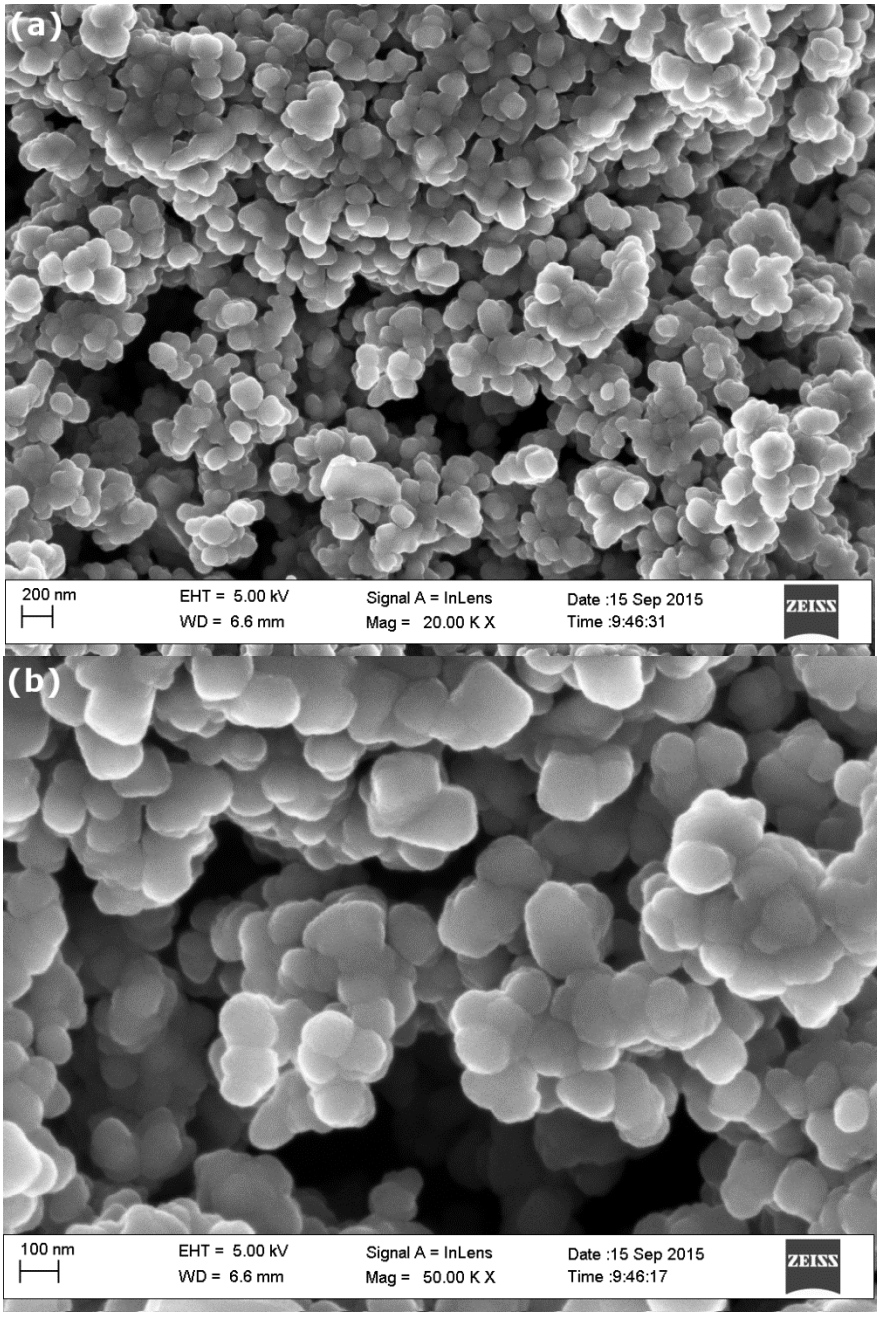

***Figure 4.35**: SEM images of VO_2 (M) nanoparticles synthesized by green process.*

High resolution transmission electron microscopy (HRTEM)

High resolution transmission electron microscopy (HRTEM) images of VO_2 nanoparticles synthesized by green process gives important information on the phase of the VO_2 sample.

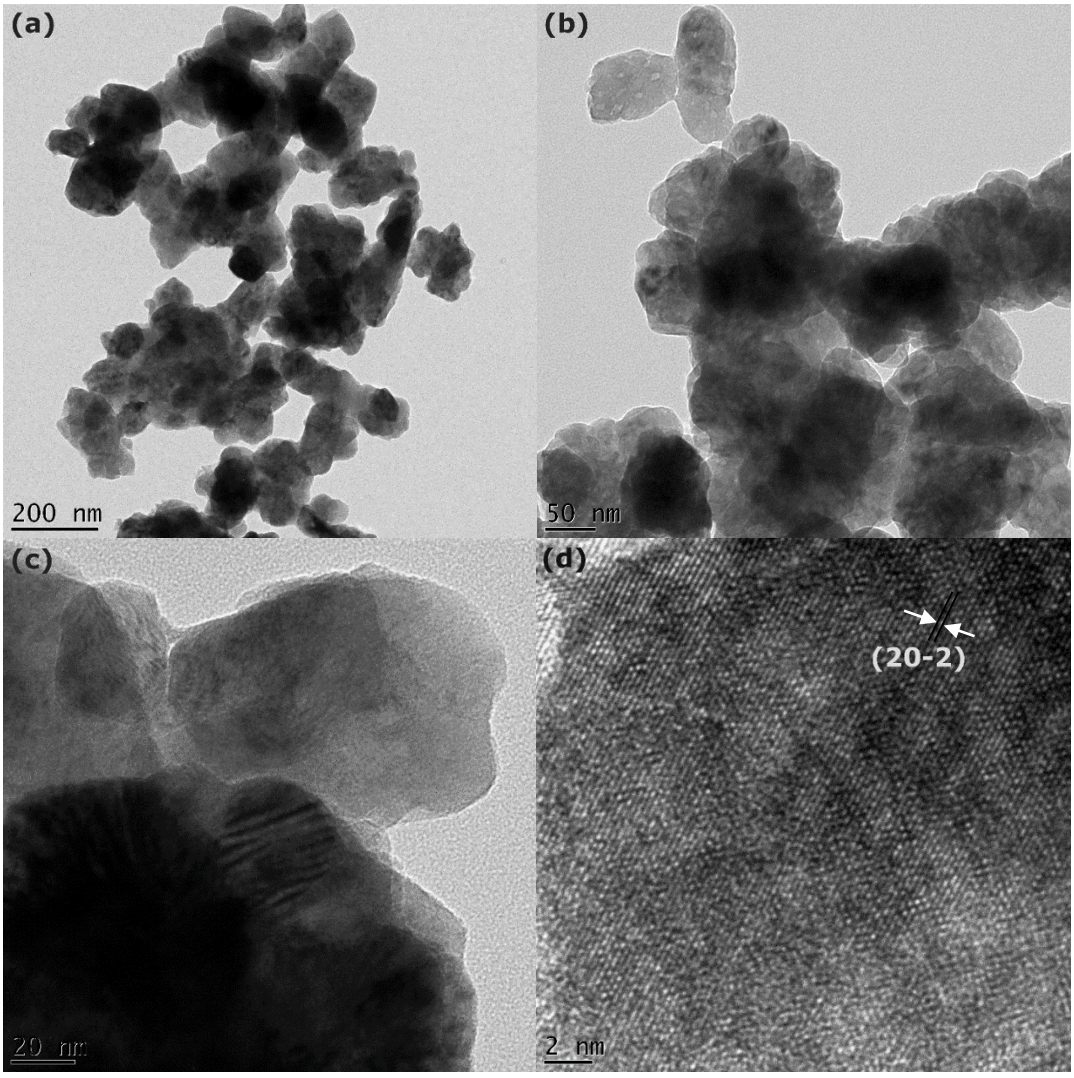

***Figure 4.36**: HRTEM images of VO_2 (M) nanoparticles by green process (a-c) with clear lattice fringes (d).*

As observed from Figure 4.36 (a-d), the nanoparticles exhibited crystalline structures and clear lattice fringes of VO_2 (M) phase. Morphology observation of the VO_2 (M) nanoparticles, Figure 4.36 (a, b), clearly shows granular structure with an average size of 50–100 nm.

Selected area electron diffraction (SAED) patterns of VO_2 nanoparticles in Figure 4.37 shows that the synthesized particles are crystalline.

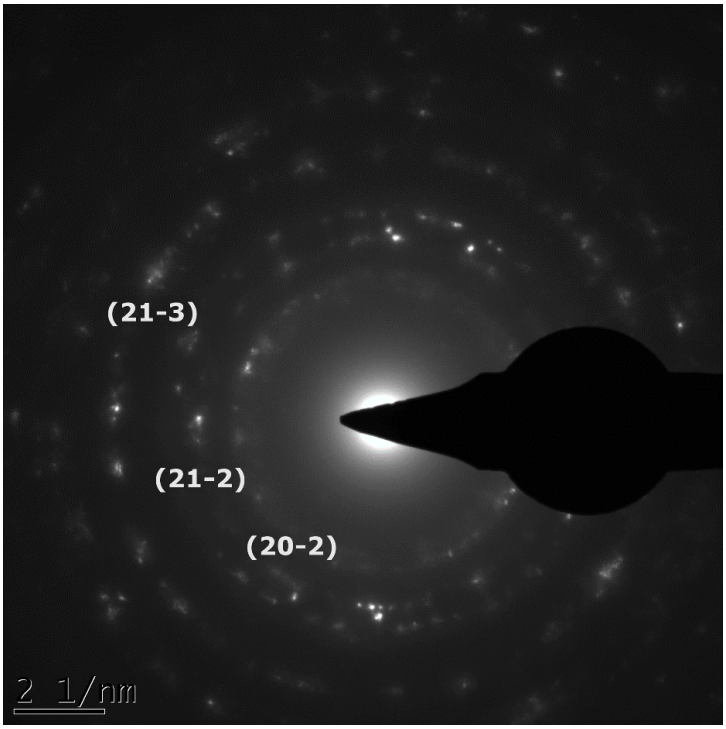

***Figure 4.37**: SAED ring patterns of VO_2 (M) by green process.*

Energy-dispersive X-ray spectroscopy (EDS)

Energy dispersive X-ray spectroscopy (EDS) analysis were made on a representative specimen to determine the chemical composition of undoped VO_2 nanoparticles synthesized by the green process, The EDS result as shown in Figure 4.38 revealed that the nanoparticles contain V and O only. From EDS spectrum it is observed that monoclinic VO_2 nanoparticles were successfully synthesized by the green process. The Cu peaks observed in the spectrum were from the instrument.

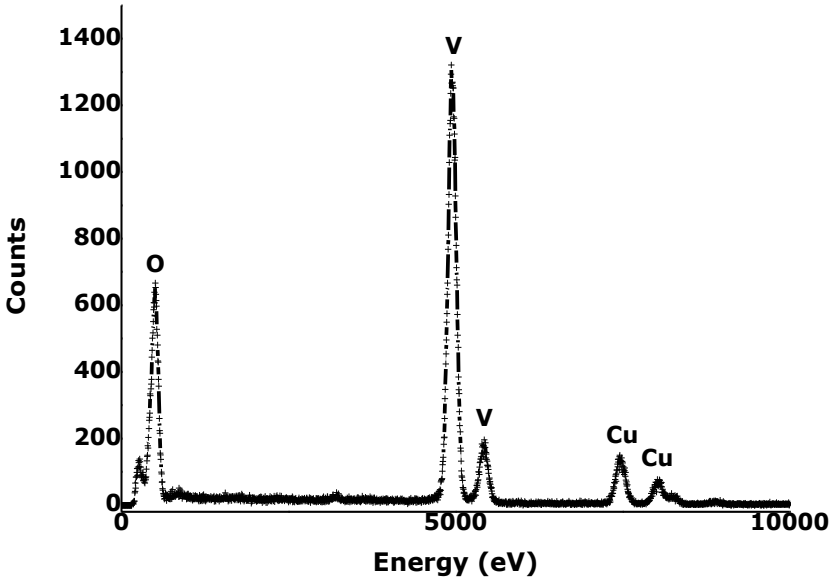

***Figure 4.38**: EDS spectrum of VO_2 (M) nanoparticles by green process.*

Fourier transformed infrared spectroscopy (FTIR)

FTIR measurement was conducted to study the chemical bonding between vanadium and oxygen atoms in the nanostructure of VO_2 synthesized by the green process. In Figure 4.39, the absorption at 2988.6 cm^{-1} is assigned to the stretching and bending vibration of H_2O [90] and the feature at 2013.5 cm^{-1} is due to CO_2 in the instrument [154]. The other three peaks at 1066.9 cm^{-1}, 961.1 cm^{-1} and 407.6 cm^{-1} are attributed to the stretching of V=O and V–O–V coupled vibration, respectively [153, 154].

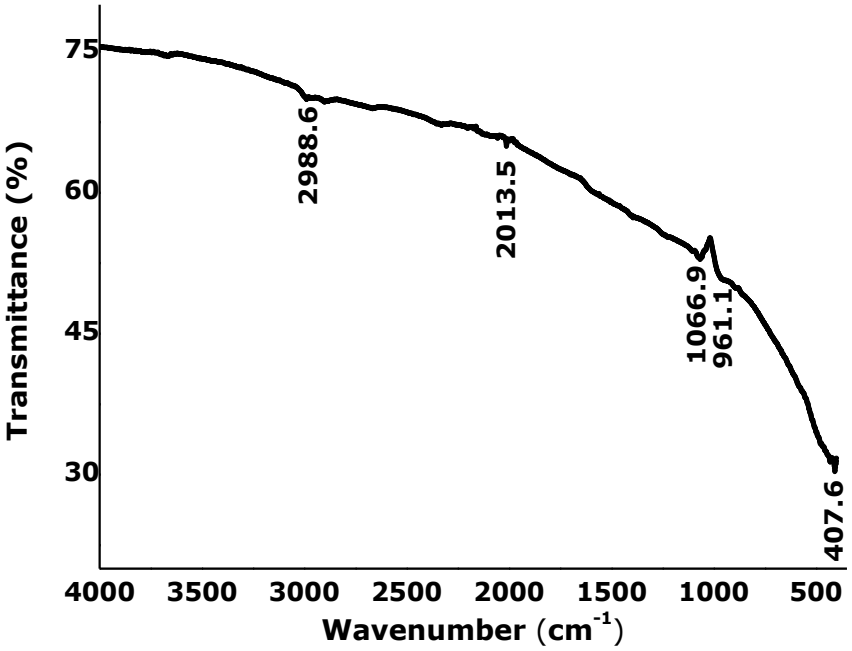

***Figure 4.39**: FTIR spectrum of VO_2 (M) nanoparticles by green process.*

CHAPTER FIVE

CONCLUSIONS AND FUTURE WORK

5.1 Conclusions

One of the dissertation's objectives was syntheses of undoped and doped VO_2 nanostructures by hydrothermal method, and characterization of the product to investigate various physical properties. In this regard, undoped VO_2 and Mg-, Mo-, Cr-doped VO_2 nanoparticles have been successfully synthesized and different techniques have been employed to characterize the products with the aim of investigating different physical properties of nanostructures.

XRD results showed that undoped VO_2 nanoparticles have been successfully synthesized and the doping has significant effect on reducing the phase transition temperature to lower values. SEM and HRTEM results revealed the nanoparticles are rod shaped for hydrothermal method and are granular in shape for green process. DSC curves showed transition temperature were in the range of 66-68 ^{0}C for undoped VO_2 and found to decrease with increasing dopant concentration.

The second and major objective of this dissertation was synthesis of pure VO_2 nanostructures by green process, and characterization of the product to investigate various physical properties. In this regard, VO_2 nanoparticles have been successfully synthesized and different techniques have been employed to characterize the products with the aim of investigating different physical properties of nanostructures.

In conclusion,

1. Undoped thermochromic VO_2(M) and Mg, Cr, Mo doped thermochromic VO_2(M) have been successfully synthesized with 6-48 hours hydrothermal process followed by two hours thermal annealing under vacuum at 500°C. Lower values of MIT were achieved for annealing at 6 hours. Moreover, the MIT decreases with increasing dopant concentration as observed from DSC curves for the synthesized Mg-, Cr- Mo doped nanoparticles. Our result, thus, revealed that the phase transition temperature of VO_2 decreases due to Mg-, Mo, Cr- doping. Moreover, the Mg/Mo codoping of VO_2 has been conducted for the first time and results in better reduction of the phase transition temperature.

2. The plant extract based nanoparticles synthesis technique is not expensive, easily scalable to mass production and environmentally friendly. Moreover, convenient for synthesis of non-toxic nanoparticles of multifunctional purposes.

5.2 Future Work

Optimization of results for the green process and doping with various transition metals for multifunctional material synthesis will be considered in future studies. Green syntheses of vanadium dioxide and tungsten oxide are the researcher's future interest. Specifically, for applications such as in SRD space crafts, Li-ion batteries improvement making graphene-vanadium composites will be the researcher's future task. Due to time constraint (six months only to conduct the whole Lab. work), the researcher didn't perform optical property and transport measurement tests for the synthesized samples. In future, transport measurements and optical properties studies would be emphasized to obtain complete information.

References

[1] L. H. Yeo, A. Srivastava, M. A. Majidi, R. Sutarto, F. He, S. M. Poh, et al., Anomalous spectral-weight transfers un ravelling oxygen screening and electronic correlations in the insulator-metal transition of VO_2, Phys. Rev. B 91 (2015) 081112-5.

[2] M. M. Qazilbash, M. Brehm, B. G. Chae, P. C. Ho, G. O. Andreev, B. J. Kim, S. J. Yun, A. V. Balatsky, M. B. Maple, F. Keilmann, H. T. Kim, and D. N. Basov, Mott transition in VO_2 revealed by infrared spectroscopy and nano-imaging, Science 318 (2007)1750-1753.

[3] M. Maaza, B.D. Ngom, M. Achouri, K. Manikandan, Functional nanostructured oxides, Vacuum 114 (2015) 172-187.

[4] W. -T. Liu, J. Cao, W. Fan, Z. Hao, M. C. Martin, Y. R. Shen, J. Wu, and F. Wang, Intrinsic Optical Properties of Vanadium Dioxide near the Insulator-Metal Transition, Nano Lett. 11 (2011) 466–470.

[5] A. P. Ramirez, Colossal magnetoresistance, J. Phys.: Condens. Matter 9 (1997) 8171.

[6] A. Cavalleri, Th. Dekorsy, H. H. W. Chong, J. C. Kieffer, and R. W. Schoenlein, Evidence for a structurally-driven insulator-to-metal transition in VO_2: A view from the ultrafast timescale, Phys. Rev. B 70 (2004) 161102 (R); J. Wei and D. Natelson, Nanostructure studies of strongly correlated materials, Nanoscale 3 (2011) 3509-3521.

[7] G. Kotliar, D. Vollhardt, Strongly correlated materials: Insights from dynamic-mean field theory, Phys. Today 57(2004) 53-59.

[8] D. Adler and H. Brooks, Theory of Semiconductor-To-Metal Transitions, Phys. Rev. 155 (1967) 826-840.

[9] D. Adler, Mechanism for Metal-Nonmetal Transitions in Transition –Metal Oxides and Sulfides, Rev. Mod. Phys. 40 (1968) 714-736.

[10] M. M. Qazilbash,1, A. A. Schafgans, K. S. Burch, S. J. Yun, B. G. Chae, B. J. Kim, H. T. Kim, and D. N. Basov, Electrodynamics of the vanadium oxides VO_2 and V_2O_3, Phys. Rev. B 77 (2008) 115121-10.

[11] D. Fu, K. Liu, T. Tao, K. Lo, C. Cheng, B. Liu, R. Zhang, H. A. Bechtel, and J. Wu, Comprehensive study of the metal-insulator transition in pulsed laser deposited epitaxial VO_2 thin films, J. Appl. Phys. 113(2013) 043707.

[12] D. H. Kim and H. S. Kwok, Pulsed laser deposition of VO_2 thin films, Appl. Phys. Lett. 65(1994) 3188-3190.

[13] M. M. Qazilbash, A. Tripathi, A. A. Schafgans, Bong-Jun Kim, Hyun-Tak Kim, Zhonghou Cai, M. V. Holt, J. M. Maser, F. Keilmann, O. G. Shpyrko, and D. N. Basov, Nanoscale imaging of the electronic and structural transitions in vanadium dioxide, Phys. Rev. B 83 (2011) 165108.

[14] W. Li, S. Ji, Y. Li, A. Huang, H. Luo and P. Jin, Synthesis of VO_2 nanoparticles by a hydrothermal assisted homogeneous precipitation approach for thermochromic applications, RSC Adv. 49 (2014) 13026-13033.

[15] F.J. Morin, Oxides which show a metal-to-insulator transition at the nèel temperature, Phys. Rev. Lett.3 (1959) 34–36.

[16] T. J. Huffman, Peng Xu, A. J. Hollingshad, M. M. Qazilbash, Lei Wang, R. A. Lukaszew, S. Kittiwatanakul, Modification of electronic structure in compressively strained vanadium dioxide films, Phys. Rev. B 91 (2015) 205140.

[17] M. Maaza, D. Hamidi, A. Simo, T. Kerdja, A. K. Chaudhar, J. B. Kana Kana, Optical lmiting in pulsed laser deposited VO_2 nanostructures, Opt. Commun. 285 (2012) 1190-1193.

[18] M. Maaza, A. Simo, B. M. Itani, J. B. Kana Kana, S. El Harthi, K. Bouziane, M. L. Saboungi, T. B. Doyle, I. Luk'yanchuk, Phase transition in a single VO_2 nano-crystal: potential femtosecond tunable opto-electronic nano-gating, J. Nanopart. Res. 16 (2014) 2397.

[19] Z. Chen, Y. Gao, L. Kang, C. Cao, S. Chena and H. Luo, Fine crystalline VO_2 nanoparticles: synthesis, abnormal phase transition temperatures and excellent optical properties of a derived VO_2 nanocomposite foil, J. Mater. Chem. A 2 (2014) 2718.

[20] X. Gong, J. Li, S. Chen, and W. Wen, Copolymer solution-based smart window, Appl. Phys. Lett. 95 (2009) 251907; DOI: 10.1063/1.3276289.

[21] F.Y. Kong, M. Li, S.S. Pan, Y.X. Zhang, G.H. Li, Synthesis and thermal stability of W-doped VO_2 nanocrystals, Mater. Res. Bull. 46 (2011) 2100–2104.

[22] Z. Peng, W. Jiang, and H. Liu, Synthesis and Electrical Properties of Tungsten- doped Vanadium Dioxide Nanopowders by Thermolysis, J. Phys. Chem. C 111(2007) 1119-1122.

[23] J. Zou, Y. Peng and H. Lin, A low-temperature synthesis of monoclinic VO_2 in an atmosphere of air, J. Phys. Chem. A 1 (2013) 4250–4254.

[24] K.R. Speck, H.S.-W. Hu, M.E. Sherwin and R.S. Potember, Vanadium dioxide films grown from vanadium tetra isopropoxide by the sol-gel process, Thin Solid Films 165 (1988) 317-322.

[25] N. Yuan, J. Li, G. Li, X. Chen, The large modification of phase transition characteristics of VO_2 films on SiO_2/Si substrates, Thin Solid Films 515 (2006) 1275–1279.

[26] K. C. Kam, A. K. Cheetham, Thermochromic VO_2 nanorods and other vanadium oxides nanostructures, Mater. Res. Bull.41 (2006) 1015–1021.

[27] L. Dai, C. Cao, Y. Gao, H. Luo, Synthesis and phase transition behavior of undoped VO_2 with a strong nano-size effect, Sol. Energy Mater. Sol. Cells 95 (2011) 712–715.

[28] G. Karaoglan-Bebek, M. N. F. Hoque, M. Holtz, Z. Fan, and A. A. Bernussi, Continuous tuning of W-doped VO_2 optical properties for terahertz analog applications, Appl. Phys. Lett. 105 (2014) 201902; DOI: 10.1063/1.4902056.

[29] B. W. Mwakikunga, E. Sideras-Haddad, M. Maaza, First synthesis of vanadium dioxide by ultrasonic nebula-spray pyrolysis, Opt. Mater. 29 (2007) 481–487.

[30] M. Pan, H. Zhong, S-w Wang, Z. Li, X. Chen, W. Lu, First-principle study on the chromium doping effect on the crystal structure of metallic VO_2, Chem. Phys. Lett. 398 (2004) 304–307.

[31] I. P. Parkin and T. D. Manning, Intelligent Thermochromic Windows, J. Chem. Educ. 83 (2006) 393-400.

[32] W. Ning, H. Yizhong, S. Magdassi, D. Mandler, L. Hai and L. Yi, Formation of VO_2 zero-dimensional/nanoporous layers with large supercooling effects and enhanced thermochromic properties, RSC Adv. 3 (2013) 7124.

[33] N. Wang, S. Magdassi, D. Mandler, Y. Long, Simple sol–gel process and one-step annealing of vanadium dioxide thin films: Synthesis and thermochromic properties, Thin Solid Films 534 (2013) 594-598.

[34] Y. Ningyi, L. Jinhua, L. Chenglu, Valence reduction process from sol-gel V_2O_5 to VO_2 thin films, Appl. Surf. Sci. 191 (2002) 176-180.

[35] X. Xiao, H. Zhang, G.Q. Chai, Y.M. Sun, T. Yang, H.L. Cheng, L.H. Chen, L. Miao, G. Xu, A cost-effective process to prepare VO_2 (M) powder and films with superior thermochromic properties, Mater. Res. Bull. 51 (2014) 6–12.

[36] S. H. Chen, H. Ma, X. J. Yi, T. Xiong, H. C. Wang, and C. J. Ke, Smart VO_2 thin film for protection of sensitive infrared detectors from strong laser radiation, Sens. Actuators A 115 (2004) 28-31.

[37] Z. Huang, S. Chen, C. Lv, Y. Huang, and J. Lai, Infrared characteristics of VO_2 thin films for smart window and laser protection applications, Appl. Phys. Lett. 101 (2012)191905.

[38] M. Benkahoul, M. Chaker, J. Margot, J. E. Haddad, R. Kruzelecky, B. Wong, W. Jamroz, P. Poinas, Thermochromic VO_2 film deposited on Al with tunable thermal emissivity for space applications, Sol. Energy Mater. Sol. Cells 95 (2011) 3504–3508.

[39] A. Hendaoui, N. Émond, S. Dorval, M. Chaker, E. Haddad, VO_2-based smart coatings with improved emittance-switching properties for an energy-efficient near room-temperature thermal control of space crafts, Sol. Energy Mater. Sol. Cells 117 (2013)494–498.

[40] A. Hendaoui, N. Émond, S. Dorval, M. Chaker, E. Haddad, Enhancement of the positive emittance-switching performance of thermochromic VO_2 films deposited on Al substrate for an efficient passive thermal control of spacecrafts, Curr. Appl. Phys. Lett.13 (2013) 875-879.

[41] Y.-B. Kang, Critical evaluation and thermodynamic optimization of the VO–$VO_{2.5}$ system, J. Eur. Ceram. Soc. 32 (2012) 3187–3198.

[42] J. Y. Suh, R. Lopez, L. C. Feldman, and R. F. Haglund, Jr., Semiconductor to metal phase transition in the nucleation and growth of VO_2 nanoparticles and thin films, J. Appl. Phys. 96 (2004) 1209-1213.

[43] M.J. Miller and J. Wang, Influence of grain size on transition temperature of thermochromic VO_2, J. Appl. Phys. 117 (2015) 034307.

[44] A. Lafort, H. Kebaili, S. Goumri-Said, O. Deparis, R. Cloots, J. De Coninck, M. Voué, F. Mirabella, F. Maseri , S. Lucas, Optical properties of thermochromic VO_2 thin films on stainless steel: Experimental and theoretical studies, Thin Solid Films 519 (2011) 3283–3287.

[45] D. Vernardou, P. Paterakis, H. Drosos, E. Spanakis, I. M. Povey, M. E. Pemble, E. Koudoumas, N. Katsarakis, A study of the electrochemical performance of vanadium oxide thin films grown by atmospheric pressure chemical vapour deposition, Sol. Energy Mater. Sol. Cells 95 (2011) 2842–2847.

[46] T. Maruyama, Y. Ikuta, Vanadium dioxide thin films prepared by chemical vapour deposition from vanadium (III) acetylacetonate, J. Mater. Sci. 28 (1993) 5073-5078.

[47] P. H. Jampani, O. Velikokhatnyi, K. Kadakia, D. H. Hong, S. S. Damle, J. A. Poston, A. Manivannan and P. N. Kumta, High energy density titanium doped-vanadium oxide-vertically aligned CNT composite electrodes for supercapacitor applications, J. Mater. Chem. A 3 (2015) 8413-8432.

[48] M. Borek, F. Qian, V. Nagabushnam, and R. K. Singh, Pulsed laser deposition of oriented VO_2 thin films on Rcut sapphire substrates, Appl. Phys. Lett. 63 (1993) 3288.

[49] L. Mathevula, B.D. Ngom, L. Kotsedi, P. Sechogela, T.B. Doyle, M. Ghouti, M. Maaza, Thermochromic VO_2 on Zinnwaldite Mica by pulsed laser deposition, Appl. Surf. Sci. 314 (2014) 476–480.

[50] M. Maaza, K. Bouziane, J. Maritz, D.S. McLachlan, R. Swanepool, J.M. Frigerio, M. Every, Direct production of thermochromic VO_2 thin film coatings by pulsed laser ablation. Opt. Mater. 15 (2000) 41-45.

[51] E. M. Heckman, L. P. Gonzalez, S. Guha, J. O. Barnes, A. Carpenter, Electrical and optical switching properties of ion implanted VO_2 thin films, Thin Solid Films 518 (2009) 265–268.

[52] P. Jin, S. Nakao, S. Tanemur, Tungsten doping into vanadium dioxide thermochromic films by high-energy ion implantation and thermal annealing, Thin Solid Films 324 (1998) 151–158.

[53] L. Zhao, L. Miao, S. Tanemura, J. Zhou, L. Chen, X. Xiao, G. Xu, A low cost preparation of VO_2 thin films with improved thermochromic properties from a solution-based process, Thin Solid Films 543 (2013) 157–161.

[54] J.D. Zhou, Y.G. Gao, X.L. Liu, Z. Chen, L. Dai, C.X. Cao, H.J. Luo, M. Kanahira, C. Sun and L. Yan, Mg-doped VO_2 nanoparticles: hydrothermal synthesis, enhanced visible transmittance and decreased metal–insulator transition temperature, Phys. Chem. Chem. Phys.15 (2013) 7505-7511.

[55] S. Wang, M. Liu, L. Kong, Y. Long, X. Jiang, A. Yu, Recent progress in VO_2 smart coatings: Strategies to improve the thermochromic properties, Prog. Mater. Sci. 81 (2016) 1–54.

[56] Y.-T.Wang, C.H. Chen, Facile growth of thermochromic VO_2 nanostructures with greatly varied phases and morphologies, Inorg. Chem. 52 (2013) 2550–255.

[57] L. Zhong, M. Li, H. Wang, Y. Luo, J. Pana and G. Li, Star-shaped VO_2 (M) nanoparticle films with high thermochromic performance, CrystEngComm 17 (2015) 5614-5619.

[58] G. P. Nagabhushana and G. T. Chandrappa, Facile solution combustion synthesis of monoclinic VO_2: a unique and versatile approach, J. Mater. Chem. A 1 (2013) 11539.

[59] V. Kumar and S. K. Yadav, Plant-mediated synthesis of silver and gold nanoparticles and their applications, J. Chem. Technol. Biotechnol. 84 (2009) 151–157.

[60] R. Satyavathi, M. B. Krishna, S. V. Rao, R. Saritha, D. N. Rao, Biosynthesis of silver nanoparticles using Coriandrum sativum leaf extract and their application in non-linear optics, Adv. Sci. Lett. 3 (2010) 1-6.

[61] J. K. Patra and K-H. Baek, Green Nanobiotechnology: Factors Affecting Synthesis and Characterization Techniques, J. Nanomater. http://dx.doi.org/10.1155/2014/417305

[62] J. Jeevanandam, Y.S. Chan, M. K. Danquah, Biosynthesis of Metal and Metal Oxide Nanoparticles, ChemBioEng Rev 3 (2016) 55–67.

[63] S. Baker, D. Rakshith, K. S. Kavitha, P. Santosh, H. U. Kavitha, Y. Rao, S. Satish, Plants: Emerging as Nanofactories towards Facile Route in Synthesis of Nanoparticles, BioImpacts 3 (2013) 111-117.

[64] A. K. Mittal, Y. Chisti, U. C. Banerjee, Synthesis of metallic nanoparticles using plant extracts, Biotechnol. Adv. 31 (2013) 346–356.

[65] M. Shah, D. Fawcett, S. Sharma, S. K. Tripathy and G. E. Jai Poinern, Green Synthesis of Metallic Nanoparticles via Biological Entities, Materials 8 (2015) 7278–7308.

[66] V. V. Makarov, A. J. Love, O. V. Sinitsyna, S. S. Makarova, I. V. Yaminsky, M. E. Taliansky, N. O. Kalinina, "Green" Nanotechnologies: Synthesis of Metal Nanoparticles Using Plants, Acta Nature 6(2014)35-44.

[67] Z. Chen, Y. Gao, L. Kang, J. Dua, Z. Zhang, H. Luo, H. Miao, G. Tan, VO_2-based double-layered films for smart windows: Optical design, all-solution preparation and improved properties, Sol. Energy Mater. Sol. Cells 95(2011)2677–2684.

[68] C. G. Granqvist, Solar energy materials, Adv. Mater. 15(2003) 1789-1803.

[69] M. Kamalisarvestani, R.Saidur, S.Mekhilef, F.S.Javadi, Performance, materials and coating technologies of thermochromic thin films on smart windows, Renew. Sustain. Energy Rev. 26(2013)353–364.

[70] M. J. Powell, P. Marchand, C. J. Denis, J. C. Bear, J. A. Darr and I. P. Parkin, Direct and Continuous Synthesis of VO_2 Nanoparticles, Nanoscale, DOI: 10.1039/c5nr04444h

[71] C.G. Granqvist, Electrochromics for smart windows: Oxide-based thin films and devices, Thin Solid Films 564 (2014) 1-38.

[72] C.-J. Liu, U. Burghaus, F. Besenbacher, and Z.L. Wang, Preparation and characterization of Nanomaterials for Sustainable Energy Production, ACSNANO 4 (2010) 5517–5526.

[73] Y. Zhang, C. Chen, W. Wu, F. Niu, X. Liu, Y.Zhong, Y. Cao, X. Liu, C. Huang, Facile hydrothermal synthesis of vanadium oxides nanobelts by ethanol reduction of peroxovanadium complexes, Ceram. Int. 39(2013)129–141.

[74] J. Nag, R. F. H. Jr, Synthesis of vanadium dioxide thin films and nanoparticles, J. Phys.: Condens. Matter 20 (2008) 264016.

[75] N. Shen, S. Chen, Z. Chen, X. Liu, C. Cao, B. Dong, H. Luo, J. Liu and Y. Gao, The synthesis and performance of Zr-doped and W–Zr-codoped VO_2 nanoparticles and derived flexible foils, J. Phys. Chem. A 2 (2014) 15087–15093.

[76] S. Lysenko, A.J. Rua, V. Vikhnin, J. Jimenez, F. Fernandez, H. Liu, Light-induced ultrafast phase transitions in VO_2 thin film, Appl. Surf. Sci. 252 (2006) 5512-5515.

[77] A. Cavalleri, Cs. Tóth, C.W. Siders, and J. A. Squier, Femtosecond Structural Dynamics in VO_2 during an Ultrafast Solid-Solid Phase Transition, Phys. Rev. Lett. 87 (2001) 237401-1.

[78] G. Stefanovich, A. Pergament, D. Stefanovich, Electrical switching and Mott transition in VO_2, J. Phys.: Condens. Matter 12 (2000) 8837-8845.

[79] H.-T. Kim, B.-G. Chae, D.-H. Youn, G. Kim, K.-Y. Kang, S.-J. Lee, K. Kim, and Y.-S.

Lim, Raman study of electric-field-induced first-order metal-insulator transition in VO_2-based devices, Appl. Phys. Lett. 86 (2005) 242101.

[80] J. Jeong, N. Aetukuri, T. Graf, T. D. Schladt, M. G. Samant, S.P. Parkin, Suppression of Metal-Insulator Transition in VO_2 by Electric Field–Induced Oxygen Vacancy Formation, Science, 339 (213) 1402-1405.

[81] H. Zhang, X. Xiao, X. Lu, G. Chai, Y. Sun, Y. Zhan, G. Xu, A cost-effective method to fabricate VO_2 (M) nanoparticles and films with excellent thermochromic properties, J. Alloys Compd. 636 (2015) 106–112.

[82] J. Livage, D. Ganguli, Sol–gel electrochromic coatings and devices: a review, Sol. Energy Mater. Sol. Cells 68 (2001) 365–381.

[83] S. Ji, F. Zhang, P. Jin, Preparation of high performance pure single phase VO_2 nanopowder by hydrothermally reducing the V_2O_5 gel, Sol. Energy Mater. Sol. Cells 95 (2011) 3520–3526.

[84] J. Lu, H. Liu, S. Deng, M. Zheng, Y. Wang, J. A. van Kan, S. H. Tang, X. Zhang, C. H. Sow and S.G. Mhaisalkard, Highly sensitive and multispectral responsive phototransistor using tungsten-doped VO_2 Nanowires, Nanoscale 2014; DOI: 10.1039/c4nr00898g.

[85] Y. Gao, C. Cao, L. Dai, H. Luo, M. Kanehira, Y. Ding and Z. L. Wang, Phase and shape controlled VO_2 nanostructures by antimony doping, Energy Env. Sci. 5 (2012) 8708.

[86] X. Xiao, H. Cheng, G. Dong, Y. Yu, L. Chen, L. Miao and G. Xu, A facile process to prepare one dimension VO_2 nanostructures with superior metal–semiconductor transition, CrystEngComm. 15 (2013) 1095–1106.

[87] D. Li, M. Li, J. Pan, Y. Luo, H. Wu, Y. Zhang, and G. Li, Hydrothermal Synthesis of Mo-Doped VO_2/TiO_2 Composite Nanocrystals with Enhanced Thermochromic Performance, ACS Appl. Mater. Interf. 2014, 6, 6555−6561.

[88] H. Hayashi and Y. Hakuta, Hydrothermal Synthesis of Metal Oxide Nanoparticles in Supercritical Water, Materials 3 (2010) 3794-3817; DOI: 10.3390/ma3073794

[89] C. Wu, X. Zhang, J. Dai, J. Yang, Z. Wu, S. Wei, Y. Xie, Direct hydrothermal synthesis of monoclinic VO_2 (M) single-domain nanorods on large scale displaying magnetocaloric effect, J. Phys. Chem. 21 (2011) 4509–4517.

[90] W. Chen, J.F. Peng, L.Q. Mai, H. Yu, Y.Y. Qi, Synthesis and characterization of novel vanadium dioxide nanorods, Solid State Commun. 132 (2004) 513–516.

[91] J.F. Liu, Q.H. Li, T.H. Wang, D.P. Yu, Y.D. Li, Metastable vanadium dioxide nanobelts: hydrothermal synthesis, electrical transport, and magnetic properties, Angew. Chem. Inter. Edit. 43 (2004) 2409–2411.

[92] L. Sikong, P. Kumbour, A new route for thermochromic vanadium dioxide synthesis, Dig. J. Nanomater. Biostruct. 10 (2015)135-140.

[93] M. Li, X. Wu, L. Li, Y. Wang, D. Li, J. Pan, S. Li, L. Sun and G. Li, Defect-mediated phase transition temperature of VO_2 (M) nanoparticles with excellent thermochromic performance and low threshold voltage, J. Phys. Chem. A 2(2014) 4520-4523.

[94] N. R. Mlyuka, G. A. Niklasson, and C. G. Granqvist, Mg doping of thermochromic VO_2 films enhances the optical transmittance and decreases the metal-insulator transition temperature, Appl. Phys. Lett. 95, 171909 (2009); DOI: 10.1063/1.3229949.

[95] S. Surnev, M.G. Ramsey, F.P. Netzer, Vanadium oxide surface studies, Prog. Surf. Sci. 73 (2003) 117–165.

[96] N. Bahlawane and D. Lenoble, Vanadium Oxide Compounds: Structure, Properties, and Growth from the Gas Phase, Chem. Vap. Deposition 2014, 20, 299–311.

[97] S. Shin, S. Suga, M. Taniguchi, M. Fujisawa, and H. Kanzaki, A. Fujimori, H. Daimon, Y. Ueda, K. Kosuge, and S. Kachi, Vacuum-ultraviolet reflectance and photoemission study of the metal-insulator phase transitions in VO_2, V_6O_{13}, and V_2O_3, Phys. Rev. B 41 (1990) 4993-5009.

[98] M. Imada, A. Fujimori, and Y. Tokura, Metal-insulator transitions, Rev. Mod. Phys. 70 (1998) 1039-1263.

[99] J. Cao, W. Fan, K. Chen, N. Tamura, M. Kunz, V. Eyert, and J. Wu, Constant threshold

resistivity in the metal-insulator transition of VO_2, Phys. Rev. B 82 (2010) 241101.

[100] D. Guo, C. Hua, Q. Yang, H. Hua, W. Li, C. Kong, Room-temperature ferromagnetism properties of monoclinic VO_2 (M_1) Nanobelts, Mater. Res. Bull. 53 (2014) 102–106.

[101] S. Biermann, A. Poteryaev, A. I. Lichtenstein, and A. Georges, Dynamical singlets and Correlation-assisted Peierls transition in VO_2, Phys. Rev. Lett. 94(2) (2005) 026404.

[102] A. Tselev, I. A. Luk'yanchuk, I. N. Ivanov, J. D. Budai, J. Z. Tischler, E. Strelcov, A. Kolmakov, and S. V. Kalinin, Symmetry Relationship and Strain-Induced Transitions between Insulating M1 and M2 and Metallic R phases of Vanadium Dioxide, Nano Lett. 10 (2010) 4409-4416.

[103] J. M. Booth and P. S. Casey, Anisotropic Structure Deformation in the VO_2 Metal-Insulator Transition, Phys. Rev. Lett. 103 (2009) 086402.

[104] B. J. Kim, Y. W. Lee, S. Choi, J. W. Lim, S. J. Yun, H. T. Kim, T. J. Shin, and H. S. Yun, Micrometer x-ray diffraction study of VO_2 films: Separation between metal-insulator transition and structural phase transition, Phys. Rev. B 77 (2008) 235401.

[105] G. Anderson, Studies on Vanadium Oxides, Acta Chem. Scand. 10 (1956) 623- 628.

[106] D. B. McWhan, M. Marezio, J. P. Remeika, and P. D. Dernier, X-ray diffraction study of metallic VO_2, Phys. Rev. B 10 (1974) 490-495.

[107] J. B. Goodenough, Two Components of Crystallographic Transition in VO_2, J. Solid State Chem. 3 (1971) 490-500.

[108] T. Christmann, B. Felde, W. Niessner, D. Schalch, A. Scharmann, Thermochromic VO_2 thin films studied by photoelectron spectroscopy, Thin Solid Films 287 (1996) 134-138.

[109] J. Narayan and V. M. Bhosle, Phase transition and critical issues in structure-property correlations of vanadium oxide, J. Appl. Phys. 100 (2006)103524.

[110] V. Eyert, The metal-insulator transitions of VO_2: A band theoretical approach, Ann. Phys. (Leipzig) 11 (2002) 650-702.

[111] V. Eyert, VO_2: A Novel View from Band Theory, Phys. Rev. Lett. 107 (2011)

016401.

[112] I. G. Austin and N. F. Mott, Metallic and Nonmetallic Behavior in Transition Metal Oxides, Science 168 (1970) 71-77.

[113] N.F. Mott, The transition to the metallic state, Philos. Mag. 6 (1961) 287-309.

[114] T. M. Rice, H. Launois, and J. P. Pouget, Comment on VO_2 - Peierls or Mott-Hubbard A view from Band theory, Phys. Rev. Lett. 73 (1994) 3042-3042.

[115] R. M. Wentzcovitch, W. W. Schulz, and P. B. Allen, VO_2-Peierls or Mott-Hubbard – A view from Band Theory, Phys. Rev. Lett. 72 (1994) 3389-3392.

[116] B. Lazarovits, K. Kim, K. Haule, and G. Kotliar, Effects of strain on the electronic structure of VO_2, Phys. Rev. B 81 (2010) 115117.

[117] A. Zylbersztejn and N. F. Mott, Metal-insulator transition in vanadium dioxide, Phys. Rev. B 11 (1975) 4383-4395.

[118] F. Evers & A. D. Mirlin, Anderson transitions. Rev. Mod. Phys. 80 (2008)1355-1417.

[119] N.B. Aetukuri, A.X. Gray, M. Drouard, M. Cossale, L. Gao, A. H. Reid, et al., Control of the metal–insulator transition in vanadium dioxide by modifying orbital occupancy, Nat. phys. 2013; DOI: 10.1038/NPHYS2733.

[120] M. Abbate, F. M. F. de Groot, J. C. Fuggle, Y. J. Ma, C. T. Chen, F. Sette, et al. Soft-x-ray-absorption studies of the electronic-structure changes through the VO_2 phase transition, Phys. Rev. B 43 (1991) 7263-7266.

[121] H. Kim, Y. Kim, T.Y. Kim, A-R. Jang, H. Y. Jeong, S. H. Han, D. H. Yoon, H. S. Shin, D.J. Bae, K.S Kim and W. S. Yang, Enhanced optical response of hybridized VO_2/graphene films, Nanoscale 5 (2013) 2632–2636.

[122] M. Pan, H. Zhong, S. Wang, J. Liu, Z. Li, X. Chen, W. Lu, Properties of VO_2 thin film prepared with precursor $VO(acac)_2$, J. Cryst. Growth 265 (2004) 121–126.

[123] C.N. Berglund and H.J. Guggenheim, Electronic properties of VO_2 near the semiconductor-metal transition, Phys. Rev. 185 (1969) 1022-1033.

[124] A.C. Serena, M. Grossman, J. D. Furman, B. C. Melot, A. K. Cheetham, K. R. Heier,

and R. Seshadri, Controlled Reduction of Vanadium Oxide Nanoscrolls: Crystal Structure, Morphology, and Electrical Properties, Chem. Mater. 20 (2008) 6396–6404.

[125] Y. Zhao, C. Chen, X. Pan, Y. Zhu, M. Holtz, A. Bernussi, and Z. Fan, Tuning the properties of VO_2 thin films through growth temperature for infrared and terahertz modulation applications, J. Appl. Phys. 114 (2013) 113509-5.

[126] M. Nakano, K. Shibuya, N. Ogawa, T. Hatano, M. Kawasaki, Y. Iwasa, and Y. Tokura, Infrared-sensitive electrochromic device based on VO_2, Appl. Phys. Lett. 103(2013) 153503.

[127] W.R. Roach, Holographic Storage in VO_2, Appl. Phys. Lett. 19 (1971) 453.

[128] Y. Liu, E. Uchaker, N. Zhou, J. Li, Q. Zhang and G. Cao, Facile synthesis of nanostructured vanadium oxide as cathode materials for efficient Li-ion batteries, J. Phys. Chem. 22 (2012) 24439–24445.

[129] Y. Shi, S.-L. Chou, J.-Z. Wang b, H.-J. Li, H.-K. Liu, Y.-P. Wu, In-situ hydrothermal synthesis of graphene woven VO_2 nanoribbons with improved cycling performance, J. Power Sources 244 (2013) 684-689.

[130] S. Zhang, M. A. Kats, Y. Cui, Y. Zhou, Y. Yao, S. Ramanathan, and F. Capasso, Current-modulated optical properties of vanadium dioxide thin films in the phase transition region, Appl. Phys. Lett. 105 (2014) 211104; DOI: 10.1063/1.4902924.

[131] M. Liu, H. Y. Hwang, H. Tao, A. C. Strikwerda, K. Fan, G. R. Keiser, et.al, Terahertz-field-induced insulator-to-metal transition in vanadium dioxide metamaterial, Nature 487(2012) 345-348.

[132] M.A. Kats, R. Blanchard, S. Zhang, P. Genevet, C. Ko, S. Ramanathan, and F. Capasso, Vanadium Dioxide as a Natural Disordered Metamaterial: Perfect Thermal Emission and Large Broadband Negative Differential Thermal Emittance, Phys. Rev. X 3 (2013) 041004.

[133] M. D. Goldflam, M. K. Liu, B. C. Chapler, H. T. Stinson, A. J. Sternbach, A. S. McLeod, J. D. Zhang, K. Geng, M. Royal, Bong-Jun Kim, R. D. Averitt, N. M. Jokerst, D. R. Smith, H-T. Kim, and D. N. Basov, Voltage switching of a VO_2 memory metasurface using ionic gel, Appl. Phys. Lett. 105 (2014) 041117; DOI: 10.1063/1.4891765.

[134] T. Driscoll, S. Palit, M. M. Qazilbash, M. Brehm, F. Keilmann, B.-G. Chae, S.-J. Yun, H.-T. Kim, S. Y. Cho, N. M. Jokerst, D. R. Smith, and D. N. Basov, Dynamic tuning of an infrared hybrid-metamaterial resonance using vanadium dioxide, Appl. Phys. Lett. 93 (2008) 024101.

[135] C.M. Zheng, J.L. Zhang, G.B. Luo, J.Q. Ye, M.M. Wu, Preparation of vanadium dioxide powders by thermolysis of a precursor at low temperature, J. Mater. Sci. 35 (2000) 3425–3429.

[136] C.S. Blackman, C. Piccirillo, R. Binions, Ivan P. Parkin, Atmospheric pressure chemical vapour deposition of thermochromic tungsten doped vanadium dioxide thin films for use in architectural glazing, Thin Solid Films 517 (2009) 4565–4570.

[137] P.-C.Lin, S.Lin, P.C.Wang, R.Sridhar, Techniques for physicochemical characterization of nanomaterials, Biotechnol. Adv. 32 (2014) 711–726.

[138] L. Long & H. Ye, How to be smart and energy efficient: A general discussion on thermochromic windows, Scientific Reports 4 (2014) 6427;DOI: 10.1038/srep06427.

[139] Z. Zhang, Y. V. Kaneti, X. Jiang, A. Yu, Hydrothermal synthesis of sodium vanadium oxide nanorods for gas sensing application, Sens. Actuators B 202(2014)803–809.

[140] A. Simo, B. Mwakikunga, B. T. Sone, B. Julies, R. Madjoe, M. Maaza, VO_2 nanostructures based chemiresistors for low power energy consumption hydrogen sensing, Int. J. Hydrogen Energy 39 (2014) 8147-8157.

[141] A. Simo, B. Mwakikunga and M. Maaza, One-Dimensional Vanadium Dioxide Nanostructures for Room Temperature Hydrogen Sensors, Sens. Transducers 189 (2015) 143-149.

[142] T. Guo, M.-S. Yao, Y.-H. Lin and C.-W. Nan, A comprehensive review on synthesis

methods for transition-metal oxide nanostructures, CrystEngComm 2015 DOI: 10.1039/c5ce00034c.

[143] H. Duan, D. Wang and Y. Li, Green chemistry for nanoparticle synthesis, Chem. Soc. Rev. 2015. DOI: 10.1039/c4cs00363b.

[144] C. H. Griffiths and H. K. Eastwood, Influence of stoichiometry on the metal-semiconductor transition in vanadium dioxide, J. Appl. Phys. Lett. 45 (1974) 2201-2206.

[145] S.A. Lawton, E.A. Theby, Synthesis of vanadium-oxide powders by evaporative decomposition of solutions, J. Am. Ceram. Soc. 78 (1995) 104–108.

[146] K. Maruszewski, W. Strek, M. Jasiorski and A. Ucyk, Technology and Applications of Sol-Gel Materials, Radiat Eff. Defects Solids, 158(2003) 439–450.

[147] Y. Dimitriev, Y. Ivanova, R. Iordanova, History of Sol-Gel Science and technology, J. Univ. Chem. Technol. Metall. 43 (2008) 181-192.

[148] G. Guzman, F. Beteille, R. Morineau and J. Livage, Electrical switching in VO_2 sol-gel films, J. Phys. Chem. 6(3) (1996) 505-506.

[149] Z. Zhang, Y. Gao, Z. Chen, J. Du, C. Cao, L. Kang, and H. Luo, Thermochromic VO_2 Thin Films: Solution-Based Processing, Improved Optical Properties, and Lowered Phase Transformation Temperature, Langmuir 26 (13) (2010) 10738–10744.

[150] C. Zhang, W. Cao, A. V. Adedeji, H. E. Elsayed-Ali, Preparation and properties of VO_2 thin films by a novel sol–gel process, J. Sol-Gel Sci. Technol. 69 (2014) 320–324.

[151] L. Jacques, Hydrothermal Synthesis of Nanostructured Vanadium Oxides, Materials 3 (2010) 4175-4195; DOI: 10.3390/ma3084175.

[152] C. Zhang, J. Cheng, J. Zhang, X. Yang, Simple and Facile Synthesis W-doped VO_2 (M) Powder Based on Hydrothermal Pathway, Int. J. Electrochem. Sci. 10 (2015) 6014.

[153] F.J. Quites, H.O. Pastore, Hydrothermal synthesis of nanocrystalline VO_2 from poly (diallyldimethyl ammonium) chloride and V_2O_5, Mater. Res. Bull. 45 (2010) 892–896.

[154] R. Li, C.-Y. Liu, VO_2 (B) nanospheres: Hydrothermal synthesis and electrochemical

properties, Mater. Res. Bull. 45 (2010) 688–692.

[155] Y. Zhang, M. Fan, F. Niu, Y. Zhong, C. Huang, X. Liu, B. Wang, H. Li, Hydrothermal synthesis of VO_2 (A) nanobelts and their phase transition and optical switching properties, Micro Nano Lett. 6 (2011) 888–891.

[156] B.D. Ngom, M. Chaker, A. Diallo, I.G. Madiba, S. Khamlich, N. Manyala, O. Nemraoui, R. Madjoe, A.C. Beye, M. Maaza, Competitive growth texture of pulsed laser deposited vanadium dioxide nanostructures on a glass substrate, Acta Mater. 65 (2014) 32–41.

[157] B. Chen, D. Yang, P.A. Charpentier, M. Zeman, Al^{3+}-doped vanadium dioxide thin films deposited by PLD, Sol. Energy Mater. Sol. Cells 93 (2009) 1550–1554.

[158] K. C. Patil, S. T. Aruna and S. Ekambaram, Combustion synthesis, Curr. Opin. Solid State Mater. Sci. 2(1997) 158-165.

[159] K.C. Patil, S.T. Aruna, Tanu Mimani, Combustion synthesis: an update, Curr. Opin. Solid State Mater. Sci. 6 (2002) 507–512.

[160] S. T. Aruna, A. S. Mukasyan, Combustion synthesis and nanomaterials, Curr. Opin. Solid State Mater. Sci. 12 (2008) 44–50.

[161] H. Futaki and M. Aoki, Effects of doping elements on the transition temperature of vanadium oxide semiconductors, Jpn J. Appl. Phys. 8 (1969) 1008- 1013.

[162] M. Marezio, D. B. McWhan, J. P. Remeika, and P. D. Dernier, Structural Aspects of the Metal-Insulator Transitions in Cr-Doped VO_2, Phys. Rev. B 5 (1972) 2541-2551.

[163] L. Song, Y. Zhang, W. Huang, Q. Shi, D. Li, Y. Zhang, Y. Xu, Preparation and thermochromic properties of Ce-doped VO_2 films, Mater. Res. Bull. 48 (2013) 2268.

[164] A. Pergament, G. Stefanovich, O. Berezina, D. Kirienko, Electrical conductivity of tungsten doped vanadium dioxide obtained by the sol–gel technique, Thin Solid Films 531 (2013) 572–576.

[165] Z. YaBin, H. Fan & N. Jie, Au doping effects on electrical and optical proper ties of vanadium dioxides, Sci. China - Phys. Mech. Astron. 55 (2012) 409–412.

[166] Y. Zhang, J. Zhang, X. Zhang, C. Huang, Y. Zhong, Y. Deng, The additives W, Mo, Sn and Fe for promoting the formation of VO_2(M) and its optical switching properties, Mater. Lett. 92(2013)61–64.

[167] S. -Y. Li, G. A. Niklasson, and C. G. Granqvist, Thermochromic undoped and Mg-doped VO_2 thin films and nanoparticles: Optical properties and performance limits for energy efficient windows, J. Appl. Phys. 115 (2014) 053513; DOI: 10.1063/1.4862930.

[168] J. Yea, L. Zhou, F. Liu, J. Qi, W. Gong, Y. Lin, G. Ning, Preparation, characterization and properties of thermochromic tungsten-doped vanadium dioxide by thermal reduction and annealing, J. Alloys Compd. 504 (2010) 503–507.

[169] M.K. Dietrich, B. G. Kramm, M. Becker, B. K. Meyer, A. Polity, and P. J. Klar, Influence of doping with alkaline earth metals on the optical properties of thermochromic VO_2, J. Appl. Phys. 117 (2015) 185301.

[170] H. Zhang, Z. Wu, R. Niu, X. Wu, Q. he, Y. Jiang, Metal–insulator transition properties of sputtered silicon-doped and un-doped vanadium dioxide films at terahertz range, Appl. Surf. Sci. 331 (2015) 92–97.

[171] F. Y. Kong, M. Li, J. Zhang, Y. Xu, D. B. Li, Z. Zeng and G. H. Li, Hydrothermal Synthesis of W and Mo co-doped VO_2 (R) Microrods at Low Temperature, Open J. Adv. Mater. Res. (2013) 1-6.

[172] W. Burkhardt, T. Christmann, B.K. Meyer, W. Niessner, D. Schalch, A. Scharmann, W- and F-doped VO_2 films studied by photoelectron spectrometry, Thin Solid Films 345 (1999) 229-235.

[173] W. Burkhardt, T. Christmann, S. Franke, W. Kriegseis, D. Meister, B.K. Meyer, W. Niessner, D. Schalch, A. Scharmann, Tungsten and fluorine co-doping of VO_2 films, Thin Solid Films 402 (2002) 226–231.

[174] Y.Jiazhen, Z. Yue, H. Wanxia, T. Mingjin, Effect of Mo-W Co-doping on semiconductor-metal phase transition temperature of vanadium dioxide film, Thin Solid Films 516 (2008) 8554–8558.

[175] N. Wang, S. Liu, X. T. Zeng, S. Magdassic and Y. Long, Mg/W-codoped vanadium dioxide thin films with enhanced visible transmittance and low phase transition temperature, J. Mater. Chem. C 2015; DOI: 10.1039/c5tc01062d.

[176] C.N.R. Rao and Kanishka Biswas, Characterization of Nanomaterials by Physical Methods, Annu. Rev. Anal. Chem. 2 (2009) 435–62.

[177] M. Suga, S. Asahina, Y. Sakuda, H. Kazumori, H. Nishiyama, T. Nokuo, et. Al., Recent progress in scanning electron microscopy for the characterization of fine structural details of nano materials, Prog. Solid State Chem. 42 (2014) 1-21.

[178] B. Akbari, M. P. Tavandashti, and M. Zandrahimi, Particle Size Characterization of Nanoparticles–A Practical approach, IJMSE 8 (2011) 48-56.

[179] P.-C. Lin, S. Lin, P.C.Wang, R. Sridhar, Techniques for physicochemical characterization of nanomaterials, Biotechnol. Adv. 32 (2014) 711–726.

[180] R. Das, Md. E. Ali and S. B. Abd Hamid, Current Applications of X-Ray Powder, Rev. Adv. Mater. Sci. 38 (2014) 95-109.

[181] A. Bogner, P.-H. Jouneau, G. Thollet, D. Basset, C. Gauthier, A history of scanning electron microscopy developments: Towards "wet-STEM" imaging, Micron 38 (2007) 390–401.

[182] O. Johari, S. Bhattacharyya, The application of scanning electron microscopy for the characterization of powders, Powder Technol. 2 (1969) 335-348.

[183] https://www.purdue.edu/REM/rs/sem.htm

[184] https://en.wikipedia.org/wiki/Transmission_electron_microscopy

[185] https://en.wikipedia.org/wiki/High-resolution transmission electron microscopy

[186] C.Baudot, C.M. Tan, J.C. Kong, FTIR spectroscopy as a tool for nano-material characterization. Infrared Phys. Technol. 53 (2010) 434–8.

[187] L. Chen, C. Huang, G. Xu, L. Miao, J. Shi, J. Zhou, and X. Xiao, Synthesis of Thermochromic W-Doped VO_2 (M/R) Nanopowders by a Simple Solution-Based Process, J. Nanomater. 2012; DOI:10.1155/2012/491051.

Publication

1. **A.B. Habtemariam**, D.M. Kabtamu, M. Maaza, One-step hydrothermal synthesis and characterization of Mg/Mo co-doped VO_2 nanorods, SN Applied Sciences, 1 (2019) 413.